



QUANTIFICATION OF DIFFERENT SOURCES OF UNCERTAINTY
IN A REGIONAL CLIMATE MODEL

CUANTIFICACIÓN DE DIFERENTES FUENTES DE INCERTIDUMBRE
EN UN MODELO CLIMÁTICO REGIONAL

TESIS DOCTORAL | ÁLVARO LAVÍN GULLÓN

Directores: José Manuel Gutiérrez Llorente y Jesús Fernández Fernández
Universidad de Cantabria
Programa de Doctorado en Ciencia y Tecnología - Santander, 2021

CUANTIFICACIÓN DE DIFERENTES FUENTES
DE INCERTIDUMBRE EN UN MODELO
CLIMÁTICO REGIONAL

QUANTIFICATION OF DIFFERENT SOURCES OF
UNCERTAINTY IN A REGIONAL CLIMATE
MODEL

Álvaro Lavín Gullón

Directores:

Dr. Jesús Fernández Fernández

y

Dr. José Manuel Gutiérrez Llorente

Universidad de Cantabria

Programa de Doctorado en Ciencia y Tecnología



Santander, 2021

Quantification of different sources of uncertainty in a Regional Climate Model

Álvaro Lavín Gullón
Instituto de Física de Cantabria (IFCA)
Universidad de Cantabria

Santander, Spain
April 2021

To those who were and to those who are

Acknowledgements

First of all, I want to express my gratitude to my directors José Manuel Gutiérrez and Jesús Fernández. To the former for trusting me and giving me the opportunity to carry out this thesis, to the latter for his indefatigable support and his constant willingness to help me. I can't thank both of you enough.

Thanks also to all my colleagues in the Santander Meteorology Group. In particular, I am really grateful to Rodri for supporting me with his friendship. Josipa, for all those good moments and her unfailing disposition to help. Zequi, for our passionate debates and for being such a good colleague. Mikel, for those long after-lunch conversations trying to sort out the world. Juan, for setting me a good example of so many things. Antonio, for helping me with the technical issues and offering me the opportunity to give my first lectures. The list is very long... Fer, Dolo, Juaco, the people from IFCA, my Argentinians from CIMA... For one reason or another, everybody has contributed to my reaching this moment.

Finally, at a more personal level, I would like to thank all my family, and especially my parents for teaching me that effort is always worthwhile. Thank you too Tamara for all these years, not forgetting Javi, Sofía, Elena, Vir, Noe... Thanks everybody.

En primer lugar, me gustaría expresar mis agradecimientos a mis directores José Manuel Gutiérrez y Jesús Fernández. Al primero por confiar en mí y darme la oportunidad de llevar a cabo esta tesis, al segundo por su infatigable apoyo y su constante disposición a ayudarme. No tengo palabras para agradecerlos.

Gracias también a todos mis compañeros del Grupo de Meteorología de Santander. En particular a Rodri, por apoyarme con su amistad. A Josipa,

II

por todos esos buenos momentos y su inagotable entusiasmo por ayudar. A Zequi, por nuestros apasionados debates y por ser tan buen compañero. A Mikel, por esos largos cafés de sobremesa intentando arreglar el mundo. A Juan, por llegar a ser un referente en tantas cosas. A Antonio, por ayudarme con los aspectos técnicos y ofrecerme la oportunidad de dar mis primeras clases. La lista es muy larga... Fer, Dolo, Juaco, la gente del IFCA, mis argentinos del CIMA... Por una razón u otra, todos han contribuido para llegar hasta aquí.

Finalmente, en un terreno más personal me gustaría dar las gracias a mi familia, y especialmente a mis padres, por enseñarme que el esfuerzo siempre merece la pena. Gracias también a Tamara por todos estos años, sin olvidar a Javi, Sofía, Elena, Vir, Noe... Gracias a todos.

Preface

This thesis is the work carried out in the Santander Meteorology Group (<http://www.meteo.unican.es>), part of Consejo Superior de Investigaciones Científicas (CSIC) and Universidad de Cantabria (UC), under the supervision of José Manuel Gutiérrez and Jesús Fernández. The work has been written following the requirements of Universidad de Cantabria to obtain the title as "Doctor en Ciencia y Tecnología", with international commendation. The investigation was initiated in 2016, prior to get the contract "Ayudas para contratos predoctorales para la formación de doctores" in 2017, funded by the Spanish government (grant BES-2016-078158). The work developed in the thesis has been mainly summarized in the following publications:

- **Lavin-Gullon, A.**, Milovac, J., Fernández, J., *Spin-up time and internal variability analysis for overlapping time slices in a regional climate model*. Submitted to Journal of Advances in Modeling Earth Systems.
- **Lavin-Gullon, A.**, Feijoo, M., Solman, S., Fernández, J., da Rocha, R. P., Bettolli, M. L., *Synoptic forcing associated with extreme precipitation events over Southeastern South America as depicted by a CORDEX FPS set of convection-permitting RCMs*. Climate Dynamics (2021) 10.1007/s00382-021-05637-8
- **Lavin-Gullon, A.**, Fernández, J., Bastin, S., Cardoso, R.M, Fita, L., Giannaros, T.M., Goergen, K., Gutiérrez, J.M., Kartsios, S., Katragkou E., Lorenz T., Milovac, J., Soares P.M.M., Sobolowski S., Warrach-Sagi, K., *Internal variability versus multi-physics uncertainty in a regional climate model*. International Journal of Climatology (2020) 10.1002/joc.6717

IV

- **Lavin-Gullon, A.**, Fernández, J., Cardoso, R.M., Goergen, K., Knist, S., Lorenz, T., Milovac, J., Soares, P. M., Sobolowski, S., Truhetz, H., Warrach-Sagi, K., *Convective processes in high resolution models: Impact of the lead time of the simulation*. Acta de las Jornadas Científicas de la Asociación Meteorológica Española (2018) 10.30859/ameJrCn35p388

In addition, part of the thesis work is also included in the following community publications:

- Coppola E., Sobolowski S., Pichelli E., Raffaele F., Ahrens B., Anders I., Ban N., Bastin S., Belda M., Belusic D., Caldas-Alvarez A., Cardoso R.M., Davolio S., Dobler A., Fernandez J., Fita L., Fumiere Q., Giorgi F., Goergen K., Güttler I., Halenka T., Heinzeller D., Hodnebrog Ø., Jacob D., Kartsios S., Katragkou E., Kendon E., Khodayar S., Kunstmann H., Knist S., **Lavín-Gullón A.**, Lind P., Lorenz T., Maraun D., Marelle L., van Meijgaard E., Milovac J., Myhre G., Panitz H.J., Piazza M., Raffa M., Raub T., Rockel B., Schär C., Sieck K., Soares P.M.M., Somot S., Srncic L., Stocchi P., Tölle M.H., Truhetz H., Vautard R., de Vries H., Warrach-Sagi K., *A first-of-its-kind multi-model convection permitting ensemble for investigating convective phenomena over Europe and the Mediterranean*. Climate Dynamics (2020) 10.1007/s00382-018-4521-8
- Bettolli M. L., Solman, S., da Rocha R. P., Llopart, M., Gutiérrez, J.M., Fernández, J., Olmo, M. E., **Lavin-Gullon, A.**, Chou, S., Carneiro Rodrigues, D., Coppola, E., Balmaceda Huarte, R., Barreiro, M., Blázquez, J., Doyle, M., Feijoo, M., Huth, R., Machado, L., Vianna Cuadra, S., *The CORDEX Flagship Pilot Study in South-eastern South America: A comparative study of statistical and dynamical downscaling models in simulating daily extreme precipitation events*. Climate Dynamics (2021) 10.1007/s00382-020-05549-z
- Ban, N., Caillaud C., Coppola, E., Pichelli, E., Sobolowski, S., Adinolfi, M., Ahrens, B., Alias, A., Anders, I., Bastin S., Belusic, D., Berthou, S., Brisson, E., Cardoso, R.M., Chan, S., Christensen, O. B., Fernández, J., Fita, L., Frisius, T., Gašparac, G., Giorgi, F., Goergen, K., Haugen, J. E., Hodnebrog, O., Kartsios, S., Katragkou, E., Kendon, E. J., Keuler, K., **Lavin-Gullon, A.**, Lenderink, G., Leutwyler, D., Lorenz, T., Maraun, D., Mercogliano, P., Milovac, J.,

Panitz, H. J., Raffa, M., Remedio, A. R., Schär, C., Soares, P. M. M., Srnec, L., Steensen, B. M., Stocchi, P., Tölle, M. H., Truhetz, H., Vergara-Temprado, J., de Vries, H., Warrach-Sagi, K., Wulfmeyer, V., Zander, M., *The first multi-model ensemble of regional climate simulations at kilometer-scale resolution, Part I: Evaluation of precipitation*. Climate Dynamics (In print)

All the simulations generated in the Universidad de Cantabria were carried out with WRF4G (Fernández-Quiruelas et al, 2015). This is a framework created by the Santander Meteorology Group for the execution and monitoring of the WRF model in distributed computer resources, in which I partially contributed in its development and improvement.

Along these years, the scientific formation and experience was completed by attending several international conferences and with two international stays: In 2016, in the National Center for Atmospheric Research (Boulder, US) under the supervision of Pedro Jiménez, and in Centro de Investigaciones del Mar y la Atmósfera (Buenos Aires, Argentina) in 2019, under the supervision of Silvina Solman. The latter stay led to the publication Lavin-Gullon et al (2021a).

In parallel, I had the opportunity to lecture in three Masters degrees in the Universidad de Cantabria, in different subjects related to advanced computer programming.

The format of this thesis follows the regulations of the Doctoral Studies at the Universidad de Cantabria. Although the Doctoral Programme in "Ciencia y Tecnología" does not specify any requirement, this thesis is presented as a compendium of three international peer-review publications (one still under revision).

Resumen

En las últimas décadas, el cambio climático es un tema recurrente al que se están dedicando grandes esfuerzos para entender sus causas y consecuencias. Estos interrogantes pueden ser respondidos simulando el clima pasado y futuro mediante modelos, consistentes en un conjunto de ecuaciones matemáticas con las que se representan diferentes procesos físicos. Para aplicar estas ecuaciones, el espacio se divide en celdas, representando la llamada resolución del modelo. Con la mejora de los recursos computacionales, el tamaño de las celdas se ha reducido considerablemente, aumentando la resolución. A su vez, la posibilidad de simular con más detalle el clima de una región ha llevado al uso generalizado de Modelos Climáticos Regionales.

A pesar del creciente interés en la modelización climática regional a muy alta resolución, aún permanecen sin explicar múltiples incertidumbres, entendidas como las discrepancias que surgen entre los diferentes resultados de los modelos a la hora de simular un proceso o variable física. Estas fuentes de incertidumbre, relacionadas con la propia configuración del modelo, el dominio o producidas por las propias condiciones iniciales, entre otras, son cruciales a la hora de interpretar los resultados.

Una fuente de incertidumbre destacada en un Modelo Climático Regional es la variabilidad interna. Esta incertidumbre puede ser definida como las diferentes soluciones producidas por el modelo al usar las mismas condiciones de contorno pero con una perturbación en las condiciones iniciales, la cual debido a la naturaleza caótica y no lineal del sistema climático da lugar a diferentes trayectorias en el espacio.

Durante años, y aún actualmente, diferentes iniciativas internacionales han abordado esta y otras fuentes de incertidumbre mediante la coordinación de ensembles multi-modelo. En este sentido, la iniciativa "Coordinated Regional Downscaling EXperiment" (CORDEX) adquiere un papel central en esta tesis, y en particular, los estudios piloto derivados de

VIII

ella "Extreme precipitation events in Southeastern South America" (FPS-SESA) y "Convective phenomena at high resolution over Europe and the Mediterranean" (FPS-Convection). Estos marcos de trabajo coordinaron varios experimentos con simulaciones a muy alta resolución en los que la parametrización de convección está desactivada (convection-permitting), poniendo el foco en áreas de ocurrencia de convección profunda.

El principal objetivo de esta tesis es contribuir a los diferentes planteamientos de la iniciativa CORDEX, desde la generación de simulaciones a muy alta resolución hasta la cooperación con los distintos grupos participantes, y así de esta manera evaluar y cuantificar el papel de diferentes fuentes de incertidumbre. Los objetivos específicos pueden ser resumidos en:

- Simular el clima regional de áreas de ocurrencia de eventos de precipitación extrema a muy alta resolución mediante el uso de convection-permitting en Modelos Climáticos Regionales.
- Cuantificar el papel de diferentes fuentes de incertidumbre, principalmente la resolución horizontal, la incertidumbre en el dominio, la variabilidad interna y las incertidumbre multi-modelo y multi-física.
- Explorar la incertidumbre asociada a la inicialización de variables lentas, así como su impacto en simulaciones computacionalmente costosas y que han sido partidas en varios tramos de tiempo.
- Mejorar el entendimiento de los mecanismos sinópticos que llevan a la generación de eventos de precipitación extrema.

Gran parte del trabajo se ha llevado a cabo bajo el paraguas de FPS-Convection y FPS-SESA con simulaciones convection-permitting a muy alta resolución cubriendo Europa y América del Sur, respectivamente, con un foco en los Alpes y el sureste de América del Sur. Estos dominios ofrecen diferentes condiciones climáticas y mecanismos sinópticos. Además, los diseños experimentales de estos estudios piloto permiten cubrir la mayoría de fuentes de incertidumbre que pretendemos explorar. Las simulaciones del clima regional a muy alta resolución se han llevado a cabo mediante el modelo Weather Research and Forecasting (WRF). Debido a los altos costes computacionales de simular el clima regional a una escala espacial de pocos km y un periodo temporal de años, se vio la necesidad de partir las simulaciones en tramos de tiempo, los cuales se solapan en

periodos de al menos un año para cubrir un tiempo de spin-up mínimo. Aunque los solapamientos son descartados en el postproceso final, en este trabajo son empleados para estudiar el comportamiento del spin-up.

El tema global de esta tesis es la cuantificación de incertidumbres en la modelización del clima regional, con un especial hincapié en la variabilidad interna como contexto para evaluar el tamaño relativo de otras fuentes de incertidumbre. En este trabajo, la variabilidad interna es calculada mediante ensembles multi-condiciones-iniciales en los que cada miembro del ensemble es inicializado con un día de diferencia respecto al anterior (un día antes, dos días antes y así sucesivamente), manteniendo en todos la misma configuración física. De esta forma, el ensemble es un conjunto de simulaciones con condiciones iniciales ligeramente perturbadas.

Otras fuentes de incertidumbre estudiadas son la relativa a la resolución horizontal, con un rango de resoluciones de ~ 50 km a ~ 3 km, y la incertidumbre en el dominio, con dominios sobre Europa y América del Sur. La incertidumbre multi-física es cuantificada a la luz de la variabilidad interna para evaluar la respuesta de una selección de eventos de precipitación extrema a las parametrizaciones físicas. De manera similar se explora la incertidumbre multi-modelo.

Además de estas incertidumbres, se estudian diferentes inicializaciones y periodos de spin-up. Por un lado, se explora la habilidad de los modelos de representar eventos de precipitación extrema con dos inicializaciones: unos días antes de cada evento ("weather-like") y en "climate mode", inicializando uno o más meses antes. Por otro lado, el análisis se extiende a periodos de spin-up más largos pero haciendo uso de simulaciones que han sido partidas en tramos de tiempo.

Por último, se evalúa la habilidad de las simulaciones convection-permitting a la hora de representar eventos de precipitación extrema en Europa y América del Sur. En esta última región se exploran los mecanismos sinópticos que llevan a la generación de estos eventos, identificando un precursor de los mismos.

Con respecto al primer objetivo específico de esta tesis, se ha contribuido con simulaciones propias en todos los experimentos de evaluación de FPS-Convection y FPS-SESA, siguiendo los protocolos establecidos. Los resultados de estos experimentos muestran que los mecanismos sinópticos que favorecen la convección profunda están bien representados en los dominios de alta resolución. Sin embargo, algunas discrepancias surgen en cuanto a su localización, las cuales dan lugar a discrepancias en la reproducción de los eventos en los dominios convection-permitting. Este

comportamiento es observado en ambos modos de simulación ("weather-like" y "climate mode") en el dominio de América del Sur, pero no en el de Europa donde solo se presenta en "climate mode".

La cuantificación de diferentes fuentes de incertidumbre ha revelado la importancia que tiene la variabilidad interna en variables atmosféricas, en las que la incertidumbre multi-física puede ser de igual magnitud que la variabilidad interna. En estos casos, la incertidumbre que surge de las perturbaciones de la física del modelo son vistas como perturbaciones en las condiciones iniciales. En cambio, para variables en superficie esta incertidumbre es menos relevante. De acuerdo a otros estudios de variabilidad interna en Modelos Climáticos Regionales, esta incertidumbre presenta valores más altos (bajos) en verano (invierno) y un patrón espacial con valores más bajos según nos acercamos a los bordes del dominio. Los resultados tienen una clara dependencia con el dominio, ya que el destacado papel de la variabilidad interna en el dominio sobre Europa no parece repetirse en el dominio sobre América del Sur. Además, se ha observado que la variabilidad interna no es sensible a la resolución horizontal y a su vez, que la resolución horizontal no parece jugar ningún papel destacado en el spin-up del modelo ni en las inhomogeneidades de simulaciones que han sido partidas en tramos.

Por otro lado, los resultados confirman que partir las simulaciones en tramos de tiempo es un método válido para mejorar la eficiencia de simulaciones computacionalmente costosas. No obstante, al analizar climatologías regionales se encontró un potencial efecto de usar este procedimiento en variables relacionadas con el suelo, aunque atribuidas a la variabilidad interna. El análisis mostró que estas variables, que tienen un tiempo largo de adaptación ante un cambio, presentan las mayores discontinuidades meteorológicas en las uniones entre los diferentes tramos. El momento óptimo para unir entre dos tramos de tiempo, y con ello reducir las discontinuidades, depende de la estación y las condiciones atmosféricas de la región. Además, los resultados muestran que la variabilidad inter-anual es también un factor importante ya que el spin-up puede depender de las condiciones atmosféricas dadas en el año de inicialización.

Finalmente, con respecto al último objetivo, los diseños experimentales de tanto FPS-Convection como de FPS-SESA permitieron estudiar cómo los modelos reproducen eventos de precipitación extrema bajo diferentes condiciones sinópticas. Los mecanismos que llevan a estos eventos extremos fueron analizados en el sureste de América del Sur, donde se encontró que los valores más altos de convergencia del flujo de humedad verti-

calmente integrado se correspondían con máximos de precipitación 6 horas más tarde. Esto llevó a identificar la convergencia del flujo de humedad verticalmente integrado como un importante precursor de la convección profunda en la región. No obstante, este precursor viene determinado por las condiciones climáticas del sureste de América del Sur por lo que la generalización a otros dominios debe ser tomada con cautela.

Contents

Acknowledgements	I
Preface	III
Resumen	VII
1 Introduction	1
1.1 Climatic system and its changes	1
1.2 Modeling climate	6
1.3 Representation of fine-scale processes	10
1.4 Sources of uncertainty in Regional Climate Models	13
1.5 CORDEX initiative	17
1.6 Thesis objectives	22
1.7 Structure of the thesis	23
2 Data	27
2.1 Observational data	27
2.2 Model simulations	28
2.2.1 Weather Research and forecasting model	28
2.2.2 Ensemble generation methods	28
2.2.3 Simulation modes	29
2.2.4 List of simulations produced in this thesis	29
2.2.5 Other simulations	30
3 Internal variability vs multi-physics uncertainty in a regional climate model	33
3.1 Introduction	33
3.2 Data & methods	37
3.2.1 Multi-physics ensemble	37

3.2.2	Multi-initial-conditions ensemble	40
3.2.3	Quantification of uncertainty	41
3.3	Results & discussion	43
3.3.1	Event reproducibility	43
3.3.2	Analysis over an annual cycle	48
3.3.3	Surface variables	54
3.4	Conclusions	56
4	Spin-up time and internal variability analysis for overlapping time slices in a regional climate model	61
4.1	Introduction	61
4.2	Data & methods	64
4.2.1	Data	64
4.2.2	Methodology	67
4.3	Results & discussion	69
4.3.1	Detection of meteorological inhomogeneities	69
4.3.2	Meteorological inhomogeneities in time	72
4.3.3	Meteorological inhomogeneities: spatial distribution	80
4.3.4	Simulated climate	83
4.4	Conclusions	86
5	Synoptic forcing associated with extreme precipitation events over Southeastern South America as depicted by a CORDEX FPS set of convection-permitting RCMs	89
5.1	Introduction	89
5.2	Data & methods	92
5.2.1	Observational data sets	93
5.2.2	Regional climate models	94
5.2.3	Evaluation metrics	97
5.3	Results & discussion	98
5.3.1	Case studies: peak precipitation	98
5.3.2	Synoptic forcing mechanisms	103
5.4	Conclusions	111
6	General Conclusions	115
A	Supplementary figures	119
	Bibliography	133

Chapter 1

Introduction

Despite the continuous advances in climate modeling, many uncertainties and sensitivities are still unclear and they need to be identified for a correct interpretation of the results. The spectrum of processes and mechanisms involved in a model is very wide, which requires a certain understanding. In the following sections, the different variables, mechanisms and processes involved in a simulation are briefly explained, from the components of the climate system on Earth to the initiatives that try to explain the biases and uncertainties in the models. After this context, the main objectives of the thesis are formulated, along with the structure of the rest of the document.

1.1 Climatic system and its changes

Two variables, decisive for the life on Earth, define the climate: precipitation and temperature. They determine the existence of plants and animals and their distribution across the world. But other variables are also important, such as humidity as generator of clouds affecting the amount of solar radiation reaching the surface, or wind as generator of turbulence in the surface boundary layer. They are examples of variables and processes composing the Climate system. Their interactions define the distribution of energy and water near the surface ([Hartmann, 1994](#)).

The Climate system is usually divided into several components: hydrosphere, cryosphere, biosphere, lithosphere and atmosphere. Hydrosphere refers to the liquid water available on the Earth, composed by all the water bodies including seas, lakes, rivers, subterranean waters, etc. Cryosphere

is the part including the solid water in the shape of glaciers, snow cover, ice and permafrost. Living beings and their interactions with the climate system (e.g. evapotranspiration) are included in the biosphere. Lithosphere is the most external layer of the Earth and it acts regulating many processes in the air-surface interface. Lastly, the atmosphere is a gaseous layer over the surface of the Earth, where the main energy interactions occurs (Peixoto and Oort, 1992). Each component has very different times to recover from a perturbation (response time). For example, glaciers behave very slowly in its evolution and against any change, leading the cryosphere to have the longest response time. In this work we mainly focus on the atmosphere, paying also attention to the lithosphere due to its strong interaction with the atmosphere.

The temperature of the Earth is mainly determined by the energy balance between the energy coming from the Sun and that returned by Earth's radiative emission. The absorption of solar radiation is mostly produced at the surface, especially near the equator, whereas the emission is mainly generated by the atmosphere. In general terms, the atmosphere absorbs and emits infrared radiation so that the surface is warmer than it would be in absence of the Atmosphere (Figure 1.1). This is called "Greenhouse effect", whose direct consequence is to warm the surface of the Earth. To explain the effect, we can consider a model where the Earth behaves as a blackbody. Here, the atmosphere is relatively transparent to solar radiation but at the same time absorbs and emits the terrestrial radiation, that is, surface is warmed because solar radiation goes entirely through the atmosphere and the atmosphere heats the surface via downward radiation. Therefore, the strength of the Greenhouse effect is determined by the balance between the amount of solar energy entering the atmosphere and the terrestrial radiation going through the atmosphere (outgoing long-wave radiation) (Hartmann, 1994). The blackbody model is a simplification as the energy interactions between atmosphere and surface is more complex.

First of all, energy can be transported through three mechanisms:

1) Radiation: Electromagnetic waves transporting light and heat with no mass in between. For example, solar energy reaches the Earth and enters the atmosphere where only specific wavelengths are absorbed. Most short-wave radiation reaches the surface.

2) Conduction: Heat is transmitted from warmer to cooler bodies. The diverse elements in the climate system have different thermal conductivities, so that conduction is negligible in the atmosphere but very important in the ground.

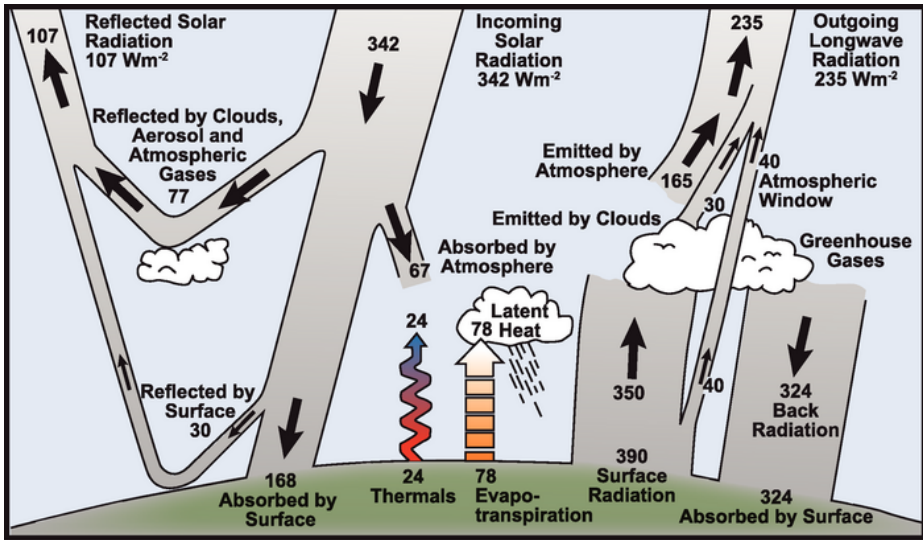


Figure 1.1: Estimations of the Earth's annual and global mean energy balance. Source: Kiehl and Trenberth (1997).

3) Convection: It is the only energy-transfer mechanism where mass is exchanged, due to the motion of heated parts in fluids or materials.

On the other hand, heat is transferred in two ways: As latent heat and sensible heat. The former is an energy transfer which involves the change of the state of a substance with no temperature change (giving rise to cloud formation, e.g.). The opposite is given in the sensible heat.

Energy coming from the Sun is transmitted as radiation, whose flux is associated with particles of solar wind, although their energy is too small to be considered in the energy balance of the Earth. In this sense, we only need to take into account the exchange of radiative fluxes. The incoming solar radiation reaches the Earth as short-wave radiation (visible, near-ultraviolet and near-infrared spectra). Then, the radiation is mostly reflected by the atmosphere, clouds and the surface, whereas the remaining is absorbed by the surface and the atmosphere as heat. The surface absorbs half of the radiation available at the top of the atmosphere, emitting it outward. Part of this energy is absorbed by clouds and atmospheric constituents such as ozone or carbon dioxide. The remaining radiative energy travels through the atmosphere via the so-called "atmospheric window", a range of wavelengths that are relatively little absorbed.

This radiation, together with that emitted outward by the atmosphere and clouds, is transmitted as outgoing long-wave radiation (thermal infrared spectra).

Clouds are a very important factor in the energy budget of the earth. They constitute a temporary thermal reservoir of the energy that reaches them and at the same time, they are an important barrier for the incoming solar radiation. However, clouds retain long-wave radiation from surface that would escape outwards in their absence. They widely vary in shape and size, but all of them develop through moist convection. Over land, a parcel of hot air rises from an instability, expanding and cooling along its rise. As the parcel ascends, it mixes with the cooler and drier environment up to reaching the saturation point and as a consequence, condensation. Over a water body, when a cool air flow moves above a relatively warmer water, an instability is induced as the lower layer of air becomes warm and moist. In turn, convection takes place and clouds are generated (Ahrens, 2009).

There are two types of cloud convection: shallow convection, vertical convective process occurring over a small part of the troposphere, and deep moist convection, spanning a much larger portion. The latter initiates from a warm surface temperature anomaly. In association with an instability, strong updrafts release latent heat vertically, generating divergence at deep upper levels. In parallel, the environment is altered by these processes. Gravity waves produced by convection warm the environment because of subsidence while the generated precipitation dries the environment by extracting water vapor. This type of convection has an important role at local and large scale. At local scale, deep convection is key because it can result in heavy precipitation events. At large scale, atmospheric vertical circulations are determined by large horizontal gradients of latent heating generated by deep convection. For example, large gradients near the tropics produce the Hadley cell, a global scale circulation moving poleward at deep upper heights, descending in the subtropics and then flowing equatorward. Likewise, phenomena like El Niño Southern Oscillation (ENSO) are influenced by deep convection occurring in the tropical eastern Pacific. Shallow convection mainly affects the processes in the near surface and it is assumed to be a non-precipitating convection (Stensrud, 2007).

The effect of the solar radiation depends on latitude, which determines daylight duration and the angle of incidence of the rays of sun. Nonetheless, the heat stored by the surface strongly depends on the albedo, that

is, how much solar radiation is reflected via outgoing radiation. Overall, the albedo determines the energy balance at the top of the atmosphere. Measurements show that lowest values can be found in tropical oceans with sparse clouds, while highest values are in polar regions, deserts and tropical regions with thick clouds (Hartmann, 1994).

The atmosphere interacts with the surface by transferring solar and infrared radiation as heat, generating fluxes of energy related with fluid motions. On the one hand, air is a very poor conductor. On the other hand, land and sea regulate the heat stored in the climate system but with different specific heat capacities. Water stores the heat easier than land, as the latter quickly emits it back to the atmosphere. The processes occurring in the sea are less efficient. However, effective heat transport is larger because of fluid motions that do not occur in land. As an example, the first two meters of soil are affected by seasonal variations (Hartmann, 1994). Heat is transmitted in land by conduction, as a function of its porosity and the moisture content so that when the latter is increased by filling the soil pores, conductivity rises. In the sea, heat is distributed to considerable depths by the turbulent mixing of water masses. Overall, due to its very high specific heat capacity, the sea behaves as a world heat reservoir (Barry and Chorley, 2003).

At the air-surface interface, turbulence is a process generated by quick chaotic fluctuations in wind velocity. When these turbulent fluctuations take place together with vertical gradients in temperature or humidity, changes of scalar properties may appear, giving rise to sensible or latent heat fluxes. Likewise, turbulence can generate vertical fluxes of mass, momentum and energy when properties of air parcels moving upward are different from those moving downward. These processes define the Planetary Boundary Layer (PBL), that is the part of the troposphere directly influenced by the surface. In turn, the PBL is usually divided into three levels: viscous sublayer, surface layer and transition layer (Pielke, 2002). On the other hand, soil, vegetation and the atmosphere interact among them, generating soil moisture or biophysical and thermodynamic processes such as evaporation and plant transpiration (evapotranspiration).

The balance between the incoming solar radiation and the outgoing long-wave radiation can be modified by processes such as fluctuations of solar cycle (van Geel et al, 1999) or aerosols (Torseth et al, 2012). It is an example of spatial and temporal variations due to external natural or anthropogenic forcings. But the climate system can be also modified by internal natural changes. Thus, both natural internal or external changes

define the climate variability.

In this context, changes in the energy-radiative balance are associated with "radiative forcing". Following [Houghton et al \(2001\)](#), radiative forcing is defined as the change in net (down minus up) irradiance (solar and long-wave radiation) at the tropopause after allowing stratospheric temperatures to readjust to radiative equilibrium, but with surface and tropospheric temperatures and state fixed. These radiative forcings produce important changes in the climate system. It should be noted that, according to the World Meteorological Organization (WMO), any climate change is a statistically significant variation in the mean state of the climate or in its variability, persisting for decades or longer. Some of the forcings have a natural origin, but we must highlight the one produced by human activities emitting greenhouse gases (GHG, [Tans, 2009](#)), which gives rise to the anthropogenic climate change.

The potential effects of future anthropogenic forcings cannot be known in advance. Therefore, different hypothesis are summarized as future emission or GHG concentration scenarios. Future greenhouse gas concentrations are calculated in terms of socio-economic, demographic and environmental activities. As a result, different scenarios describing different GHG emissions are produced. The scenarios are used to provide forcing data for climate models, which will generate future climate projections, that is, possible future states of the climate.

1.2 Modeling climate

Considering that humans can induce changes on the climate system, a common question in the research community is how climate will evolve in the future. To understand how climate behaves, we may use dynamical simulations of the atmosphere, in the manner of the weather predictions.

Weather forecasts are based on Numerical weather prediction (NWP) models, which are a computer software to solve mathematical relationships describing the motion of fluids. From the current state of the atmosphere, the model integrates the equations in order to simulate a future state. These are continuous partial differential equations that cannot be analytically solved. Therefore, numerical techniques convert them into algebraic ones ([Durrant, 1999](#)). Different techniques are used, depending on the strategies to represent the equations and to compute the derivatives ([Haltiner and Williams, 1980](#); [Durrant, 1999](#); [Kalnay, 2002](#)). The surface is

divided into grid cells (Figure 1.2), which defines the horizontal resolution and the points in which the model mathematical equations are applied. The first step in running the model is to provide the initial conditions at every grid point, as well as for several vertical layers. The way the initial conditions influence the simulation is determined by the lead time of the simulations: Weather forecasts are mainly based on the initial conditions, since their objective is to determine the state of the atmosphere at a given time. In climate modelling, the objective is to simulate the future behaviour of the atmosphere so that initial conditions are less decisive.

An accurate dataset of initial conditions is key to initiate the simulation. To determine the initial conditions, the available observations are spatially interpolated to grid points using different interpolation methods. The main problem is that the available observations are not enough to start a model, due to their irregular distribution in space and time. Some regions have more dense observational networks than others, so additional information is needed. Thus, to prepare the initial conditions, data assimilation systems employ short-range forecasts to complete the analysis (Kalnay, 2002), the most accurate representation of the state of the atmosphere at a given time. In turn, these procedure is used to generate "climate reanalysis". The reanalysis produces a comprehensive and consistent description of the observed atmospheric circulation by taking observations from different sources, whose accuracy is dealt with data assimilation. This technique consists in reprocessing available, historical observations across the entire world through a forecasting model where the equations of motion and physical processes are used to generate a gridded dataset. At the end, reanalysis produces a multidecadal set of atmospheric, sea-state, and land surface parameters, as well as variables that are not observed in-situ (Dee et al, 2014).

Depending on the purpose, models have different features or approximations. Most of the models employ the hydrostatic approximation, which consider that the pressure gradient is in balance with gravity. This is the case of the hydrostatic general circulation models (GCMs), widely used by the research community to study climate, or the hydrostatic mesoscale models, focused on mesoscale (phenomena smaller than synoptic scale and larger than microscale). Other models are non-hydrostatic, as those used to investigate specific phenomena, such as thunderstorms. Furthermore, all the three-dimensional complexities involved in the climate system (dynamic and thermodynamic processes as well as the mass and radiative exchanges) are modeled with GCMs, producing outputs covering the whole

world. The oldest GCMs included a dynamic ocean that was coupled to the atmospheric model (Atmosphere-Ocean General Circulation Models, AOGCMs) (Barry and Chorley, 2003). However, the most recent models already integrate the interactions of the atmosphere, ocean, land, biosphere and ice (Earth System models, ESMs).

Reaching this point took a long development. The first models were simple sets of numerical equations over a small region (Charney et al, 1950; Shuman and Hovermale, 1968), until major advancements arrived in the late 1980's and they were able to simulate the whole globe (Sela, 1980). Over the years, research institutions and universities started to produce their own models, increasing numerical and model complexity thanks to the availability of faster and larger computers (Stensrud, 2007).

The increasing interest to study climate change effects at regional scales led to develop a framework for a model nested into a GCM, called "Regional climate model" (RCM) (Dickinson et al, 1989; Giorgi and Bates, 1989; Giorgi et al, 1989). Due to the complexity of the climate system, composed by a wealth of interactions at multiple spatial scales, a good representation of these interactions is key in climate modeling. Computational resources limit the horizontal resolution to which GCMs can be run. It is needed to "downscale" the results, that is, to take large-scale information to produce local-scale predictions. The coarse resolution of GCMs, despite their effectivity to represent large-scale circulations (Dickinson, 1986) and their ability to respond to large-scale forcings (e.g. greenhouse gas concentrations) (McAvaney et al, 2001), are unable to solve local forcings and fine-scale processes associated with complex orography, large water bodies or complex vegetation. Regional climate modeling is a form of "dynamical downscaling", where global climate simulations outputs drive a high resolution model over a specific area. Initial and lateral meteorological boundary conditions as well as surface boundary conditions are provided by the GCM (Giorgi and Mearns, 1999). In this way, the RCM lets the GCM reach higher resolutions. These driving fields can be supplied by AOGCMs or reanalysis.

The underlying idea of driving a RCM with GCM outputs is to provide the response of the general circulation to large-scale forcings. The role of the RCM is to add regional details to large-scale forcings from a GCM. As a consequence, any error transmitted by the GCM (e.g. errors in storm tracks) is assimilated into the RCM. In this problem, so-called "garbage in - garbage out" rule, the quality of the results produced by the RCM is conditioned by the quality of the initial and boundary conditions (van

Ulden and van Oldenborgh, 2006). Therefore, prior to run the model, it is important to evaluate the large-scale fields that are provided by the GCM (Giorgi, 2006). To optimize and test RCMs, many experiments include the so-called "evaluation" simulations. Here, forcing fields are based on reanalysis, so that the driving fields are expected to be the best available and the data compare well with observations.

Nested regional modeling was not a new approach as this technique had been widely used in NWP. However, simulations were carried out for short periods as it was considered that longer simulations could propagate the error generated by the lateral boundary conditions. The underlying idea was that processes (e.g. radiative forcings or interactive soil moisture) that are irrelevant at short timescales but critical at longer timescales, could not be included. Therefore, the original proposals to run a RCM was only applied for short runs, creating a regional climatology from statistics of short-run ensembles. Several questions, such as the error propagation, the realism of the results or the accuracy of fine-scale forcings, were addressed next. Giorgi and Bates (1989) and Giorgi (1990a) carried out simulations over a complex topography in western United States showing that error did not propagate after 1-2 days of simulation and that fine-scale processes were well captured by the RCM. On the other hand, Dickinson et al (1989) and Giorgi (1990b) successfully simulated wintertime storms in month-long simulations. The storms presented realistic features and the results were close to those observed. Over the same region, Giorgi (1990a) analyzed the large-scale January climate with a GCM driving a RCM at 60 km horizontal resolution. As compared with both large-scale and high resolution observations, variables as geopotential height, wind, temperature, precipitation or storm frequencies were realistically simulated. Longer simulations were considered in order to account for the atmospheric and surface spin-up times. The model needs to reach the dynamical equilibrium between the lateral boundary forcing and the internal model physics. Also, it needs to balance the surface fields, which typically include variables evolving very slowly (e.g snow or soil moisture). Thus, long simulations were more consistent with the model physics and the model climatology. Giorgi et al (1993) and Giorgi et al (1994) run the first multi-year climate change experiment over the continental United States at the beginning of the 1990's. This approach was followed up, for example, by McGregor et al (1999), who simulated a transient climate change run of 140 years. In parallel, grid spacing has been increasing step-by-step from the initial 60 km up to below 3 kilometers (e.g. Coppola

et al, 2020).

1.3 Representation of fine-scale processes

Many important processes and interactions cannot be directly solved by the models, not only due to limitations imposed by the resolution, but also because some interactions are not dealt with the dynamical atmospheric equations. These equations do not include averaged effects of unresolved nonlinear terms, such as those related to advective terms. In this case, parameterizations (or parameterization schemes) provide the information (e.g. the effect of cumulus clouds) that the model lacks. In this regard, parameterizations compose the so-called model physics, which must be differentiated from the dynamical core, constituted by all the dynamical atmospheric equations (e.g. Navier-Stokes equations) and the ways to solve them (e.g. Lagrangian or Eulerian specifications).

Parameterizations are simplified and idealized representations of physical processes to account for their effects on the variables resolved by the model dynamics (McFarlane, 2011). These processes can be parameterized with different alternative schemes, representing different approaches and methodologies. Some of these schemes are called by the model at every integration timestep, whereas others are called less frequently, mainly those computationally more expensive. Usually, parameterization provides variable tendencies, which are added in the equations of motion as well as into the calculation of other parameterizations. The tendency given by the parameterization scheme keeps constant until it is called again by the model. This is key for the simulation as this time tendency defines how often the variables interact with others. In this sense, the relationships between the subgrid processes and the model variables are defined with the so-called scheme closure. Parameterizations usually focus on the processes within the vertical column of each model grid cell, that is the most important direction when it comes to considering energy.

When a scheme represents the effects of a process on the grid variables, the parameterization is called "implicit". However, when resolution is high enough, it is possible to solve the evolution of a subgrid process. Here, the process would be solved "explicitly".

Multiple interactions and processes are parameterized: some examples are latent and sensible heat transfer at the air-surface interface or the soil moisture that is generated because of rain. Also a cumulus cloud, gener-

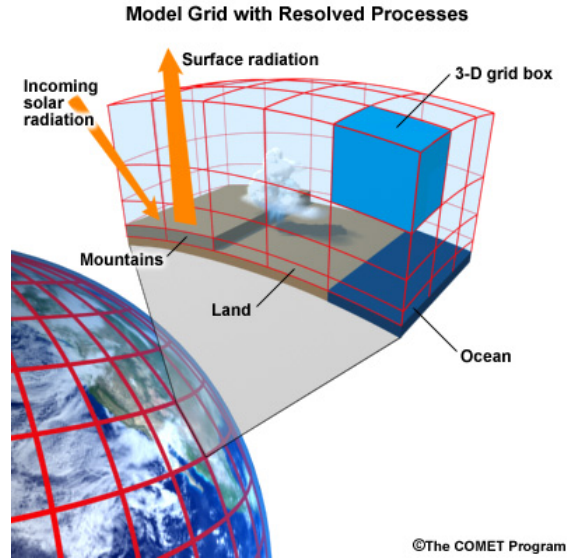


Figure 1.2: Model grid with examples of solved processes. Source: The COMET program. The University Corporation for Atmospheric Research.

ally smaller than the grid box. The effect that a cloud produces, as well as its evolution, occur at microscopic scale. In this regard, cloud microphysics focuses on the processes involved in the formation of clouds and precipitation, as well as their evolution. Microphysical variables play an important role in modeling as these processes affect multiple scales (e.g. release of latent heat due to phase changes of water or cloud-radiation interactions). Therefore, cloud microphysics parameterizations are decisive to adequately simulate formation, growth and dissipation of cloud water particles.

The effects of the vertical subgrid fluxes near the surface are usually dealt with by the surface layer and/or the PBL parameterization schemes, which are directly related. Although turbulent fluxes could be directly solved by the equations of motion, the model would require extremely high resolutions (50 m or less) and even so, some turbulent processes would still remain unresolved. The interactions are highly complex, therefore, the PBL parameterization scheme represents the evolution of the mean boundary layer state as well as the effects of the turbulence on the atmosphere (Stensrud, 2007). The surface layer parameterization focuses on calculating vertical sub-grid fluxes near the ground, such as

latent and sensible heat fluxes (Pielke, 2002). In turn, soil, vegetation and atmosphere interact in different ways between them, involving complex physiological mechanisms that need to be parameterized in the land surface parameterization schemes.

Another important component in the surface energy budget is radiation, whose mechanisms need to be parameterized due to their small scale. Indeed, the transfer of radiation through the atmosphere takes place at molecular scale, which is never resolved by the models. Radiation schemes provide a fast method of calculating the total radiative flux at the surface and the vertical radiative flux divergence, that is used to determine the radiative cooling and heating rates of the atmosphere. Usually, radiation parameterizations consider the short-wave and long-wave radiative fluxes separately.

In this thesis, deep convection takes a preeminent place so we highlight the mechanisms involved in its formation, as well as the role of the convective parameterizations. Besides, deep convection comprises a good example of process that is either explicitly or implicitly resolved. Deep convection takes place as very localized updrafts, whose order of magnitude spans between 25 m to 1 km (Stensrud, 2007), so that these processes are unrealistic in models with larger grid spacing (including typical GCMs and RCMs). Thus, the thermodynamic effects of these updrafts on the temperature and moisture profiles need to be parameterized, along with the precipitation produced in the process. In this case, when a convective process is implicitly parameterized (also called cumulus parameterization), the cumulative effects of clouds on other variables are represented on the model grid. But parameterizing convection is challenging due to the wealth of processes acting at different scales, the multiple interactions with other schemes (cloud microphysics, radiation, PBL) and the mechanisms, such as the triggering of updrafts, that remain unclear (Prein et al, 2015). Therefore, some uncertainties are inherent to cumulus parameterizations, giving rise to inaccuracies. For example, by using this parameterization, the diurnal cycle of convective precipitation is misrepresented (Brockhaus et al, 2008) and the hourly precipitation intensities are underestimated (Ban et al, 2014). Biases from the GCMs are generally carried over to the RCMs, but in parameterized convection domains, low-precipitation event frequency can be overestimated and dry days can be underestimated (Berg et al, 2013).

Although parameterization schemes have improved these common errors (e.g. Donner et al, 2011), this issues may be managed by solv-

ing convection explicitly. This kind of simulations are called with multiple names: "convection-permitting", "cloud-resolving", "convection-resolving"... Here, we use "convection-permitting" (CP) simulations, as the terminologies "cloud-resolving" and "convection-resolving" refer to processes at the smallest scales in clouds, which is not the focus in this thesis.

In CP simulations, the resolution is able to better reproduce the mechanisms involved in convection (e.g. more realistic convective updrafts). Here, microphysics scheme solves cloud processes so that they are represented directly on the grid (Arakawa, 2004). Besides, as far as it is included in the microphysics scheme, hydro-meteors that remain unresolved at coarser resolutions, can be generated now. The upper limit resolution to consider CP is generally established in 4km since Weisman et al (1997) found that horizontal resolutions equal or coarser than 4 km are unable to represent non-hydrostatic dynamics if it is explicitly parameterized. In this regard, Fosser et al (2015) showed that CP simulations at resolutions less than 4 km improved the representation of intensity distribution and diurnal cycle of precipitation. When a model reaches such high resolutions, one or more domain nesting are usually needed, depending on the grid spacing of the driving fields. Besides, CP simulations demand some other requirements. A non-hydrostatic formulation must be considered as the hydrostatic approximation is not valid above 10 km. Nevertheless, the finer horizontal resolution and its subsequent more detailed representation of orography, require higher stability in the numerical discretization by solving steeper slopes in orography (Prein et al, 2015). Resolutions between 4 km and 10 km are within the so-called "grey zone", which should be avoided as simulations in this range violate some assumptions in the cumulus parameterization and convection might not be correctly solved explicitly. Despite their expensive computational cost, reaching CP resolutions allows for getting rid of the inherent uncertainties in the cumulus parameterization, which are a remarkable source of uncertainty in RCMs.

1.4 Sources of uncertainty in Regional Climate Models

We define "uncertainty" from a quantitative perspective, as the spread in the results between ensemble members, that is, discrepancies found between different perturbed simulations. There are multiple sources of

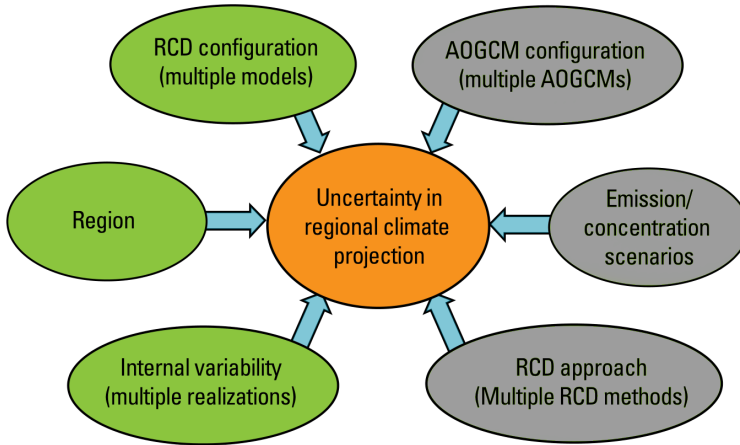


Figure 1.3: Uncertainty sources in regional climate downscaling (RCD). Adapted from Giorgi et al (2009).

uncertainty defined in previous studies (Giorgi, 2005; Giorgi et al, 2009; Giorgi and Gutowski, 2015), but we focus on a selection of them (green coloured in Figure 1.3), such as those related to the domain, initial conditions or the physical parameterizations.

First of all, an important source of uncertainty arises as regards the model domain. Both domain size and location are a very noticeable source of uncertainty as they are directly related to the influence of the lateral boundary conditions within the domain. In this sense, small-scale processes need space and time to develop and therefore, domains must be large enough to allow their development. Leduc et al (2011) observed that for comparable domains, this development is determined by the strength of the lateral boundary conditions, exhibiting a seasonal cycle for simulations in eastern Canada. At midlatitudes in the northern Hemisphere, the westerly flow in summer is weak and variable, but it becomes stronger in winter. As compared with a domain at midlatitudes, Rinke and Dethloff (2000) found a smaller predictability for the same size domain in the Arctic due to a weaker constraint of the boundaries. The observed precipitation is better captured when the domain size is smaller, although the simulation of sensitivity of precipitation to initial soil moisture can be more realistic for larger domains (Seth and Giorgi, 1998). The same study highlighted that the domain must be carefully selected, especially for sensitivity studies of physical processes internal to the domain. In fact, the selection

of the domain is an important factor that determines another source of uncertainty: the internal variability.

Internal variability is one important contribution to the uncertainty in RCMs. This variability may be defined as the different solutions produced by the model by using the same set of lateral boundary conditions (von Storch, 2006). The chaotic and non-linear behaviour of the climate system gives rise to a dependence of the simulation on the initial state. Thus, small perturbations in the initial conditions of a given state can lead to different trajectories in the state space (Palmer, 2005). The magnitude of internal variability is mainly modulated and controlled by the strength of the lateral boundary forcing. In this sense, different circulation types give rise to different degrees of internal variability, depending on the strength of the flow of information through the boundary. For example, at mid-latitudes, a positive phase of North Atlantic Oscillation (NAO) is related to low internal variability, which is explained by a stronger westerly flow (Sieck, 2013). Many meteorological fields and their statistics are very sensitive to the distance of the lateral boundaries from the region of interest (Leduc and Laprise, 2009). Thus, small domain size induces a decreasing internal variability as the distance to the lateral boundaries is shorter and therefore, the control of the boundary forcing data within the domain is stronger (Alexandru et al, 2007).

RCMs are also sensitive to the horizontal resolution (e.g. Mass et al, 2002). This source of uncertainty is decisive in many mechanisms and variables. For example, in complex orography, when horizontal resolution is increased, a general improvement of spatial correlation between simulated and observed precipitation can be found (Güttler et al, 2015). Over the Arctic, higher resolutions affect large-scale circulations, as well as the surface temperature and precipitation, leading to a strong cooling of the eastern Arctic and increased synoptic activity (Girard and Bekcic, 2005). In the same study, implications were also found in aerosol concentrations over the areas where large-scale circulation and precipitation are affected, indicating that the impact of the resolution reaches any parameter and process. The degree of this impact depends on the variable. For example, the effects of increased horizontal resolution in precipitation vary with the model and the evaluated feature (Zikova et al, 2013). In a future climate context, higher resolution may impose regional improvements in the large-scale patterns of changes in mean temperature and precipitation (Jacob et al, 2014). Nevertheless, it should be noted that some of these studies consider a single model, which in itself constitutes another source of

uncertainty that need to be considered.

The analysis of modelling uncertainty is commonly addressed with multi-model ensembles, which provide greater consistency and reliability as compared with a single-model approach (Hagedorn et al, 2005). In addition to the multi-model uncertainty, the model physics provides a remarkable uncertainty attributed to the different parameterizations that are employed. In certain models, the availability of alternative parameterization schemes for a same process allows to use a multi-physics approach, with the advantage to perturb a single physical parameterization (micro-physics, convection, radiation, etc.) and to evaluate the contribution of a specific component to total uncertainty. Two different approaches are used to explore this uncertainty (García-Díez et al, 2013). One approach consists in studying the validity of the assumptions taken in the parameterization schemes and their accuracy to represent the reality (e.g. Shin and Hong, 2011). Here, the main goal is to detect misrepresentations and inaccuracies of the parameterizations that serve to improve them. On the other hand, other studies aim to select the most adequate scheme or combination of them, focusing on several variables. For the latter, the analysis of this uncertainty is commonly carried out by using multi-physics ensembles. The literature offers a wealth of studies dealing with multi-physics ensembles. For example, over the Iberian Peninsula, Fernández et al (2007) analyzed the sensitivity to different physical parameterizations of a set of high-resolution simulations. Although they obtained different impacts depending on the parameterization scheme, the multi-physics uncertainty was comparable to the observational uncertainty. Over the same region, Jerez et al (2013a) showed that the spread from a multi-physics ensemble can be of comparable magnitude to that from a multi-model ensemble. They focused on present-day climate, but multi-physics ensemble approach is also applied for climate change projections (Jerez et al, 2013b, among others). Although it focused only on the PBL scheme, García-Díez et al (2013) found that the best-performing scheme has a seasonal dependence in a set of multi-physics ensemble simulated with the Weather Research and Forecasting (WRF) model (Skamarock et al, 2008). In this sense, the WRF model is a common choice in evaluation studies of multi-physics uncertainty. Unlike other models, whose setup is fixed, WRF offers multiple physical parameterization options.

Multiple initiatives have explored these uncertainties under international frameworks with promising results. In 2001, The Third Assessment Report of the Intergovernmental Panel on Climate Change (IPCC) recom-

mended to coordinate RCM ensembles to explore multi-model and projection uncertainties (Giorgi et al, 2001). At that time, assessments of climate change impacts were based on coarse-resolution GCMs. Therefore, in Europe, during the period 2001-2004, the project Prediction of Regional scenarios and Uncertainties for Defining European Climate change risks and Effects (PRUDENCE) represented the first comprehensive, continental-scale intercomparison of high resolution climate models and their applications (Christensen and Christensen, 2007). High resolution climate change scenarios for Europe at the end of the twenty-first century were run in order to assess projections of future climate change at regional scales, as well as to explain their uncertainties. From 2004 to 2009, the project ENSEMBLES developed an ensemble prediction system for climate change, based on the state-of-the-art of the regional climate modeling in Europe. The initiative produced objective probabilistic estimates of uncertainty in future climate at the seasonal to decadal and longer timescales. Besides, ENSEMBLES gave special importance to relate the output of the ensemble prediction system with a wealth of risk assessment applications (Doblas-Reyes et al, 2009; Weisheimer et al, 2009). These projects focused on Europe, but similar initiatives emerged for other regions, as the North American Regional Climate Change Assessment Program (NARCAPP), which intended to investigate uncertainties in regional scale projections of future climate over North America. These initiatives paved the way for a worldwide coordination of downscaling activities.

1.5 CORDEX initiative

By the end of ENSEMBLES, climate change information used by the end-user and policy-making communities was based on AOGCMs (Busalacchi and Asrar, 2009). In spite of the increasing popularity of the RCMs, their use in climate change impact assessments was relatively limited (Giorgi et al, 2009). Besides, most of the experiments followed specific targeted interests, such as the study region, which in turn, led to a fragmentation of the results. This issue was overcome in 2009 with the "Coordinated Regional Downscaling Experiment" (CORDEX), the first initiative to coordinate all the worldwide efforts involving downscaling. This initiative, under the auspices of WCRP, represented an attempt to build a common experimental framework (Giorgi and Gutowski, 2015) with the following goals:

1. Understanding different phenomena occurring at regional- and local-scale.
2. Evaluating the performance of regional climate models, as well as downscaling techniques (both dynamical and statistical downscaling).
3. Producing a complete set of experiments of downscaled climate projections.
4. Fostering communication and exchange of knowledge with the RCM users.

Within the CORDEX initiative, it is worth mentioning EURO-CORDEX, the European branch of CORDEX. This voluntary effort aims to generate a multi-model ensemble of regional climate change projections over Europe, considering different future GHG concentrations scenarios and increasing resolutions. In this sense, the project makes use of the European domain already designed in the previous experiments PRUDENCE and ENSEMBLES. In parallel, although CORDEX is an unfunded initiative, several projects in Europe support its objectives. IMPACT2C (2011-2015) was one of the first multi-disciplinary international project contributing with their activities to CORDEX. Afterwards, the ongoing European Climate Prediction (EUCP) system and PRINCIPLES gave support. The former aims at developing a climate prediction system using high-resolution RCMs to be used in climate adaptation and mitigation measures (Hewitt and Lowe, 2018), while PRINCIPLES expects to generate a large ensemble of EURO-CORDEX simulations.

During the first phase of CORDEX, the downscaling activities were based on the GCMs participating in CMIP5 (Coupled Model Intercomparison Project 5; Taylor et al, 2012). These activities, along with the use of dynamical and statistical techniques, provided valuable climate information. The techniques, applications and the user community were very varied, which showed the need to properly understand the uncertainties and results as well as to assess the limitations and strengths of the different techniques. To address these goals, a two-fold protocol was designed for a set of 14 domains covering the most areas of the world at 50 km horizontal resolution. On the one hand, an evaluation experiment was run for the period 1989-2014 with simulations driven by ERA-Interim reanalysis (Dee et al, 2011). On the other hand, a second experiment was launched

for the period 1950-2100 under different GHG scenarios with simulations driven by CMIP5 models.

After the first phase of CORDEX, several issues needed attention. First, added value of the downscaling techniques did not always result in more valuable information for Vulnerability and Impact Assessment (VIA), which was important to justify the resource expenditure of running very expensive high-resolution models. Also, simulation of key variables and phenomena for VIA studies, such as precipitation and strong local-wind systems, needed a more accurate representation (Gutowski et al, 2016). These issues, among others, were addressed in the second phase of CORDEX.

The end of the first phase cleared the path for new challenges, opening key scientific questions as the increase of the horizontal resolution to convection-permitting scales. Therefore, the CORDEX initiative considered new Flagship Pilot Studies (FPS), that is, more targeted experimental setups in which each FPS is focused on a particular sub-continental region and scientific problem. Thus, a FPS is selected in terms of importance of fine-scale processes and availability of observations. They investigate different processes, feedbacks, forcings or the role of model configuration. The research was planned to run RCMs at scales down to convection-permitting, based on targeted specific experiments and focusing on regional-scale forcings, such as aerosols or land-use changes. Analysis and evaluation are carried out by using comprehensive observational datasets in combination with dynamical and statistical techniques. To date, 9 FPSs have been endorsed, two of which are a central part in this thesis: the FPS "Extreme precipitation events in Southeastern South America: a proposal for a better understanding and modeling" (FPS-SESA) and the FPS "Convective phenomena at high resolution over Europe and the Mediterranean" (FPS-Convection).

The improvement of the computational resources, the availability of observations covering extreme events and the increasing studies with convection-permitting models allowed the submission of the FPS-Convection in 2016. The FPS was based on the fact that convective processes play an important role as regards hydrological impacts, being a noticeable damaging phenomena (Coppola et al, 2020). Thus, knowing how these events respond under climate change conditions, key for VIA studies, is one of the challenges in the study. On the other hand, explicit representation of these processes at the convection-permitting scales presents an opportunity to assess whether these models lead to a clear

added value. Both scientific aims, along with hybrid approaches considering statistical downscaling, compose the main open-ended questions to be answered. Thus, the protocol set up three general aims:

1) To investigate convective-scale events, their processes and their changes over Europe and the Mediterranean.

2) To provide an assessment of the modeling capacity at convection-permitting scale.

3) To set a coherent assessment of the impact of the climate change in convective-processes at local- and regional-scale.

The consortium, composed by 27 research groups using 9 different RCMs, built a first-of-its-kind multi-model convection-permitting ensemble. The targeted area was defined over the Alps, due to the availability of observations and the relative high frequency of heavy precipitation events.

Considering also Europe, the FPS "Impact of land use changes on climate in Europe across spatial and temporal scales" (FPS-LUCAS) (Davin et al, 2020) attempts to evaluate robust biophysical impacts of land use changes in Europe. Due to the highly heterogeneous changes of land use distribution, FPS-LUCAS requires to solve future fine-scale processes and their interactions with the terrestrial biosphere and hydrosphere.

Following the approach from FPS-Convection, FPS-SESA aims at studying multi-scale processes and interactions resulting in heavy precipitation events in Southeastern South America (Bettolli et al, 2021). The region emerges as one of the most active regions concerning deep convection. The interaction between different large-scale features, such as the South America Low-level Jet, leads to a high occurrence of extreme precipitation events. Recent studies highlight the increase of the frequency and intensity of these events during the late 20th century. However, understanding the different interactions, mechanisms and factors involved in these processes is still challenging. FPS-SESA addresses these questions by using both dynamical and statistical techniques to explore the added value of regional climate downscaling as well as to strengthen the cooperation between dynamical and statistical approaches. In this context, FPS-SESA tries to foster inter-institutional cooperation, also including research communities from out of South America, especially those participating in FPS-Convection (e.g. Universidad de Cantabria). Similarly to FPS-Convection, the first phase consisted in evaluating the capability of convection-permitting models to simulate deep convection. Three heavy precipitation events occurred in 2009 were selected and simulated in two modes (a short- and a long-term run), at 20 km and 4 km horizontal res-

olutions. The main goals are to identify the processes leading to these events and their sensitivity to different model configurations, as well as to develop actionable climate information for the impact community.

Understanding convective processes and their impacts on the future climate are also the central question in the FPS "High resolution climate modelling with a focus on convection and associated precipitation over the Third Pole region" (FPS-CPTP). The Tibetan Plateau (so-called the Third Pole) contains the third largest volume of ice in the world, reason by which the research evaluates the relation between convection and cryosphere over Central and East Asia. As FPS-Convection and FPS-SESA, the study investigates the impact of the convective processes by means of CP RCMs.

Although the first CORDEX framework established a multi-domain approach, the proposal paid special attention to Africa due to its high vulnerability (Giorgi et al, 2009). Recently, three FPSs were endorsed corresponding to three African subregions: the Southeast Africa, the Lake Victoria Basin and the Western-Southern Africa. The former, dominated by the intertropical convergence zone, the tropical monsoon and the ENSO, is strongly affected by changes in rainfall. In this sense, the FPS "Modelling the Southeast African regional Climate" proposes to evaluate how precipitation over this region will evolve in the future. The Lake Victoria Basin is used to analyze the future intensity and occurrence of extreme events under the FPS "Climate Extremes in the Lake Victoria Basin" (FPS-ELVIC). The study aims at providing robust climate information as regards to climate extremes such as droughts, heavy precipitation or heat waves. These medium- to local-scale climate extreme events are expected to be better represented in CP RCMs. Thus, similarly to FPS-SESA, the main objective is to explore the added value of the convection-permitting RCMs against those with parameterized convection. Finally, interactions between land, atmosphere and ocean are dealt within the FPS "Coupled regional modelling of land-atmosphere-ocean interactions over western-southern Africa under climate change". The region is affected by biomass-burning aerosols, which are transported via stratocumulus cloud deck, influencing the climate over the Atlantic. Hence, the research gives especial importance to the role of the aerosols. This scientific aspect is shared with the FPS "Role of the natural and anthropogenic aerosols in the Mediterranean region: past climate variability and future climate sensitivity" (FPS-Aerosol). Aerosols play an important role in the Mediterranean, strongly affecting the atmospheric circulation,

radiation and cloud cover. The study uses high-resolution RCMs to analyze the role of Mediterranean aerosols on the regional climate variability, as well as its influence on extreme events. Over the same region, the FPS "Role of the air-sea coupling and small scale ocean processes on regional climate" investigates the mechanisms through which air-sea coupling can modify the regional climate. Here, the Mediterranean is selected due to its high complexity, containing a wealth of processes and interactions between air and sea.

In parallel to the FPSs, other activities arose. The fragmentation of high resolution downscaling research, with most of the efforts mainly centered over specific regions, led to the need of worldwide high resolution information about regional climate change and its impacts. In this sense, CORDEX designed the framework "CORDEX-COMMON Regional Experiment" (CORDEX-CORE Gutowski et al, 2016). This framework addresses the needs for a more homogeneous multi-model ensemble information, constituting a complementary framework of the original CORDEX experiment. The experiment is intended to provide an ensemble of high resolution simulations spanning major inhabited regions of the world to assess future extreme events and climate change impacts. The protocol establishes finer horizontal resolutions (about 25 km) than the original CORDEX standard resolution (about 50 km). Simulations include an evaluation run together with historical and future scenarios runs.

1.6 Thesis objectives

The main aim of this thesis is to contribute to the different dimensions of the CORDEX evaluation framework, from the production of state-of-the-art RCM simulations, to the international cooperation with different research groups, in order to assess and quantify the relative role of different uncertainty sources in regional climate downscaling. We pay special attention to heavy precipitation events, as represented by new-generation convection-permitting RCMs. A natural framework to carry out this study are the CORDEX Flagship Pilot Studies that coordinate the research activity on convective precipitation. The specific objectives can be formulated as follows:

- Simulate the regional climate of heavy precipitation areas at very high, convection-permitting resolution using a state-of-the-art RCM.

- Quantify the role of different uncertainty sources. Namely, horizontal resolution, domain uncertainty, internal variability, multi-physics and multi-model uncertainties.
- Explore the uncertainty associated to the initialization of variables with long response time, and their impact on the time slicing of costly RCM simulations.
- Improve the understanding of the mechanisms leading to heavy precipitation events.

For this purpose, the thesis has been carried out within the framework of the CORDEX FPS-Convection and FPS-SESA initiatives, which focus on the Alpine and southeastern South America regions, respectively. Their target domains provide different climate conditions and forcing mechanisms for heavy precipitation events. Also, their experimental design considers most of the uncertainties we aim to assess. This experimental design has been extended in this thesis to accommodate the assessment of internal variability and domain uncertainties.

1.7 Structure of the thesis

The thesis is structured to address the main objectives across different chapters. Chapter 2 summarizes the model simulation data sets generated as a result of the thesis work, along with other observational and model output data sets used. Chapters 3 to 5 present the main results of the thesis and roughly correspond to the studies [Lavin-Gullon et al \(2020\)](#), [Lavin-Gullon et al \(2021b\)](#) and [Lavin-Gullon et al \(2021a\)](#), respectively. Each of these chapters has its own ‘Data & Methods’ section with a selection of the data generated and used for that particular study, along with the particular analysis methodology. Different ‘Conclusions’ sections summarize the main outcomes at the end of each of these chapters. Finally, general conclusions are provided in Chapter 6, recollecting the main objectives.

For the simulation of the regional climate at very high resolution, we selected the WRF modelling system (Chapter 2). With this state-of-the-art RCM, we engaged with the FPS-Convection ([Coppola et al, 2020](#)) and FPS-SESA ([Bettolli et al, 2021](#)) initiatives, producing our simulations following internationally coordinated protocols. We contributed to all model evaluation experiments within these initiatives (Section 2.2.4),

extending our contribution to additionally explore RCM internal variability. The computationally-demanding task of performing multi-year, km-scale regional climate simulations led us to consider split simulations, by overlapping different time slice simulations (Chapter 4).

The overarching theme of the thesis is the quantification of regional climate modelling uncertainties, with an emphasis on internal variability as a background to assess the relative size of other sources of uncertainty. Internal variability is introduced in Chapter 3, along with the methodology used to measure it. In this Chapter, we also extend the internal variability metric to quantify multi-physics uncertainty. Internal variability plays also a leading role in Chapter 4, limiting the perfect match between overlapping time slice simulations. In Chapter 5, internal variability is also compared to multi-model uncertainty, and used to assess the robustness of the simulation of individual precipitation events.

Other sources of uncertainty are also considered. The sensitivity of the results to the horizontal resolution is assessed in Chapters 4 and 5. Horizontal grid spacings range from ~ 50 km to ~ 3 km. Domain uncertainty, i.e. the dependence of the results on the region of the globe, is considered by simulating over regions with different climatic conditions. Chapter 3 focuses on Europe, Chapter 5 on South America, and Chapter 4 considers both Europe and South America and discusses regional differences. Multi-physics uncertainty is quantified in Chapter 3, to assess the response of specific heavy precipitation events to the physical parameterizations in the light of the existing internal variability. Multi-model uncertainty is also considered in Chapter 5, which includes results from the RegCM4 model along with two configurations of the WRF model.

In addition to these uncertainties, the initialization and spin-up transient of the model is also studied. The ability of the model to represent heavy precipitation events with a ‘weather like’ initialization (few days before the event) or in ‘climate mode’ (one or several months in advance) was considered in [Lavin-Gullon et al \(2018\)](#) and in Chapters 3 and 5. Much longer spin-up periods are considered in Chapter 4, where the length of the initial transient of the model simulations is studied for different variables, resolutions, regions and seasons. The impact of this initial transient on the simulated climate is also evaluated in this Chapter, to consider the use of overlapping time slice simulations as a mean to perform costly long-term RCM simulations.

Finally, we evaluated the high-resolution, convection-permitting simulations produced in terms of their ability to represent heavy precipitation

over Europe (Ban et al, 2021) and southeastern South America (Lavin-Gullon et al, 2021a). Part of the latter study is included as Chapter 5, where we evaluate the multi-model ensemble of FPS-SESA in two different simulation modes and considering 20 and 4 km grid spacings. Apart from evaluating heavy precipitation events in the region against several observational databases, we explore the synoptic mechanisms leading to these events, identifying a key precursor.

Chapter 2

Data

This chapter presents a description of all the model simulations and datasets which have been generated and postprocessed accomplishing the first objective established in this thesis (Section 1.6). The Chapter also describes the reanalysis and observational datasets used, as well as other datasets in the standard CORDEX resolution that are part of this thesis. In addition, the chapter includes model simulations that while they are not part of the following content, they were generated during the development of this thesis. Nevertheless, it should be noted that all the datasets are detailed in the corresponding Data section of every chapter.

2.1 Observational data

Initial and lateral boundary conditions for the simulations used in this thesis were taken from the European Center for Medium Range Weather Forecasts (ECMWF) ERA-Interim reanalysis. The uncertainty in the reanalysis was taken into account by considering also the National Centers for Environmental Prediction reanalysis (Reanalysis-1) and the Japanese 55-year reanalysis (JRA55).

In this thesis, reanalysis was considered as a reference. Observational datasets are not relevant since we are mainly focus on quantifying the uncertainty, without exploring the error with respect an observation. Nevertheless, four different precipitation datasets were used. The high-resolution gridded E-OBS dataset (Haylock et al, 2008) was employed as observational reference in Europe. Observational uncertainty in South America was taken from the NOAA Climate Prediction Center morphing

method (CMORPH), the Precipitation Estimation from Remotely Sensed Information using Artificial Neural Networks (PERSIANN) and the Multi-Source Weighted-Ensemble Precipitation (MSWEP) datasets. A more detailed description of these datasets are found in Section 5.2.1.

2.2 Model simulations

2.2.1 Weather Research and forecasting model

The Weather Research and Forecasting (WRF) model (Skamarock et al, 2008) is a mesoscale numerical weather prediction model designed for both atmospheric research and operational forecasting applications. This is a nonhydrostatic model, whose main advantage is its modularity, that is, the possibility to combine its components and in turn, to design different model configuration setups. WRF offers two dynamical cores: the Advanced Research WRF (ARW-WRF) core maintained by the National Center for Atmospheric Research (NCAR) and the Nonhydrostatic Mesoscale Model (NMM) core, maintained by the National Centers for Environmental Prediction (NCEP). It also includes a software architecture supporting parallel computation. The model also supports two nesting strategies. On the one hand, one-way nesting, where there is no communication between each domain and its corresponding parent domain. On the other hand, two-way nesting, where domains simultaneously communicate with each other. Nevertheless, the most important feature refers to the wealth of parameterization schemes that can be chosen for different subgrid processes. Alternative parameterization schemes can be selected for microphysics, cumulus parameterization, both short-wave and long-wave radiation, PBL, land surface model, surface layer or shallow convection, among others. In addition, WRF allows to manage many other options not related to parameterizations, such as advection and diffusion parameters.

In this thesis, WRF is preminent since most of the simulations have been generated with this model. In this regards, all the simulations were carried out by using the ARW-WRF core with one-way nesting strategy.

2.2.2 Ensemble generation methods

Besides the multi-model ensembles coordinated under the frameworks of FPS-Convection and FPS-SESA, an additional coordination was given in the FPS-Convection, where the institutions participating and using

WRF generated a multi-physics ensemble (MPE) by setting different physical configurations so that at least one option differs among them (Table 2.1). The MPE considered different options varying the parameterization schemes for cloud micro-physics processes, surface and land processes, planetary boundary layer, and radiative processes. The other model configuration and experimental setup were fixed, including the model version (ARW-WRF v3.8.1). Also, a MPE was built in Experiment CCPS (see Table 2.1) by activating or not the shallow cumulus parameterization.

The role of internal variability is assessed by building a multi-initial conditions ensemble (MICE). The set of perturbed initial conditions was generated using the lagged method (see for example, Laux et al (2017)), that is, by starting the simulations the day before, 2 days before, and so on (r0, r1, r2... in Table 2.1). This is a simple way of perturbing the initial conditions while maintaining the physical consistency among variables.

2.2.3 Simulation modes

The protocols in FPS-Convection and FPS-SESA established a test to assess the ability of the models to simulate convection. The experiment consisted in simulating several extreme precipitation events in two modes: the so-called “weather-like” and “Climate-mode”. The former was a short-range simulation initialized one or a few days before the onset of each event, aiming at simulating the event as closely as possible to the reality, aided by the predictability provided by the initial conditions. Climate-mode simulations were started one or several months before the event following somehow the approach of climatic simulations. Thus, initial conditions were not a source of predictability and the models were mainly driven by the lateral boundary conditions, which is typical in regional climate modelling.

2.2.4 List of simulations produced in this thesis

In this section, we explain the framework of all the simulations generated in this thesis, whose details can be found in Table 2.1.

Experiment A consisted of a test to evaluate the capability of a multi-model ensemble to simulate three selected heavy precipitation events in “weather-like” and “climate mode”. The experiment was carried out in two different regions: southeastern South America and the Alps, as established in FPS-SESA and FPS-Convection, respectively. A particular

coordination was given in FPS-Convection, where all institutions using WRF coordinated a MPE by setting different physical configurations so that at least one option differs among them.

Experiment B consists of RCM evaluation simulations covering a 15-year period. All the WRF simulations started using the same initial conditions, with soil states generated by a 1-year spin-up run. It should be noted that the physical parameterizations for this experiment were slightly adjusted with respect to those used in experiment A of FPS-Convection, in order to consider more complex physics schemes and to avoid uncertainties from the interaction between distinct PBL and surface layer schemes. In this experiment, the highly computationally demanding 15-year simulation required to split the run into time slices (S1, S2, S3... in Table 2.1). This procedure gave the advantage of running in parallel and in turn, reducing computing time and computational resources.

Experiment CCPS is based on a previous work from Vergara-Temprado et al (2020), which showed that solving convection explicitly for resolutions finer than 25 km in a Consortium for Small-scale Modeling (COSMO) model ensemble can be beneficial. Thus, an ongoing experiment is planned to extend this study to a multi-model approach. The participating groups run an RCM ensemble to investigate biases when either using parameterizations of deep and shallow convection or deactivating them. We run the same physical configuration as Experiment B for the coarser domain (EUR-15), with cumulus parameterization deactivated. The initial soil states were generated previously by a 1-year of spin-up. An additional full-transient simulation, that is, without any split, was run with the same physical configuration as Experiment B, only for the coarser domain. In this experiment, libraries used by WRF were compiled with newer versions than those used in the *Experiment B*, aiming to run the simulation more efficiently.

2.2.5 Other simulations

MPEs generated under FPS-Convection were built with simulations from the participating groups using WRF. Similarly, multi-model ensembles in experiments under FPS-SESA were built with runs from the different participating models.

We used also simulations in the coarse EURO-CORDEX standard (EUR-44; Vautard et al, 2013) and South America CORDEX (SAM-44; Solman and Blázquez, 2019) domains were produced in the Santander

Framework	Exp	Domain	Mode	Realization	Period	
FPS-Conv.	A	EUR-11 (ALP-3)	WL-Case 1	r0	2012-10-23 - 2012-10-28	
			WL-Case 2	r0	2009-06-20 - 2009-06-27	
			WL-Case 3	r0	2014-11-02 - 2014-11-07	
			CM-Case 1	r0	2012-10-01 - 2012-11-01	
			CM-Case 2	r0	2009-06-01 - 2009-07-01	
				r0	2014-10-01 - 2014-11-07	
				r1	2014-09-30 - 2014-11-07	
			CM-Case 3	r2	2014-09-29 - 2014-11-07	
				r3	2014-09-28 - 2014-11-07	
				r4	2014-09-27 - 2014-11-07	
		r5	2014-09-26 - 2014-11-07			
			-	S1/r0	1999-01-01 - 2005-02-28	
			-	S2	2003-09-01 - 2006-05-31	
			-	S3	2005-06-01 - 2008-02-28	
			-	S4	2007-03-01 - 2009-12-31	
B	EUR-15 (ALP-3)		r1	1998-12-31 - 1999-12-31		
			r2	1998-12-30 - 1999-12-31		
			r3	1998-12-29 - 1999-12-31		
			r4	1998-12-28 - 1999-12-31		
			r5	1998-12-27 - 1999-12-31		
		CCPS	EUR-15*	-	Full-trans.	1999-01-01 - 2009-12-31
			EUR-15	-	Full-trans.	1999-01-01 - 2009-12-31
		FPS-SESA	A	CSAM-20 (SESA-4)	WL-Case 1	r0
WL-Case 2	r0				2010-01-17 - 2010-01-20	
WL-Case 3	r0				2009-11-20 - 2009-11-23	
	r0				2009-10-01 - 2010-04-01	
CM	r1				2009-09-30 - 2010-04-01	
	r2				2009-09-29 - 2010-04-01	

Table 2.1: List of simulations generated in this thesis. For each simulation, the table shows the experiment, FPS framework, domain, mode, realization and period of simulation. Realizations identified with “r” refer to runs generated for MICE, while realizations identified with “S” refer to time slices in split simulations. For the domain denoted with an asterisk (*), the cumulus parameterization was deactivated.

Meteorology Group. The former was driven by the ERA-Interim reanalysis, whereas the latter was driven by the Canadian Earth System Model (CanESM2), carried out for the historical run and for the future scenarios RCP 4.5 and RCP 8.5.

Chapter 3

Internal variability vs multi-physics uncertainty in a regional climate model

3.1 Introduction

The increasing resolution of Regional Climate Models (RCMs) has reached the so-called convection-permitting scale (Prein et al, 2015), by approaching resolutions of a few kilometers, typically used in Numerical Weather Prediction (NWP). A recent study by Coppola et al (2020) presented the largest multi-model ensemble of convection permitting RCMs to date, with an initial experiment exploring the ability of RCMs setup as NWP models and as regional climate modelling tools. Strong discrepancies between models were found in simulating three heavy precipitation events over the Alps. The explanation of these discrepancies was left open, and they speculated on three potential explanations: (1) the proximity of the event to the boundaries of the domain, (2) a failure in some RCMs to capture the response to the drivers of the event and (3) internal variability being responsible for the differences across models. This study is a follow up of Coppola et al (2020), where we investigate the role of internal variability in a selected event and we also further extend our analysis to a full annual cycle.

Internal, unforced climate variability is one of the main sources of uncertainty in global climate simulations (Hawkins and Sutton, 2009). Due to the non-linear and chaotic nature of the climate system, small perturba-

tions to a given state of the system grow and develop different trajectories in the state space (Palmer, 2005). In a relatively short period of time, two slightly perturbed simulations in which initial conditions are modified can differ as much as two randomly chosen states of the climate system (Kalnay, 2002). When considering coupled systems that exhibit modes of low-frequency variability, even mean states over long periods of time can differ considerably. This internal or natural variability of the system is commonly explored using ensembles of simulations started from perturbed initial conditions (Haughton et al, 2014). The uncertainty arising from internal variability is not negligible compared to other sources of uncertainty, such as GCM modelling or GHG-scenario uncertainty (Hawkins and Sutton, 2009; Deser et al, 2012; van Pelt et al, 2015; Kumar and Ganguly, 2018).

In contrast, internal variability emerging in regional climate models (RCMs) is usually smaller than that in GCMs (Caya and Biner, 2004). This uncertainty is also commonly assessed by using a multi-initial-conditions ensemble (MICE) in order to separate RCM internal variability from the signal of forced variability (Giorgi and Bi, 2000; Christensen et al, 2007; Caya and Biner, 2004; Lucas-Picher et al, 2008b; Giorgi, 2019; Bassett et al, 2020). Several studies concluded that at least 5-6 members should be considered to obtain robust estimates of internal variability (Lucas-Picher et al, 2008b; Laux et al, 2017). Recent studies (Bassett et al, 2020) point to the need of even larger ensembles. The amplification of perturbations in the initial conditions is damped somewhat by the continuous flow of information through the boundaries of the limited area domain. Lucas-Picher et al (2008a) quantified the relation between the RCM internal variability and the lateral boundary forcing over the domain. In mid-latitudes, internal variability has a seasonal behaviour with higher (lower) values in summer (winter), when the boundary forcing (e.g. storm track intensity) is weaker (stronger) and the model is more (less) free to develop its own circulation (Caya and Biner, 2004; Lucas-Picher et al, 2008b).

According to the general atmospheric circulation, prevalent winds (e.g. westerlies in mid-latitudes) force a flow of information through the boundary. As a result, this forcing imposes a typical pattern that exhibits increasing internal variability as one travels downwind across the domain. Flow perturbations develop and grow as they travel through the RCM domain, reaching a maximum near the downwind boundary where they are forced back to the flow of the GCM in the relaxation zone (Lucas-Picher

et al, 2008b).

Despite its relevance, few studies have addressed other RCM uncertainties in the light of internal variability. Regarding multi-model uncertainty, Sanchez-Gomez et al (2009) explored the impact of internal variability for four different weather regimes, which showed different sensitivity depending on the lateral boundary conditions. The fraction of multi-model uncertainty in RCMs that can be explained by internal variability can be relatively large. For example, Gu et al (2018) suggest that it could be up to 70% of the total uncertainty for the precipitation in Asia. Also, Fathalli et al (2019) reported that internal variability was comparable to the inter-model precipitation spread in Tunisia during summertime, when the lateral forcing constraint is reduced. As for GCMs, the magnitude of RCM internal variability depends on the synoptic circulation, model configuration, region and season (Giorgi and Bi, 2000; Alexandru et al, 2007).

The relevance of RCM internal variability is also recognized by the Coordinated Regional climate Downscaling Experiment (CORDEX; Giorgi and Gutowski, 2015), an international ongoing initiative endorsed by the World Climate Research Program which coordinates the regional climate downscaling community. Under this framework, multiple institutions are producing and analysing the largest regional multi-model ensemble in history, covering all populated areas in the world with a standard set of continental-scale domains.

Multi-RCM ensembles sample the dynamical downscaling methodological uncertainty. As such, it is challenging to discern the contributions to uncertainty from other sources (e.g. physical process parameterizations, internal variability). This is because RCMs developed by different groups differ in so many aspects that the results from different models and members cannot be used to understand the processes responsible for the spread. There have been different attempts to decompose multi-model uncertainty into other sources of uncertainty that can be more systematically explored. Perturbed-Physics Ensembles (PPE; Yang and Arritt, 2002; Bellprat et al, 2012) consider a given RCM and explore the uncertainty associated to selected parameters, by sweeping a range of acceptable parameter values. This approach allows to link the resulting uncertainty to a specific parameter. Multi-physics ensembles (MPE; see e.g. García-Díez et al, 2015) provide a way to link modelling uncertainties to specific processes. These ensembles are generated using a single RCM by switching between different alternative physical parameterizations, which are the

model components representing sub-grid-scale processes such as cloud microphysics, radiation, turbulence, etc. Physical parameterization are one of the key differences between different RCMs and, therefore, MPEs mimic multi-model ensembles with the advantage of a fixed dynamical core and the rest of non-sampled physics schemes. Of course, these fixed components also limit model diversity and, therefore, MPEs cannot replace multi-model ensembles. Quite a few analyses tested the ability of different MPEs to encompass the regional climate in different areas (Fernández et al, 2007; Evans et al, 2012; Solman and Pessacg, 2012; Jerez et al, 2013b; García-Díez et al, 2015; Katragkou et al, 2015; Stegehuis et al, 2015; Devanand et al, 2018). Some of these analyses mentioned internal variability as potential source of background noise that impacts the sensitivity to the physical parameterization schemes (Tourpali and Zanis, 2013; Stegehuis et al, 2015), though internal variability was not formally investigated.

Few studies consider both physics sensitivity and internal variability. For instance, Laux et al (2017) explicitly aim to separate the effects of internal variability from those of changes in land-use, suggesting that internal variability has a significant impact on precipitation. Crétat and Pohl (2012) also studied the effect of physical parameterizations on internal variability and questioned the robustness of previous physics sensitivity studies which did not take into account internal variability.

The Flagship Pilot Study on Convective phenomena at high resolution over Europe and the Mediterranean (FPS-Convection) is an ongoing initiative endorsed by CORDEX. This initiative aims at studying convective processes with CPM over the Alpine region (Coppola et al, 2020) by producing both multi-model and multi-physics ensembles of RCM simulations. The initial results showed large discrepancies between individual ensemble members in their representation of selected heavy precipitation events. In this work, we take advantage of the ensembles produced in the FPS-Convection to follow up the study of Coppola et al (2020), in which the origin of these discrepancies was determined out of the scope. Since causation is difficult to address in a multi-model approach, we focus on the multi-physics ensemble within the FPS-Convection RCMs that serve to drive the CPM. We quantitatively compare the signal arising from the use of different model components (physical parameterizations) against that associated to the background noise referred to internal variability at different time scales. The objective is twofold: (1) to assess whether modelling discrepancies in Coppola et al (2020) fall within the range of internal variability and (2) to quantify how much uncertainty in a multi-physics

ensemble can be explained by internal variability.

The paper is structured as follows: The methodology and data used in this work are detailed in Section 3.2. Section 3.3 presents and discusses the results. First, applied to a case study presented in Coppola et al. (2020) and, second, we extend the study to consider the role and relative magnitude of internal variability with respect to multi-physics uncertainty over an annual cycle. Finally, the conclusions are summarized in Section 3.4.

3.2 Data & methods

3.2.1 Multi-physics ensemble

In this work, we explore the uncertainty associated to physical parameterizations by using multi-physics ensembles (MPE, hereafter) generated in the context of the FPS-Convection. This initiative considers multiple RCMs, but here we will focus only on the sub-ensemble of simulations using the Weather Research and Forecasting (WRF) model (Skamarock et al, 2008). This modelling system provides the ability to switch among different physical parameterization schemes for a given sub-grid-scale process. Additionally, WRF allows for online telescopic nesting, running several nested domains simultaneously and exchanging information across domains at each time step. This approach gives rise to much smaller artifacts close to the borders of the inner domains, as compared to the standard procedure of running the model offline, nested into the output of a coarser resolution domain.

All institutions participating in FPS-Convection and using WRF have coordinated a MPE by setting different physical configurations so that at least one option differs among them (Table 3.1). The MPE considers different options varying the parameterization schemes for cloud microphysics processes, surface and land processes, planetary boundary layer, and radiative processes. All other model configuration and experimental setup are fixed, including the model version (ARW-WRF v3.8.1).

All FPS-Convection WRF simulations consider a high-resolution (~ 3 km), convection-permitting domain centered over the Alpine region (ALP-3) nested into a coarser-resolution (~ 12 km), and much larger, pan-European domain. Except for the deep convection parameterization scheme, that is switched off in ALP-3, physical configuration does not differ between both domains. All WRF ensemble members used one-way nesting, so there is no communication from the convection-permitting back

Exp	Id.	Institution	MP	PBL	LSM	ShC
A	AB	Forschungszentrum Jülich (FZJ-IBG3), Germany	Thomp.	YSU	NOAH	GRIMS
	AC	National Observatory of Athens (NOA), Greece	Thomp.	MYNN2	NOAH	GRIMS
	AD	University of Hohenheim (UHOH), Germany	Thomp.	MYNN2*	NOAH-MP	GRIMS
	AE	Intitute Pierre Simon Laplace (IPSL), France	Thomp.	MYNN2	NOAH-MP	UW
	AF	Bjerknes Centre for Climate Research (BCCR), Norway	Thomp.	YSU	NOAH-MP	GRIMS
	AG	Aristotle University of Thessaloniki (AUTH), Greece	WDM6	YSU	NOAH	GRIMS
	AH	Instituto Dom Luiz (IDL), Portugal	WDM6	MYNN2	NOAH	GRIMS
	AI	Universidad de Cantabria (UCAN), Spain	WDM6	MYNN2*	NOAH-MP	GRIMS
	B	BB	Forschungszentrum Jülich (FZJ-IBG3), Germany	Th-AA	YSU	NOAH
BC		National Observatory of Athens (NOA), Greece	Thomp.	MYNN2	NOAH	GRIMS
BD		University of Hohenheim (UHOH), Germany	Th-AA	MYNN2	NOAH-MP	GRIMS
BE		Intitute Pierre Simon Laplace (IPSL), France	Th-AA	MYNN2	NOAH-MP	UW
BF		Bjerknes Centre for Climate Research (BCCR), Norway	Thomp.	YSU	NOAH-MP	GRIMS
BG		Aristotle University of Thessaloniki (AUTH), Greece	WDM6	YSU	NOAH-MP	GRIMS
BH		Instituto Dom Luiz (IDL), Portugal	WDM6	MYNN2	NOAH	GRIMS
BI		Universidad de Cantabria (UCAN), Spain	WDM6	MYNN2	NOAH-MP	GRIMS

Table 3.1: WRF multi-physics configurations considered in this study (see Section 3.2.1) for experiment A (one-month simulation, EUR-11 domain) and experiment B (one-year simulation, EUR-15). For each ensemble member, the table shows an Id. code, the institution performing the simulation and the physical parameterizations used. The ensembles explore the use of different schemes for micro-physics (MP), planetary boundary layer and surface layer (PBL), land surface (LSM), and shallow convection (ShC) processes. The PBL schemes denoted with asterisk (*) used a different surface layer scheme despite sharing the MYNN2 PBL. See Table 3.2 for details of each parameterization scheme.

Acronym	Physical scheme
Thomp.	Thompson et al (2008) scheme with ice, snow and graupel processes suitable for high-resolution simulations
Th-AA	New Thompson aerosol-aware scheme considering water- and ice-friendly aerosols
WDM6	WRF Double-Moment 6-class microphysics scheme with cloud condensation nuclei for warm processes
YSU	Yonsei University non-local closure PBL scheme with revised MM5 Monin-Obukhov surface layer
MYNN2	Mellor-Yamada Nakanishi and Niino Level 2.5 (*combined with revised MM5 Monin-Obukhov surface layer)
NOAH	Noah LSM with multilayer soil temperature and moisture, snow cover and frozen soil physics
NOAH-MP	Noah LSM-Multi Physics. NOAH with multiple options for land-atmosphere processes
GRIMS	Shallow cumulus scheme from the Global/Regional Integrated Modeling System
UW	University of Washington shallow cumulus scheme from the Community Earth System Model

Table 3.2: Physical schemes used in the multi-physics experiments shown in Table 3.1.

to the coarser domain. Therefore, the convection-permitting inner domain did not alter in any way the results for the pan-European domain used in this work. Our analyses focus only on this pan-European domain, since we are interested in the uncertainty of the synoptic conditions over Europe, which drive the needed moisture that leads to unstable conditions over the Alpine area (see Section 3.3.1). The ALP-3 domain is not large enough to alter significantly the large-scale synoptic conditions, so, in order to reproduce the case studies of Coppola et al (2020) in the ALP-3 domain, the right sequence of observed events should be preserved first in the pan-European domain forcing simulations.

We use WRF data from two different FPS-Convection experiments driven by 6-hourly initial and lateral boundary conditions taken from the ERA-Interim Reanalysis (Dee et al, 2011):

Experiment A is described in Coppola et al (2020) and consisted of a preliminary test with all participating models, including WRF. Three heavy precipitation events in the Alpine region were simulated in two modes, identified as “weather-like” and “climate mode”. Weather-like simulations were started one day before the onset of the events, aiming at simulating the event as closely as possible to the reality, aided by the

predictability provided by the initial conditions. As the proximity of the initial conditions constrains the internal variability, we did not consider weather-like simulations in this study. Climate-mode simulations were started one month before the event, so that initial conditions were not a source of predictability in this case and the models were mainly driven by the lateral boundary conditions, which is typical in regional climate modeling. We focus on a single event that occurred around the 23rd June, 2009, and was covered by climate-mode simulations running for the period from 1st June to 1st July, 2009 (see Section 3.3.1). WRF members of the ensemble showed the largest differences in terms of predictability of this particular event. WRF simulations for this experiment used a pan-European domain at $0.11^\circ \times 0.11^\circ$ horizontal resolution (EUR-11), corresponding to the official EURO-CORDEX domain setup.

Experiment B consists of RCM evaluation simulations covering a 15-year period starting in 1999. All the WRF simulations started using the same initial conditions, with soil states generated by a 1-year spin-up run (1998). As in experiment A, the WRF model contributed with a MPE. However, the physical parameterizations for this experiment were slightly adjusted with respect to those used in experiment A (see Table 3.1) in order to consider more complex physics schemes and to avoid uncertainties from the interaction between distinct PBL and surface layer schemes. It should be noted that WRF simulations for this experiment used a slightly coarser ~ 15 km horizontal resolution (EUR-15) than those in Experiment A, covering the same domain. This change was motivated to comply with the recommended odd nesting ratios for telescopic domains (5:1 in this case, from EUR-15 to ALP-3), which avoids interpolation between the staggered Arakawa-C grids used. In this way, fluxes across nested domains are more accurate and computationally efficient. In this study we used the first year (1999) of these simulations.

3.2.2 Multi-initial-conditions ensemble

A MICE was run to assess the role of internal variability in explaining the uncertainty developed by the MPE. We used WRF configurations AI and BI (see Table 3.1) to match the setup of experiments A and B, respectively, using a set of 6 different initial conditions. The set of perturbed initial conditions was generated using the lagged method (see e.g. Laux et al, 2017), i.e. by starting the simulations the day before (AI-r1), 2 days

before (AI-r2), and so on, up to a 5-day lag (AI-r5). This is a simple way of perturbing the initial conditions while maintaining the physical consistency among variables. The extra simulated days are excluded, and we analyze only the period common to the MPE. The standard, no-lag runs AI and BI (say, AI-r0 and BI-r0) are part of both the 8-member MPE and this 6-member MICE.

We ran the 1-year MICE corresponding to experiment B (BI-r1 to BI-r5) only for the EUR-15 domain, without the inner ALP-3 nesting, so as to significantly reduce computational demands. Since no feedback from ALP-3 back to EUR-15 was allowed in the MPE, our EUR-15 MICE is fully comparable to EUR-15 MPE.

3.2.3 Quantification of uncertainty

In order to quantify the uncertainty (spread) in the two ensembles, we followed the approach of [Lucas-Picher et al \(2008b\)](#), who used an unbiased estimator of the inter-member variance:

$$\sigma_X^2(s, t) = \frac{1}{M-1} \sum_{m=1}^M (X(s, t, m) - \langle X \rangle(s, t))^2 \quad (3.1)$$

where $X(s, t, m)$ is the value of a given variable X at position s (summarizing, in this case, typical bi-dimensional position indices i, j), at time step t and from ensemble member m . M is the total number of ensemble members. The term $\langle X \rangle(s, t)$ is the ensemble mean at a given position s and time t :

$$\langle X \rangle(s, t) = \frac{1}{M} \sum_{m=1}^M X(s, t, m). \quad (3.2)$$

To avoid confusion, we keep in this methodological summary the notation of [Lucas-Picher et al \(2008b\)](#) and earlier publications on internal variability, although the use of Greek letters (σ^2) to refer to a sample variance estimator is uncommon, and usually reserved for the population parameters to be estimated ([Wilks, 2011](#)). Note that even though this measure was proposed to quantify internal variability, it is just a measure of spread or uncertainty, that can be applied to any ensemble. This is typically employed to quantify internal variability on MICE. In this work, we apply it to both MPE and MICE.

The uncertainty, as represented by Eq. 3.1, is a spatio-temporal field. The evolution of uncertainty in time (UT) is calculated by considering the spatial average of the inter-member variance σ_X^2 as

$$UT^2 \equiv \overline{\sigma_X^2}^s(t) = \frac{1}{S} \sum_{s=1}^S \sigma_X^2(s, t) \quad (3.3)$$

where S is the total number of grid cells in the domain. UT^2 represents the domain average of the inter-member variance. To emphasize the quadratic nature of this uncertainty measure, we use the symbol UT^2 in Eq. 3.3 but, in the following, we consider always its square root UT , which has the units of the variable, and allows for an easier interpretation. In the same way, a spatial distribution of the uncertainty (US) is obtained by considering the time average of the inter-member variance σ_X^2 as

$$US^2 \equiv \overline{\sigma_X^2}^t(s) = \frac{1}{T} \sum_{t=1}^T \sigma_X^2(s, t) \quad (3.4)$$

where T is the total number of time steps in the period. This expression is an estimate of the expected value of the inter-member variance over a period of interest.

We consider transient eddy variability (TEV) as a reference for inter-member variability. Passing weather systems create a natural time variability in meteorological fields, which sets a limit to the maximum variability attainable at a given location. This variability is seasonally dependent, so [Caya and Biner \(2004\)](#) proposed to use a monthly estimator and compute a spatial average to make it comparable to UT :

$$TEV^2 \equiv \hat{\sigma}_X^2(\tau, m) = \frac{1}{S} \sum_{s=1}^S \overline{(X(s, t, m) - \bar{X}^\tau(s, m))^{2\tau}} \quad (3.5)$$

where the $\overline{\quad}^\tau$ operator computes the monthly average, i.e. the mean for all time steps t corresponding to a given month τ . Again, the σ -notation is from previous literature but, in the following, we will simply refer to this monthly-averaged, transient-eddy variance as TEV . Note that TEV depends on the model and also suffers from sampling uncertainty, which will be quantified by computing it from different ensemble members.

Finally, the long-term impact (LTI) of the inter-member uncertainty on the climatology of a meteorological field is estimated by calculating the variance of the climate among ensemble members as

$$LTI^2 \equiv \sigma_{\bar{X}}^2(s) = \frac{1}{M-1} \sum_{m=1}^M \left(\bar{X}^t(s, m) - \langle \bar{X}^t \rangle(s) \right)^2 \quad (3.6)$$

where $\bar{X}^t(s, m)$ is the time average (i.e. the climatology) of each ensemble member m and $\langle \bar{X}^t \rangle(s)$ is the ensemble mean of the climatologies. Note that LTI measures the "uncertainty" of climate, while US measures the "climate" of the uncertainty. The latter is sensitive to the correspondence of meteorological events (e.g. heavy precipitation convective events) in time and space, while the former measures systematic deviations among members that lead to a different mean state (climate).

3.3 Results & discussion

3.3.1 Event reproducibility

As an example, we focus first on a heavy precipitation case study analyzed by Coppola et al (2020). The event was mostly driven by large-scale features, which consisted of a cut-off low over the Balkans inducing a persistent northeasterly flow over Austria. This unstable flow was warm and wet enough to trigger extreme precipitation by orographic lifting upon reaching the Alps. Observations reveal precipitation peaking on the 23rd June, 2009, over Austria. RCM simulations consistently reproduced this heavy precipitation event under weather-like initialization (see Section 3.2.1), but Coppola et al (2020) reported mixed results when considering the climate-mode initialization. Some members of the multi-model/multi-physics ensemble completely missed the precipitation event or represent highly damped versions of it (see Figure 4 of Coppola et al (2020)). They speculated on a potentially weak background synoptic forcing for this event, which we investigate in this work.

Notably, the WRF MPE alone also exhibited mixed results in reproducing the event. For illustration, Figure 3.1 (left) shows the accumulated precipitation on 23rd June for 4 WRF configurations. Only WRF configuration AF is able to reproduce the event, with extended precipitation over Austria. Other WRF configurations (AB, AE, AD) miss the event and show some precipitation over southern Italy or very scarce precipitation (configurations AC, AG, AI, not shown in Figure 3.1).

The synoptic situation, as represented by the 850hPa geopotential height (Figure 3.1, right), shows the cut-off low located as observed (ERA-

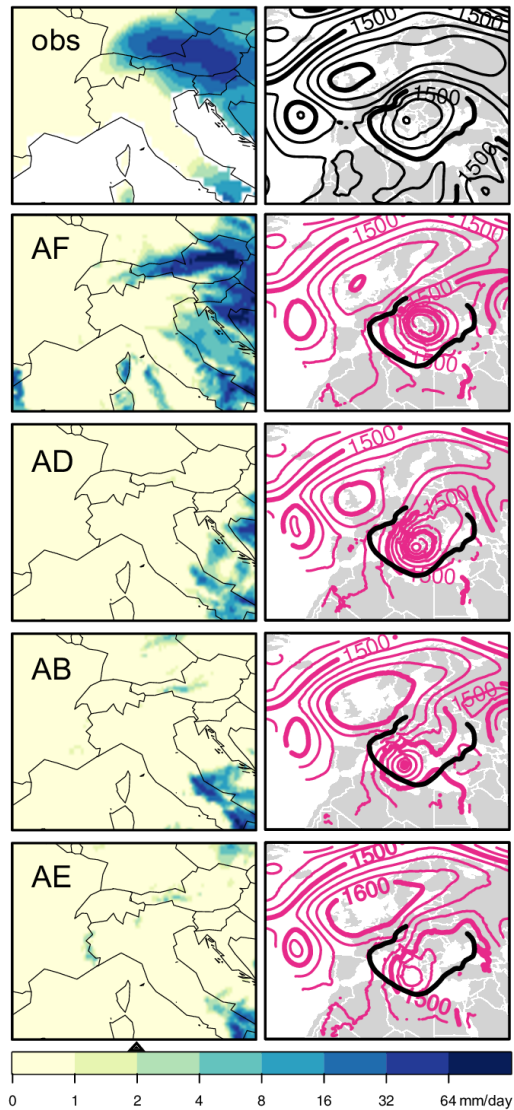


Figure 3.1: Left: Accumulated precipitation (mm) on June, 23rd 2009 according to E-OBS (Haylock et al (2008); top) and as simulated in the ALP-3 domain by experiment A for WRF MPE members AF, AD, AB and AE. Right: 850hPa geopotential height (m) according to ERA-Interim (top) and the corresponding MPE ensemble members in the EUR-11 domain in pink. An ERA-Interim 1500m-isoline (the same in all panels) is represented for reference in black.

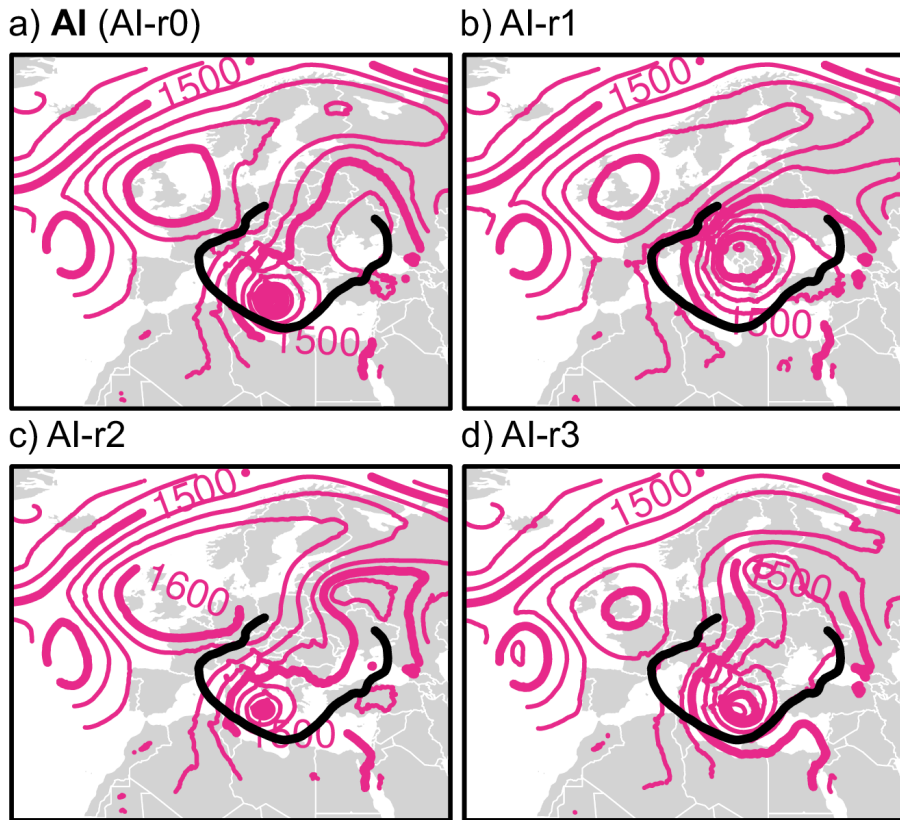


Figure 3.2: As Figure 3.1 (right), but for 4 MICE members: AI-r0 to AI-r3.

Interim) over the Balkans for the AF configuration. For the rest of the MPE members, a low-pressure system is simulated in southern Italy, which alters the circulation so that the warm-moist airflow over the Alps is strongly reduced and precipitation is eventually not occurring or occurring over other areas (southern Italy).

Given that MPE members differ only in their physical parameterization schemes, one might be tempted to assume that configuration AF outperforms the rest. That would imply e.g. that the use of the YSU non-local boundary layer scheme somehow helps in developing the cut-off low at the right location, as opposite to the MYNN2 local mixing scheme. This is the only difference between configurations AF and AD. Moreover, YSU alone cannot explain the ability of AF to represent the event, be-

cause configuration AB also used this PBL scheme. The only difference between configurations AF and AB is the land surface model (LSM). AF used Noah-MP, a much extended version (Niu et al, 2011) of the Noah LSM (used in AB), considering a multi-layer snow model with more realistic snow physics, canopy shadows, snow on canopy, an aquifer layer, and many other improvements. Other configurations used Noah-MP (AD, AE or AI), though, and the low pressure system and precipitation still did not occur on the right place. Therefore, either the exact parameterization combination of configuration AF is the key or there must be a different explanation for the discrepancies.

Note that WRF was run using one-way, online telescopic nesting and, therefore, we can also rule out the proximity of the high precipitation event to the ALP-3 domain boundaries as potential cause for the different model results in Coppola et al (2020). Boundary artifacts close to the inner boundaries are greatly reduced in this setup and still some WRF members reproduced the event while others missed it.

An alternative hypothesis is that the different development of the event in the different MPE members is just the result of internal variability. To test this hypothesis, we considered a MICE based on configuration AI, which did not develop the event under the standard MPE initialization setup (start date: 00UTC, 1st June, 2009). Configuration AI (AI-r0) developed a low over southern Italy (Figure 3.2a), as many of the other configurations (Figure 3.1). Many of the MICE members also developed a low over this area (see e.g. Figure 3.2), but member AI-r1 (start date: 00UTC, 31st May, 2009) presents a low in the right place, when compared against ERA-Interim. This was achieved by perturbing the initial conditions, starting the simulation one day earlier, and preserving exactly the same model configuration. Note that this is not a matter of improved initial conditions, since there are more than 20 days simulated from the geopotential height fields shown in Figures 3.1 (right) and 3.2, well beyond the limit of deterministic predictability of an atmospheric state. This is the result of internal variability. The slight perturbations in the initial conditions grew up by the non-linear dynamical model. This process is in competition with the constraints imposed by the lateral boundary conditions, which bring the flow towards that of ERA-Interim close to border of the domain. This constraint can be seen in Figures 3.1 (right) and 3.2.

In this particular flow state, there seem to be two preferred weather regimes over the southern Mediterranean area or, at least, our model simulations were only able to generate these two weather regimes: one with a

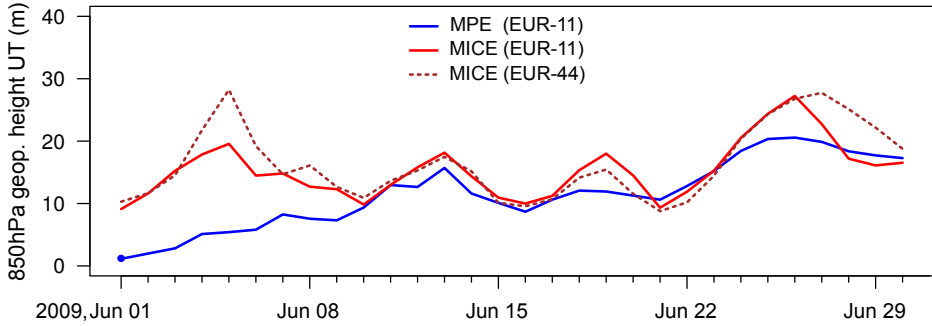


Figure 3.3: Inter-member variance in time (Equation 3.3) for 850hPa geopotential height (m) in EUR-11 domain of experiment A (June 2009). The spread is computed separately for MPE (blue) and MICE (red). The latter was computed both at 0.11° and 0.44° horizontal resolution with similar number of ensemble members.

low evolving over southern Italy and the other with the low positioned over the Balkans. The observed flow took the Balkan low path even though the model has difficulties to reproduce this path. Note that these weather regimes and their probability of occurrence are likely model dependent. In any case, this is just one particular event. Once we have shown that internal variability can trigger flow deviations similar to those from different physical parameterizations, we focus on quantifying their relative uncertainty, i.e. the spread of MPE and MICE ensembles.

The evolution of inter-member variance in time for MPE and MICE (Figure 3.3) can reach comparable values. MPE member simulations take exactly the same initial and lateral boundary conditions from ERA-Interim, hence the uncertainty (essentially the member-to-member variability) at the start is very small (close to zero during the first day), indicating that all members produce similar circulation patterns. As the different physical parameterizations have an effect on the model, each member simulated a different synoptic situation and the uncertainty increases. Regarding the MICE, since its members were initialized before the MPE start date shown in Figure 3.3, the spread among members is larger than in the MPE in the beginning of June. MICE uncertainty (i.e. internal variability) remains fairly stable along the 1-month time span of the simulation. After about 10 days, the magnitude of MPE and MICE inter-member variance are comparable, with internal variability (MICE

spread) generally larger than MPE spread. This suggests that the different physical parameterizations used in the MPE introduce smaller differences among members than those arising from internal variability.

A qualitative look at the UT evolution (Figure 3.3) shows that, even if uncertainty remains quite stable, there are periods of increased uncertainty that seem to be synchronous in both ensembles. These must be periods of either weaker lateral boundary forcing (the only external forcing) or increased internal variability due to a particular situation of the internal dynamics. Notably, the period 22-26 June, when the heavy precipitation event occurred over Austria, is a period of increased uncertainty, where internal variability surpasses MPE spread. Also, MPE spread seems to develop a linear trend along the 1-month period. If sustained, this trend would overcome internal variability in longer periods. Unfortunately, FPS-Convection experiment A only considered 1-month-long simulations. In order to explore MPE vs. MICE uncertainty over a longer period, we use the output from FPS-Convection experiment B in the next section.

Experiment B produced a MPE with slightly different model configurations (Table 3.1) and also on a slightly coarser domain (EUR-15). In order to discard a sensitivity to this coarser resolution, we simulated a new MICE using AI configuration but on a much coarser $0.44^\circ \times 0.44^\circ$ horizontal resolution (EUR-44). Its spread (dashed line on Figure 3.3) is very similar to that of EUR-11, which suggests that a major part of the uncertainty is due to the large-scale synoptic pattern and not to smaller scale variability.

3.3.2 Analysis over an annual cycle

We extended the analysis to an one-year period taking advantage of FPS-Convection experiment B (Section 3.2.1). In particular, we extended Figure 3.3 to one year using the year 1999 from the WRF MPE of experiment B and a MICE based on configuration BI. The resulting inter-member variance in time (Figure 3.4) shows a very similar behaviour of MPE spread and internal variability (MICE spread) along the whole year. MPE members started again from the same initial conditions. Therefore, they show very low differences on January 1st, which increases after about 10 days. After this 10-day transient evolution affected by the initial conditions, both ensembles show comparable inter-member variance, exhibiting an annual cycle with increased uncertainty in summer. Moreover, even weekly to monthly variability in these UT time series seems to match in both

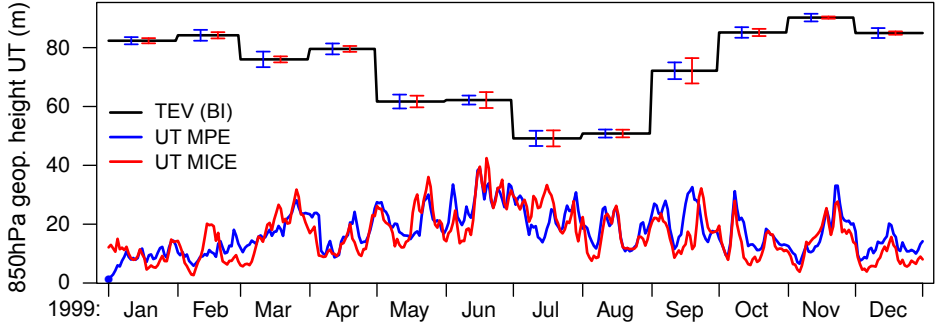


Figure 3.4: Inter-member variance in time (UT) for 850hPa geopotential height (m) in EUR-15 domain of experiment B (year 1999). The uncertainty is computed separately for MPE (blue) and MICE (red). Transient-eddy variability (Equation 3.5, black line) was computed from BI configuration and error bars show its standard deviation for MPE and MICE.

ensembles. Notably in the last months (Oct-Dec), and also in many other peaks along the year. This suggests that the differences introduced by the different physics formulations along the time are amplified by the model in a similar way than the perturbations of the initial conditions. No systematic effect is noticeable in the circulation. Put in another way, for this variable at least, multi-physics uncertainty can be fully explained by internal variability.

As in previous studies (Caya and Biner, 2004; Lucas-Picher et al, 2008b), we used transient-eddy variability (Equation 3.5) as a reference for uncertainty. This is the natural variability of a meteorological field associated to weather systems traveling along the storm track. TEV can be computed from any of the ensemble members. We used simulation BI (top line in Figure 3.4), which is the only member common to both MPE and MICE. To evaluate the uncertainty associated to the selection of this particular member, we computed the monthly TEV from each member, and its standard deviation for each ensemble and for each month is shown as error bars in Figure 3.4. TEV spread is very low and any member could have been used as the reference. As already found in previous studies in mid-latitudes, TEV is larger in winter than in summer, due to the more frequent passage of weather systems from the Atlantic. The faster atmospheric circulation in winter imposes a strong boundary forcing, which may explain the lower spread among ensemble members. TEV and the as-

sociated boundary forcing is lower during summer. As a result, the model has more freedom to develop its own circulation features, increasing the spread between the members. During summer, the spread reaches approximately half of the TEV, which would be the maximum attainable. This maximum is what one would expect from a GCM, which has no lateral boundary constraints. For such a model, MICE spread (i.e. internal variability) would increase during 1-2 weeks to reach the TEV line and remain around this limit along the year. In this sense, RCM internal variability is negligible compared to GCM internal variability during winter, but it represents an important fraction (approximately one half, in this example) during summer.

The similarity between MPE and MICE uncertainty is not restricted to domain averages. In Figure 3.5, we show the spread in space, by averaging inter-member variance in time for each model grid point (Equation 3.4). Both maps show a typical spatial distribution of internal variability in mid-latitudes, with increasing variability from the southwestern to the northeastern part of the domain. The patterns are remarkably similar, with MPE inter-member variance (Figure 3.5a) only slightly larger than internal variability (Figure 3.5b). Both reach about 35 m over the Baltic Sea and a steeper gradient towards the outflow (eastern) boundary than in the inflow (western) one. The westerly input flow is slowly modified by the RCM as it travels along the domain, but it is suddenly modified at the outflow boundary to match again the ERA-Interim flow at the eastern border. Christensen et al (2007) suggested that, for a domain over Europe, the lower uncertainty in south-western Europe is also due to the fact that the area is mainly sea, and not only due to the distance to the boundaries. Seasonal winter (DJF) and summer (JJA) patterns of MPE and MICE inter-member variance (not shown) are very similar to those in Figure 3.5. They show higher (lower) intensity in JJA (DJF), reaching 45 m (25 m) over the Baltic Sea.

The systematic effects of the physical parameterizations on the circulation can be seen in the long-term impact (Figure 3.6a). LTI summarizes the variability of the climatology for the different ensemble members (Equation 3.6). Note that this variability is about one order of magnitude smaller than the uncertainty measures shown previously (cf. the scales of Figures 3.5 and 3.6). Nevertheless, LTI has an impact on the simulated climate, while the (time) mean inter-member variance explored previously is mainly due to a lack of correlation (Caya and Biner, 2004). The largest differences among the simulations using different parameterizations occur

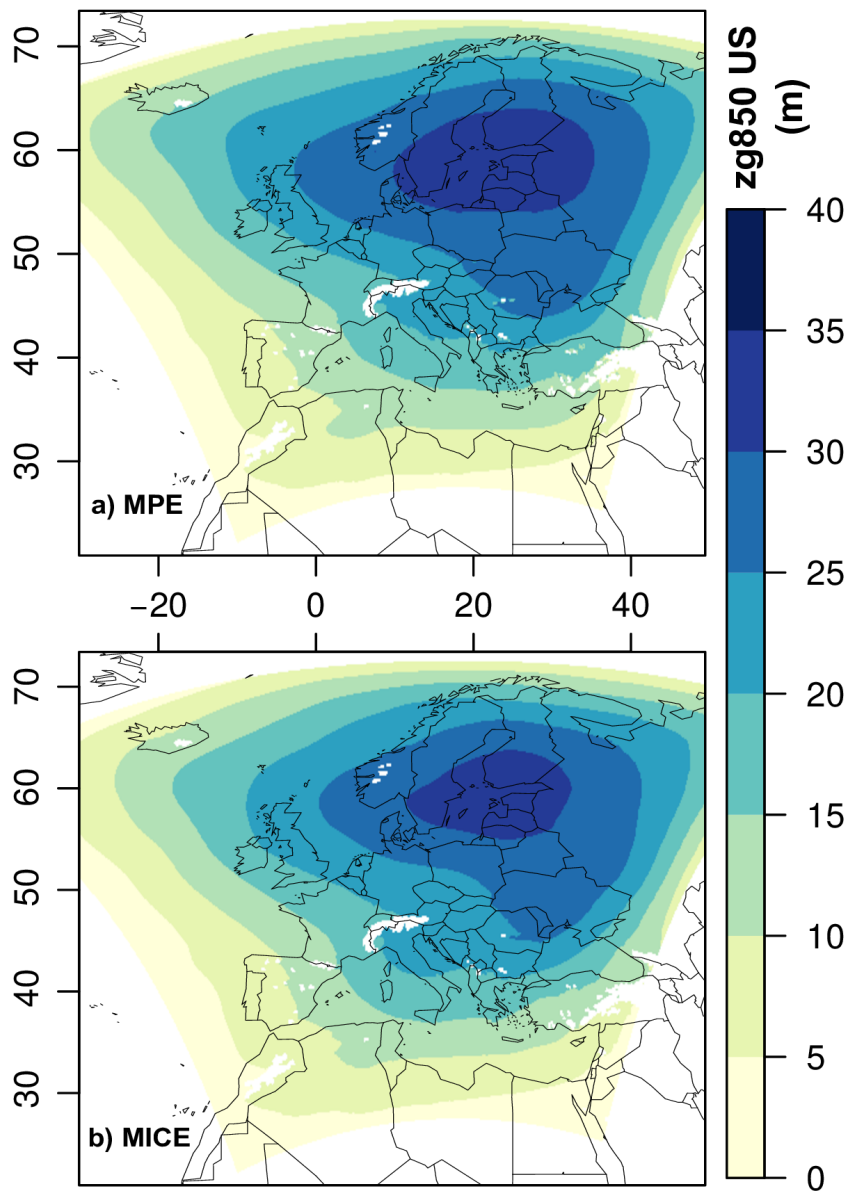


Figure 3.5: Spatial distribution of the inter-member variance (US) for the 850 hPa geopotential height (m) in EUR-15 domain of experiment B (year 1999). a) multi-physics ensemble. b) multi-initial-conditions ensemble.

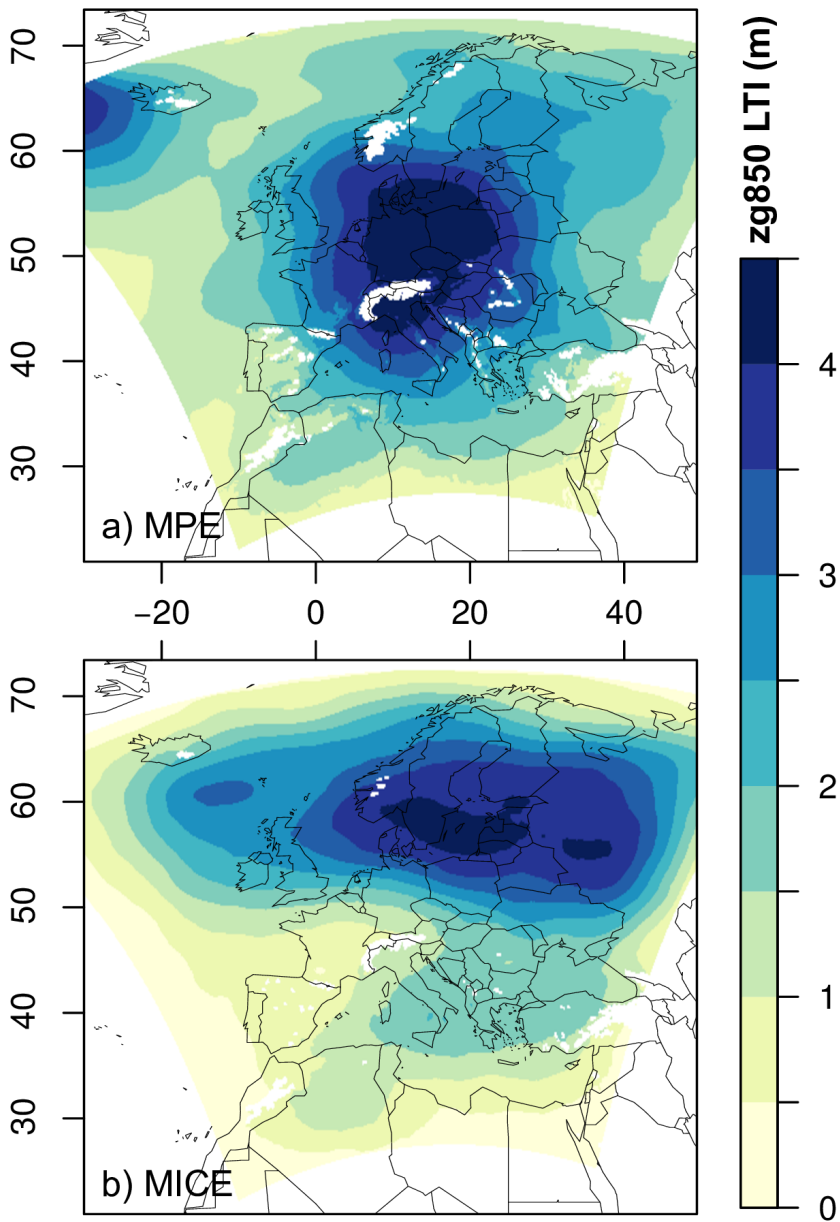


Figure 3.6: Long-term impact of multi-physics (a) and multi-initial-conditions (b) on 850hPa geopotential height (m).

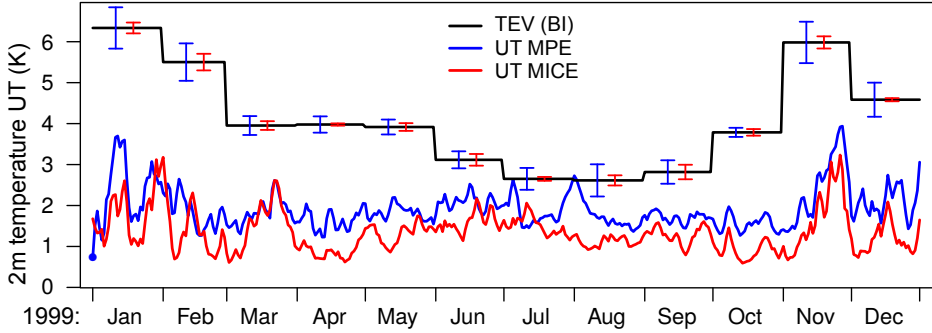


Figure 3.7: As Fig. 3.4 but for surface temperature over land.

in the center of the domain, between Germany and Poland, and extend towards the Alpine region. Remarkably, systematic differences develop also on the northwestern boundary.

The LTI of internal variability (Figure 3.6b) shows a distinct pattern, with the largest values in the northern half of the domain. The magnitude is comparable to that of the MPE, though. Therefore, even though the spatial patterns are different, the systematic differences among MPE members are still comparable to the internal variability. This would suggest that one-year simulations are not enough to distinguish the systematic effect of a particular parameterization configuration compared to the impact of different initial conditions on the circulation. Since the MICE is just composed of multiple realizations of the same model configuration, its LTI must tend to zero as the simulation length increases and the climatology of all members tends towards the “true” model climatology. Longer simulations, such as those currently under way in the FPS-Convection, should provide a better assessment of the LTI of the MPE. For example, for 10-year simulations, the values on Figure 3.6b should be divided by a factor of $\sqrt{10} \approx 3.2$ (Lucas-Picher et al, 2008b). Up to this point, we have focused on the circulation (850 hPa geopotential height) and we have seen that multi-physics uncertainty is hard to distinguish from internal variability. The results for the circulation at 700 hPa or 500 hPa (not shown) are qualitatively similar.

3.3.3 Surface variables

Since circulation is only indirectly affected by physical parameterizations, in this section we focus on near-surface (2-meter) temperature. This is just one example of a variable affected by surface radiative and heat flux balances, which are parameterized in RCMs. In particular, the set of parameterizations tested in the FPS-Convection WRF ensemble (Table 3.1) directly affects cloud cover, surface energy (and mass) exchange and transport. As a result, this MPE shows a spread in surface temperature that substantially exceeds internal variability (Figure 3.7). Other near-surface variables, such as 10-meter wind, were also checked (not shown) and showed qualitatively similar results as near-surface temperature.

The evolution of inter-member variance for near-surface temperature, both for the MPE and MICE is different from the geopotential height shown in Figure 3.4. The annual cycle is clearer in the TEV than in the variance, which only shows a hint of a seasonal cycle during April through October. In summer, MPE and MICE spread evolution is uncorrelated, with some peak MPE uncertainty events (e.g. end of July) clearly standing out of internal variability. However, the strong winter variability seems coherent between MPE and MICE spread. Even if multi-physics spread is usually the greatest, internal variability seems to modulate it. This is in apparent contradiction with the results of Cr  tat and Pohl (2012), who claimed that physical parameterizations modulate IV. They show that two MICE under different physical parameterization configurations develop a different amount of IV on average. However, they also show (their Figure 4b) a coherent evolution in time of the IV between model configurations. In our setup, physical parameterizations cannot modulate IV time evolution since the model configuration is fixed in the MICE. Still, Figure 3.7 shows that, despite the different spread amounts in MICE and MPE, both evolve coherently in time. It is likely that a third variable, such as the strength of the external forcing (i.e. boundary conditions), modulates the degree to which both physics and IV uncertainties can grow.

Transient-eddy variability for surface temperature (monthly step line in Figure 3.7) shows again the mid-latitude maximum during winter. A key difference compared to the geopotential height is the large variability of TEV within MPE members, as compared to the MICE members. In fact, uncertainty in MPE nearly doubles internal variability during some months. Notably, a peak uncertainty event by the end of July reaches the

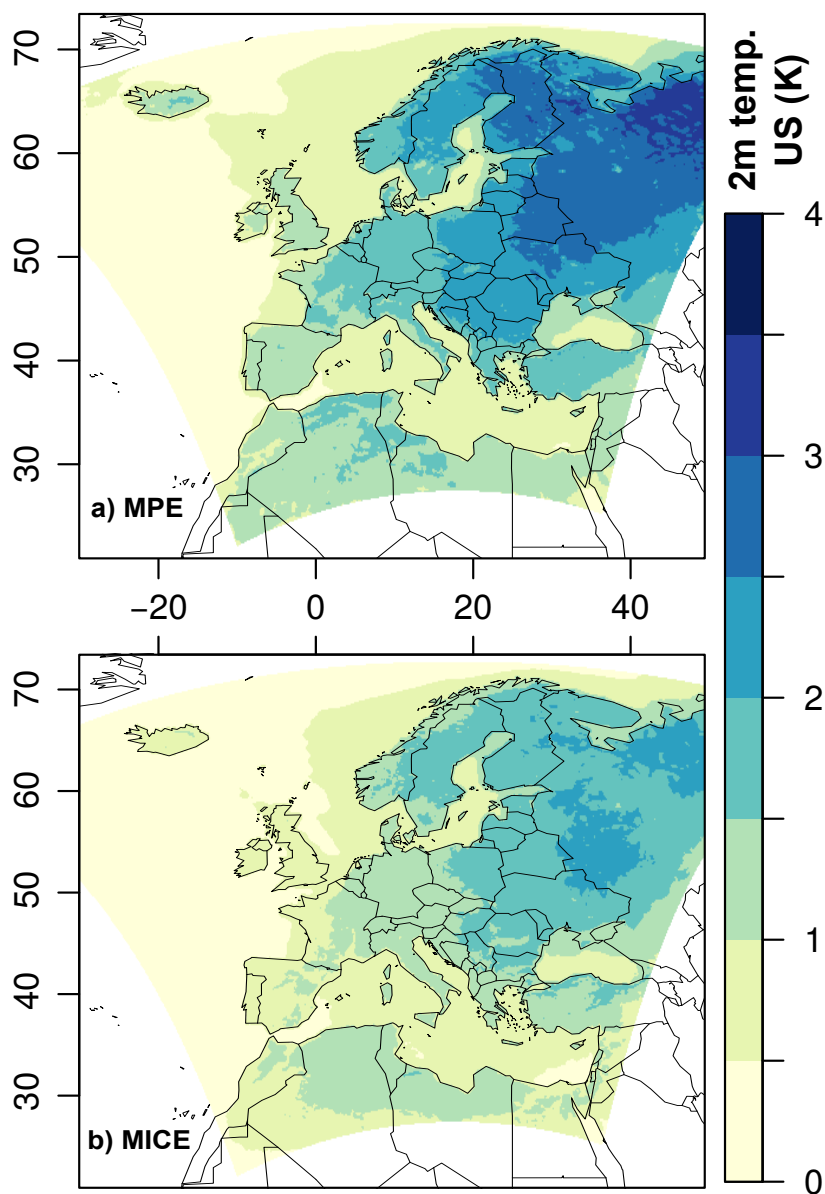


Figure 3.8: Spatial distribution of the inter-member variance for surface temperature (K) in EUR-15 domain of experiment B (year 1999). a) multi-physics ensemble. b) multi-initial-conditions ensemble.

TEV line (especially, when considering its uncertainty), indicating that surface temperature patterns for the different physics differ as much as two random temperature patterns in this month. Note, however, that TEV was computed using a single month and, therefore, this estimate does not consider interannual variability. This might explain the reversal of the TEV cycle during November and December. The strong uncertainty in the November UT estimate is likely pushing up the TEV value for this month.

The spatial distribution of the inter-member variance for surface temperature (Figure 3.8) reveals, as before, a similar pattern of increasing spread towards the northeast in both ensembles. In this case, despite the similar pattern, MPE shows larger spread values in accordance with Figure 3.7. MPE reaches a maximum value of about 3.5 K while MICE reaches about 2 K.

Finally, apart from the higher day-to-day uncertainty of the MPE for surface temperature, a systematic, long-term impact is clearly developed for this variable (Figure 3.9a). Unlike the circulation variable, the long-term impact of MPE for temperature is of comparable magnitude to its uncertainty. Also, it falls well above the long-term impact of internal variability (Figure 3.9b), suggesting that for variables directly influenced by physical parameterizations (such as surface temperature), one-year simulations suffice to discern the systematic effect of a given parameterization with respect to another. Not only the magnitude, but also the spatial pattern of LTI differs between that of internal variability and the effect of parameterizations. The latter shows three main maxima over Africa, central Europe and Russia. As expected, impact is negligible over the sea, where surface temperatures are prescribed.

3.4 Conclusions

In this study we quantified the uncertainty arising from WRF model MPEs, on two different time scales, developed within the FPS-Convection international initiative. Additionally, for each MPE, new MICEs were performed to assess the role of internal variability in explaining the different ability of MPE members to reproduce specific convective events. The study was carried out for a one-month period focusing on a particular case study of heavy precipitation over Austria, and extended to one-year timescale.

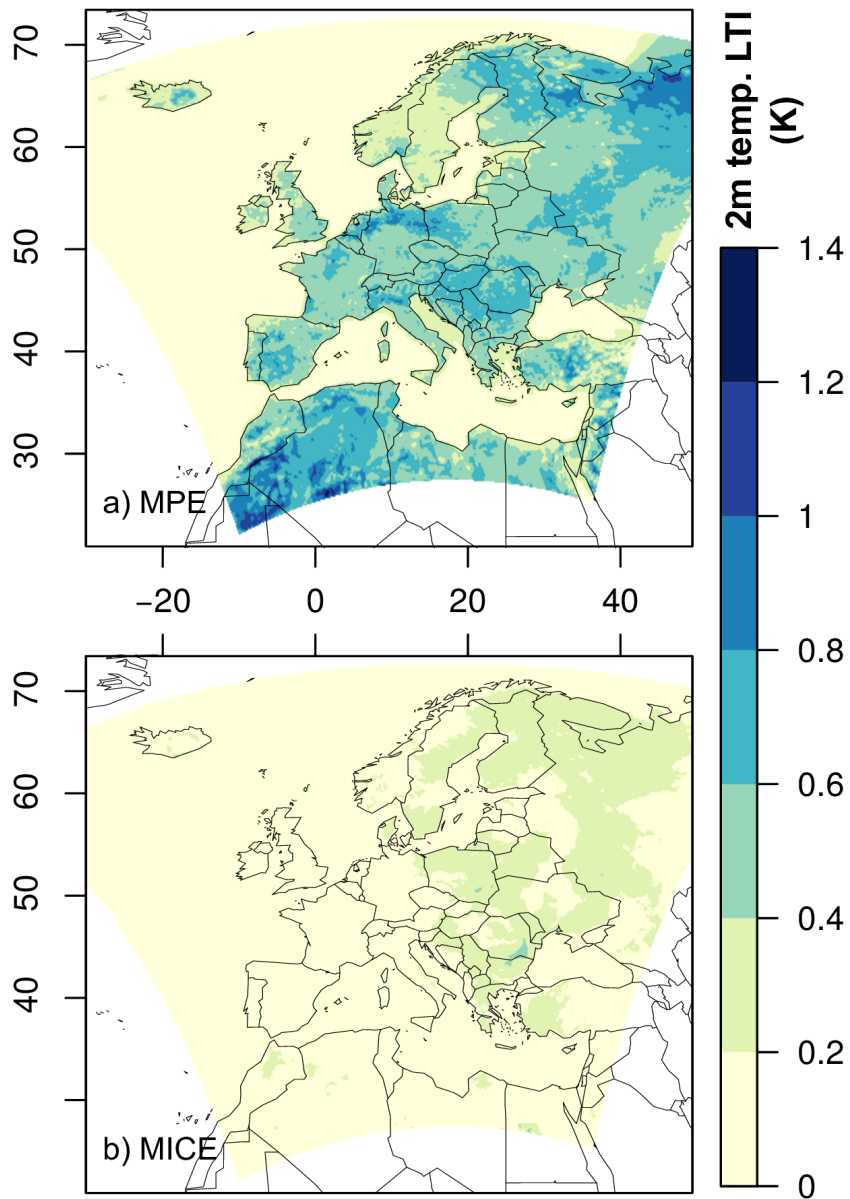


Figure 3.9: Long-term impact of multi-physics (a) and multi-initial-conditions (b) on surface temperature (K).

The analyses over the one-month period already shed light on the 2 main objectives of this work: (1) The failure of some WRF model configurations to reproduce the case study, as reported by [Coppola et al \(2020\)](#), is not related to physical parameterizations, but to the absence of a synoptic circulation pattern that favoured the event. Some members of the MICE were able to reasonably reproduce the observed synoptic pattern without modifying the model parameterization setup. (2) From a quantitative perspective, the spread due to the parameterization differences has a magnitude comparable to that from internal variability. Therefore, in these one-month simulations, the effect of the different physical parameterizations on the circulation cannot be distinguished from internal variability.

The extended study over a one-year period showed similar results for circulation variables (geopotential height). Multi-physics spread is comparable to internal variability both in its time evolution along the year and its spatial pattern. In this regard, we found multi-physics circulation uncertainty to behave according to previous RCM internal variability studies ([Lucas-Picher et al, 2008b](#)), with an annual cycle exhibiting increased uncertainty during summer and a spatial pattern of increased uncertainty towards the outflow boundaries of the regional domain.

The results, however, depend on the variable, with surface variables (known to be sensitive to parameterized processes) showing higher MPE spread. For example, for near-surface temperature the spread associated to parameterizations was above that due to the internal variability. This suggests that it is easier to discern both sources of uncertainties when analyzing variables more constrained by the model physics, which is typically the case in RCM parameterization sensitivity studies ([Fernández et al, 2007](#); [Evans et al, 2012](#); [Solman and Pessacg, 2012](#); [Jerez et al, 2013b](#); [García-Díez et al, 2015](#); [Katrakou et al, 2015](#); [Stegehuis et al, 2015](#); [Devanand et al, 2018](#)).

As a reference for uncertainty, we computed transient-eddy variability, and quantified its spread due to the multi-physics and to internal variability. This type of uncertainty also depends on the variable. For the circulation, transient-eddy variability of the different physical model configurations is similar to the internal variability range. However, for near-surface temperature, the different physics configurations exhibit a different level of transient-eddy variability. This requires further analysis on longer simulations to properly estimate the inter-annual contribution, but this is beyond the scope of the present work.

The long-term impact of the internal variability has been found to be of comparable magnitude to that of multi-physics for atmospheric circulation variables on year-long simulations. For surface temperature, however, the long-term impact of the multi-physics is larger, standing out of internal variability. For both variables, the spatial patterns of MPE and MICE differ, and this calls for a detailed study of each physical parameterization considered.

The techniques for quantification of internal variability (Lucas-Picher et al, 2008b) were applied here to explore also multi-physics spread, which proved to be a useful method for comparing both sources of uncertainty. They revealed that uncertainty arising from perturbations of the model physics (full replacement of a physics scheme) are seen from the circulation point of view as perturbations of initial conditions, i.e. as internal variability “noise”. Both types of perturbations seem amplified in a similar way by the dynamical system and synchronously constrained by the lateral boundary conditions. This view of a structured near-surface perturbation as a random upper air circulation noise was also found, in a completely different context, by Fernández et al (2009).

The inability of an RCM to reproduce the observed day-to-day circulation due to internal variability is not a matter of concern for mean climate studies, given that long-term climate is preserved (Caya and Biner, 2004). However, with the arrival of convection-permitting simulations and the increasing interest in the climate of extremes, RCM internal variability re-emerges as a matter of concern for model evaluation. As an example, the FPS-Convection focuses on high-impact (low probability) convective phenomena that occur mainly during the summer season, when lateral boundary forcing is the weakest. The evaluation of models under these conditions poses a real challenge that can only be addressed by computationally expensive experiments including the simulation of long periods and/or the simulation of a corresponding MICE to disentangle the role of internal variability in the results. Other alternatives would be to constrain internal variability by using techniques such as spectral nudging, which has its own drawbacks (Alexandru et al, 2009), or frequently reinitializing the RCM (Lo et al, 2008; Lucas-Picher et al, 2013).

Finally, the magnitude of internal variability in an RCM has been shown to depend on the domain size and location (Giorgi and Bi, 2000; Rinke and Dethloff, 2000; Alexandru et al, 2007). Given that, for circulation variables, MPE variability behaves as internal variability, we could argue that a similar dependence on domain size and location might af-

fect MPE variability. The generalization of these results for other domain sizes and for regions with a weaker lateral boundary forcing is left for a forthcoming study.

Chapter 4

Spin-up time and internal variability analysis for overlapping time slices in a regional climate model

4.1 Introduction

Climate model resolution has always increased hand in hand with the available computer power. As an example, 30 years ago, the computational demand of the first regional climate models (RCMs; Giorgi, 2019) limited their use to 60 km grid spacing for a month-long simulation (Dickinson et al, 1989; Giorgi and Bates, 1989). Currently, centennial RCM simulations at ca. 10 km grid spacing are routinely carried out at different research centers (Jacob et al, 2020). Still, the experiments with the highest spatial resolution (currently at kilometer-scale grid spacing) can only be afforded for time slices of about a decade (Coppola et al, 2020). This approach considers a decadal simulation driven by a future scenario and a reference decade driven by historical conditions to explore changes in climate. This pushes the period to carry out climate analyses well below the minimal standard of a 30-year period (WMO, 2017). In the near future, centennial simulations of a kilometer-scale RCM will be feasible, especially if the RCM community adopts the latest advances in computing (Leutwyler et al, 2016). However, time slices will still be required for the ever-increasing model resolution, complexity and coupling with other

demanding model components. In this work, we consider the use of a set of overlapping time slices to accomplish multi-decadal RCM simulations and we explore the effects of this approach on the simulated climate.

The idea of splitting a climate simulation into slices is nearly as old as regional climate modelling (Pan et al, 1999). There are different reasons for doing so, though. A common reason to re-initialize a climate simulation is to keep it close to the observations. For this purpose, a frequent reinitialization is advocated (Pan et al, 1999; Qian et al, 2003; Lo et al, 2008). The frequent cold-start from reanalysis initial conditions constrains the weather trajectory of the model close to the observed one. This approach can introduce discontinuities in the weather events and, more importantly for climate analyses, may disrupt the proper evolution of variables with slow response times, such as deep soil variables. To prevent this disruption, the so-called poor man’s reanalysis approach (Berg and Christensen, 2008; Stahl et al, 2011; Lucas-Picher et al, 2013) keeps the soil variables across the different re-initializations, and updates only the atmospheric initial conditions from reanalysis data. In this latter approach, the simulation slices are not independent of each other and there is no computational advantage in the re-initialization. This computational advantage has been put forward (Jimenez et al, 2010; Menendez et al, 2014) to use the frequent cold-start re-initialization instead of the poor man’s reanalysis.

A second reason to split an RCM simulation into slices is the computational advantage of running the resulting slices in parallel. This form of parallelism can be more efficient than standard high-performance parallel computing paradigms such as OpenMP or MPI (Jerez et al, 2009). Using these parallel computing approaches, computing time scales reasonably only up to a given number of processors, which is usually much less than those available. Even for a reasonable scaling, there is always a loss in using an increasing number of computing cores. Computing time is therefore used more efficiently when splitting the simulation and running the slices on a smaller amount of cores. For their use in climate studies, the initial part of each simulation slice must be disregarded as model spin-up. This spin-up period is, typically, at least one year (Christensen, 1999), although a few months might suffice depending on the season when the slices start (Jerez et al, 2020). This computing time trade-off between the gain by a more efficient use of the processors and the waste to spin-up of each simulation slice, can be used to optimize the length of the slices (Jerez et al, 2009).

RCM simulation splitting is hardly avoidable for very long simulations, such as those for the last millenium (Gómez-Navarro et al, 2011). This procedure can also alleviate the computational burden for research groups to perform centennial climate change RCM simulations. As an example, in this work, we analyze RCM simulations carried out in the last decade at Universidad de Cantabria (UCAN) as split runs and also as continuous simulation (Section 2.1). A form of simulation splitting is also used for the most computationally demanding RCM simulations (Coppola et al, 2020), where only a couple of decadal time slices can be afforded. Time slicing is just a simulation split into pieces, but where the pieces do not usually overlap. Here, we analyse the effect that overlapping a set of time slices would have on the simulated regional climatology.

Due to internal variability in the RCM (Christensen et al, 2007; Lucas-Picher et al, 2008b), a perfect match of the weather trajectory in two consecutive time slices is not possible. Internal variability is unavoidable and is triggered by the different initial conditions in the time slices, so there will always be a 'weather jump' at the joints. On top of the internal variability, the coarse initial conditions from the driving GCM or reanalysis need some time (spin-up time) to be assimilated by the RCM dynamics. This spin-up time depends on the variable. It is quite short for atmospheric variables, but it can extend for several months or even years for other slow-varying variables (Christensen, 1999; Cosgrove et al, 2003; Jerez et al, 2020).

The objective of this study is to show the effect of the overlapping time slice approach on the regional climate simulated by an RCM. For this purpose, we used state-of-the-art CORDEX simulations carried out at UCAN using the Weather Research & Forecasting (WRF) modelling system (Section 2.1). Analyses were carried out for variables with different response time, using simulations for different regions, with different resolutions and with time slices initialized in different seasons. We studied the weather jumps in split simulations, locating their occurrence (Section 4.3.1), analysing their evolution in time (Section 4.3.2) and their geographical location (Section 4.3.3). Finally, we analysed the potential effect of splitting the simulations into time slices on the simulated climate (Section 4.3.4).

4.2 Data & methods

4.2.1 Data

In this study we analyse three sets of simulations using the WRF model (Skamarock et al, 2008), with different parameterization schemes, domains, spatial resolutions and time periods. Simulations were performed over three model domains as defined within the Coordinated Regional climate Downscaling Experiment (CORDEX; Giorgi and Gutowski, 2015). One set of simulations was carried over the CORDEX South America domain at the standard 0.44° horizontal resolution (SAM-44), regular on a rotated latitude-longitude projection (Falco et al, 2019; Solman and Blázquez, 2019). These simulations were carried out for the historical period 1951–2005 and for the future scenarios RCP 4.5 and RCP 8.5 for the period 2002–2100, all driven by the Canadian Earth System Model (CanESM2; Arora et al, 2011). The other two sets consisted of evaluation simulations over Europe at 0.44° (EUR-44) and ~ 15 km (EUR-15) horizontal grid spacing, driven by the ERA-Interim reanalysis (Dee et al, 2011). EUR-44 simulations span the period 1979–2010 (Vautard et al, 2013), while the EUR-15 simulations were generated under the CORDEX FPS-Convection, covering the period 1999–2009 (Coppola et al, 2020). An additional convection-permitting (CP) simulation at ~ 3 km horizontal resolution, is also analysed to evaluate the effect of the resolution. This CP simulation was nested into the EUR-15 domain and centered on the Alpine region (ALP-3). The model setup is the same as EUR-15, except for the cumulus parameterization, which was deactivated (Ban et al, 2021).

Two different model configurations were used in terms of physical parameterizations. Namely, EURO-CORDEX WRF configuration WRF341I (Manzanas et al, 2018) was used in EUR-44 and SAM-44, while an updated model version and configuration WRF381BI (Ban et al, 2021) was used in EUR-15. The most important difference concerning our results is the different land surface model (LSM). WRF381BI used the new Noah multi-parameterization (Noah-MP v1.1) LSM (Niu et al, 2011), while WRF341I used its predecessor, Noah (v3.4.1) LSM (Chen and Dudhia, 2001).

The three sets of simulations were performed by splitting the runs into several time slices. In order to allow for the required spin-up time, adjacent time slices were overlapped for at least one year (Figure 4.1). Additionally, the EUR-15 and EUR-44 simulations were also performed continuously. The continuous runs were produced in two different ways.

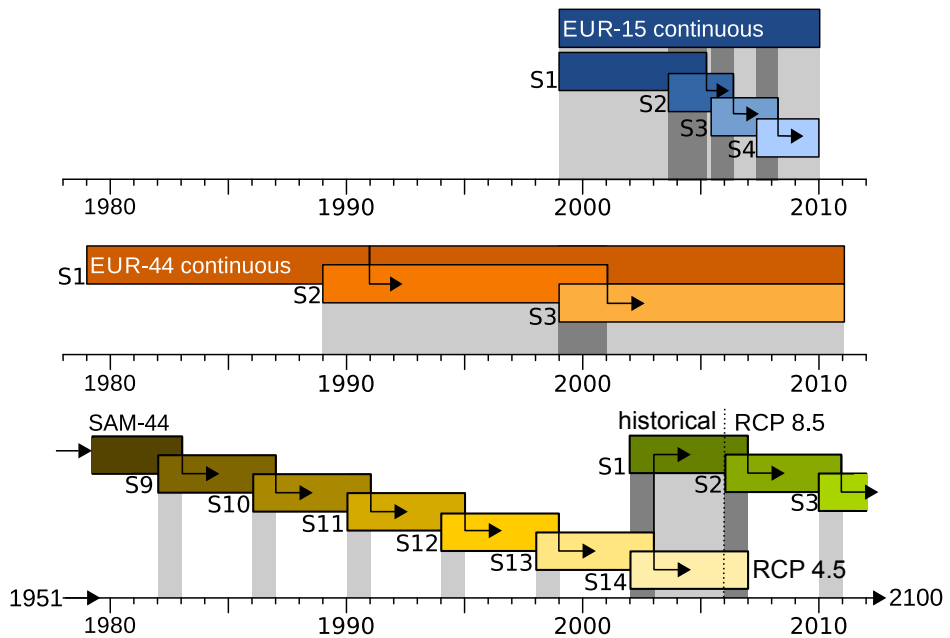


Figure 4.1: Schematic representation of the analysed simulations. Time slice simulations (S1, S2, etc.) are used to compose split simulations for each domain (switching between time slices are indicated by arrows). Continuous simulations are also represented, either as independent simulations (EUR-15) or by extending the S1 slice (EUR-44). Overlapping periods are shaded in grey, light grey for the overlapping of two simulations, and dark grey for three overlapping simulations.

For EUR-44, the first time slice (S1) was extended to cover the full period. For EUR-15, the full period was simulated again, but the model was compiled with a different compiler version and linked to a different version of the parallel computing (OpenMPI) libraries. Therefore, the differences between the EUR-15 continuous run and the first time slice of the split simulation (EUR-15-S1) will be due to different numerical round-off in the model executable. These differences are expected to grow and evolve with the flow as those caused by perturbing initial conditions, i.e. internal variability (Geyer et al, 2021). These continuous runs are considered as a reference to investigate possible inhomogeneities caused by the time slicing of the simulations.

It is worth noting that these sets of simulations were not specifically designed for this study. We use them as an ensemble of opportunity to study the spin-up length and the role of internal variability in the climate simulated by overlapping time slices. As such, we can only explore the variables available for each simulation, and the initialization seasons of the slices used in these multi-year simulations. A designed, systematic exploration of the required spin-up time has been recently carried out by Jerez et al (2020) over Europe for a 1-year test period. Our approach extends this work by considering domains in different climates, different spatial resolutions, longer spin-up lengths, and the role of interannual and internal variability.

We focus our analyses on three types of variables. First, we consider slow-varying variables as their accurate initialization and representation are of key importance for weather and climate modelling. They require significant spin-up times as their initial conditions, taken from the driving model, usually differ greatly from the conditions generated by the RCM (Jerez et al, 2020). For this purpose, among the available variables, here we analyze total soil moisture and snow depth. These variables control energy partitioning at the land surface and, through land-atmosphere feedbacks, they have an impact on the evolution of the atmospheric conditions in the planetary boundary layer (Seneviratne et al, 2006). Second, we considered near-surface temperature and precipitation, two fundamental variables that characterize the regional climate and are often considered in climate and impact studies. Both are highly variable in time and space. And third, the atmospheric circulation, which has also a strong but non-local impact on the regional climate (Zappa, 2019). Atmospheric circulation shows the shorter response time, as compared to surface or subsurface fields. We characterize the circulation by means of the geopo-

tential height at 850 hPa. The analysis was carried out for daily mean values for all variables.

4.2.2 Methodology

The analysis of discrepancies across the simulation slices is based on simple differences. For a given variable $X(s, n, t)$, taken from simulation slice s at grid point n and time step t , we define the following differences:

$$D_t X(s, n, t) = X(s, n, t) - X(s, n, t - 1) \quad (4.1)$$

$$D_s X(s, n, t) = X(s, n, t) - X(s - 1, n, t) \quad (4.2)$$

$$D_{st} X(s, n, t) = X(s, n, t) - X(s - 1, n, t - 1) \quad (4.3)$$

for consecutive time steps $t - 1$ and t , and consecutive simulation slices $s - 1$ and s . Note that

$$\begin{aligned} D_{st} X(s, n, t) &= D_s X(s, n, t) + D_t X(s - 1, n, t) \\ &= D_s X(s, n, t - 1) + D_t X(s, n, t), \end{aligned} \quad (4.4)$$

that is, the meteorological jump (D_{st}) in variable X occurring at the joint between time $t - 1$ in simulation slice $s - 1$ and time t in slice s , can be decomposed as the difference between slices D_s at time $t - 1$ plus the variable tendency in time (D_t) within slice s . In order to have a relative measure, we consider non-dimensional differences in terms of standard deviation units, by dividing each of them by the standard deviation in time at each grid point:

$$d_{st} X(s, n, t) = \frac{D_{st} X(s, n, t)}{sd D_t X(s, n)} \quad (4.5)$$

where the standard deviation is calculated as

$$sd D_t X(s, n) = \sqrt{\frac{1}{T(\tau) - 1} \sum_{t \in \tau} [D_t X(s, n, t) - \overline{D_t X}^\tau(s, n)]^2} \quad (4.6)$$

from a 45-day time period (τ) prior to the target time t . The overline represents time average over a given time period τ :

$$\overline{X}^\tau(s, n) = \frac{1}{T(\tau)} \sum_{t \in \tau} X(s, n, t) \quad (4.7)$$

with $T(\tau)$ the number of time steps in τ . This is done to use intra-seasonal variability as reference, thus preventing the annual cycle variability to mask large differences for a given season. This time period averages have also been used to assess the long-term impact of time slicing on the climatology of a given variable (Section 4.3.4).

Differences (D) are spatio-temporal fields. We summarize them by means of spatial root mean squared differences (RMSD), to avoid compensation of opposite differences across the domain. For each slice, the *intra-slice daily tendency* ($RMSD_t X$) summarizes the differences between consecutive time steps:

$$RMSD_t X(s, t) = \sqrt{\frac{1}{N} \sum_{n=1}^N D_t X(s, n, t)^2} \quad (4.8)$$

Inter-slice differences ($RMSD_s X$) are employed to quantify the differences between two slices along the overlapped period (see Section 4.3.3):

$$RMSD_s X(s, t) = \sqrt{\frac{1}{N} \sum_{n=1}^N D_s X(s, n, t)^2} \quad (4.9)$$

We can also consider the quadratic average of $D_{st} X$ ($RMSD_{st} X$), which arises in the context of split simulations; it is the $RMSD_t X$ at the slice joint time steps. This measure quantifies the inhomogeneity introduced at the joint for different variables (see Section 4.3.1).

$$RMSD_{st} X(s, t) = \sqrt{\frac{1}{N} \sum_{n=1}^N D_{st} X(s, n, t)^2} \quad (4.10)$$

Finally, as a reference for natural variability we also estimate transient eddy variability (Caya and Biner, 2004; Lucas-Picher et al, 2008b; Lavin-Gullon et al, 2020):

$$TEV(s, \tau) = \sqrt{\frac{1}{N} \sum_{n=1}^N [X(s, n, t) - \bar{X}^\tau(s, n)]^2} \quad (4.11)$$

where τ represents in this case all days in a calendar month, in order to have a monthly TEV estimate.

4.3 Results & discussion

4.3.1 Detection of meteorological inhomogeneities

Unlike continuous regional climate simulations, split simulations contain meteorological inhomogeneities, i.e. unphysical changes in the state of the system at the joints of the time slices. This is unavoidable, given that an exact match of two climate simulations is impossible due to the chaotic nature of the climate system. For RCMs, the constraint exerted by the lateral boundary conditions make the inhomogeneities much smaller than in global models. Still, substantial internal variability develops in RCMs (Lucas-Picher et al, 2008b; Bassett et al, 2020; Lavin-Gullon et al, 2020), preventing a smooth transition between simulation slices.

The ability to detect these meteorological inhomogeneities depends on the simulation sampling frequency (i.e. output frequency) used. The inhomogeneity will pass unnoticed if it is smaller than the change between consecutive output times. And this change is larger as sampling frequency lowers. Intra-slice daily tendencies ($RMSD_t$) quantify the changes between consecutive time steps. At the slice joints in a split simulation, $RMSD_t$ becomes $RMSD_{st}$ and quantifies the size of the inhomogeneity along with the variable tendency.

Of course, the relevance of the inhomogeneity depends also on the variable. For geopotential height (Figure 4.2), inhomogeneities go unnoticed. Average daily geopotential tendencies in midlatitudes (EUR-15, EUR-44) range between 20 and 100 m , with an apparent annual cycle. The geopotential change stays in an appropriate range when passing from one time slice one day to the next time slice on the next day (indicated by arrows in Figure 4.2), regardless of the season when the joint occurs. The SAM-44 domain spans mid-latitude as well as tropical regions and, thus, geopotential heights show a smaller range (20 to 80 m) and a much weaker seasonal cycle. Still, daily inhomogeneities go unnoticed. Therefore, upper atmospheric variables, such as geopotential height, do not suffer from inhomogeneities. These variables are strongly driven by the lateral boundary conditions and the pass of weather systems through the domain. Moreover, the 1-year spin-up period considered in the time slices is expected to be long enough for these variables to reach physical equilibrium within the model.

The same result applies for variables that are influenced to a greater or a lesser extent by the lateral boundary forcing, such as near-surface tem-

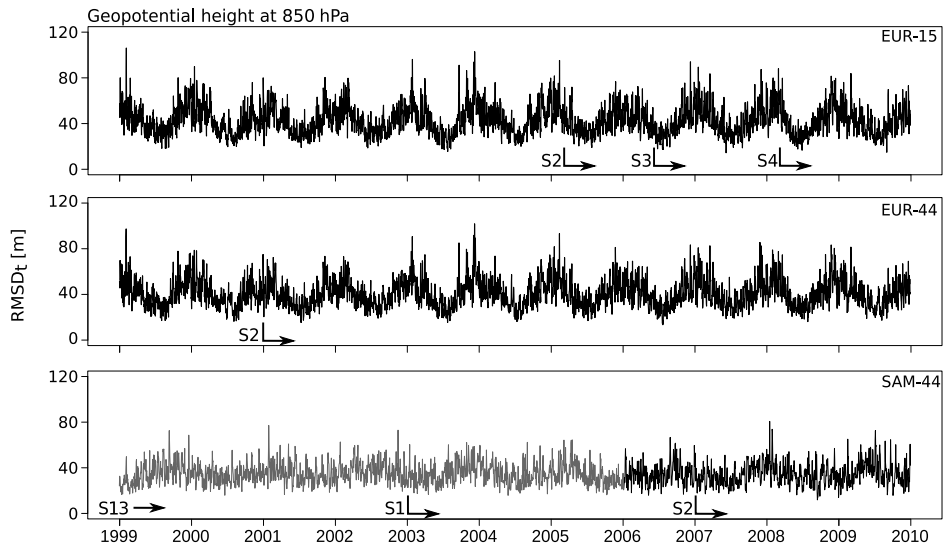


Figure 4.2: RMSD between consecutive days ($RMSD_t$) for geopotential height at 850 hPa (m) in the EUR-15, EUR-44 and SAM-44 split simulations. Time slice joints are indicated by arrows. In SAM-44, light gray shading refers to the historical run while dark gray shading corresponds to RCP 8.5 forced run.

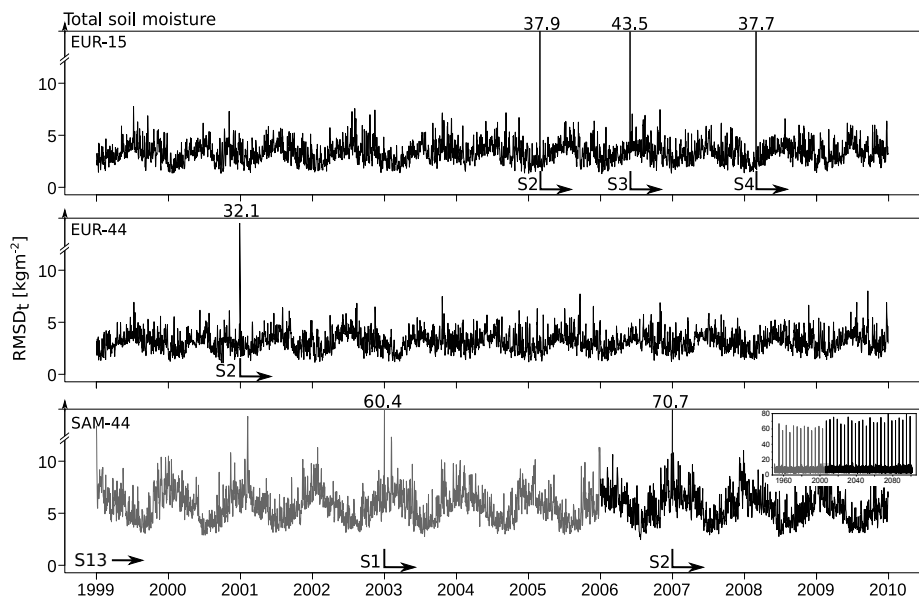


Figure 4.3: As Figure 4.2, but for the total soil moisture content (kg/m^2). The inset in the lower panel shows the whole 1950-2100 SAM-44 historical (grey) plus RCP 8.5 scenario period. Numbers at the top of the each panel represent maximum values (out of scale) at the joints of the slices.

perature, precipitation or snow depth (not shown). For snow depth, which varies slowly, regional inhomogeneities are apparent, but the domain-wide summary in $RMSD_t$ masks the differences in the relatively small snow-covered regions in the domains.

For soil variables (e.g. total soil moisture in Figure 4.3), however, large discontinuities occur. $RMSD_t$ shows inhomogeneities in the three sets of simulations, clearly unveiling the slice joints. Daily tendencies in soil moisture range between 2 and 10 kg/m^2 , except for peaks on certain days with values beyond 30 kg/m^2 , corresponding to the joints of the time slices. The order of magnitude of these peaks is not sensitive to the season in which the time slices join (winter in EUR-44, summer in SAM-44, winter and spring in EUR-15). Peaks also show low interannual variability, standing clearly out of the background variable tendency for every joint in different years (see inset in Figure 4.3). Despite the strong signal in $RMSD_t$, these peaks in the differences are still one order of magnitude smaller than the variable; e.g. the quadratic mean for total soil moisture in SAM-44 is about 600 kg/m^2 .

These strong discontinuities at the joints indicate that the discrepancies in soil moisture between two time slices is very high. The discrepancies could be due to two causes: (1) the spin-up period considered is not long enough for total soil moisture to balance within the model or (2) soil moisture internal variability is larger than the daily tendency. Or, it could also be a mixture of both. This is investigated next.

4.3.2 Meteorological inhomogeneities in time

A split simulation consists of a set of time slice simulations concatenated after removing an initial spin-up period. In principle, the longer the spin-up period, the better. Therefore, a given slice should enter the split simulation only when the previous slice has finished (as depicted in Figure 4.1). However, since the whole overlapping period is available, we could decide to switch between the slices at any time in this period. And we can quantify the size of the discontinuity by means of inter-slice differences ($RMSD_s$, Equation 4.9). As an example, Figure 4.4 shows the 1.5-year overlap between EUR-15 S1 and S2 time slices, covering the period from Sep., 2003 to Feb., 2005. The EUR-15 continuous simulation is also included in the Figure as reference for $RMSD_s$. Figure 4.5 shows another example for the 1-year overlap period between SAM-44 S1 and S2, for the overlapped period covering the complete year 2006. In this case, there is

no reference continuous run.

Total soil moisture

Total soil moisture intra-slice daily tendencies (Figure 4.4a, top panel) differ between the two time slices at the beginning of the overlapping period. At this time, total soil moisture in S2 is mainly provided by the initial conditions from ERA-Interim, while in S1 the soil state is generated by the model itself. In EUR-15, the overlap period is initiated in late summer (September) so that the difference in the daily tendencies between S1 and S2 decreases rapidly. Day-to-day variability is mainly determined by the top soil layer, which in turn depends on precipitation. Thus, under dry conditions, daily soil moisture tendencies adapt fast from the driving model soil to the soil in the long term RCM run (slice S1).

In SAM-44, intra-slice daily tendencies for soil moisture (Figure 4.5a, top panel) show that more than 3 months are necessary for the two adjacent slices S1 and S2 to evolve coherently in time. It is interesting to notice that the two slices tend to diverge again at the end of the overlapping period, which corresponds to the austral summer. This is probably associated to the discrepancies in summertime precipitation between the two slices (see Figure 4.5d top panel).

Daily soil moisture inter-slice differences ($RMSD_s$) during the overlapped period are initially very high in both domains (bottom panels of Figures 4.4a and Figure 4.5a). In EUR-15, $RMSD_s$ stabilizes at 40 kg/m^2 after about one year, while in SAM-44 the minimum value of 70 kg/m^2 is reached after just a few months. Thus, spin-up is shorter in SAM-44, despite of being initiated in summer. This highlights that not only the season determines the spin-up time, but also the synoptic regimes specific over the region. In SAM-44, the overlapped period starts in the austral summer (DJF) but, unlike in EUR-15, summer is the wet season in Central South America (Liebmann and Mechoso, 2011), which largely contributes to the annual precipitation (and soil moisture) in the whole SAM-44 domain. As a consequence, vertical transport of soil moisture between the deepest layers and the other layers is more efficient under the moist conditions of the wet season (Khodayar et al, 2015)

Inter-slice differences cannot reach a zero value due to internal variability (Lavin-Gullon et al, 2020). The afterwards stabilization is a sign of internal variability overcoming the initial spin-up transient. We can use the continuous run as reference to distinguish internal variability from in-

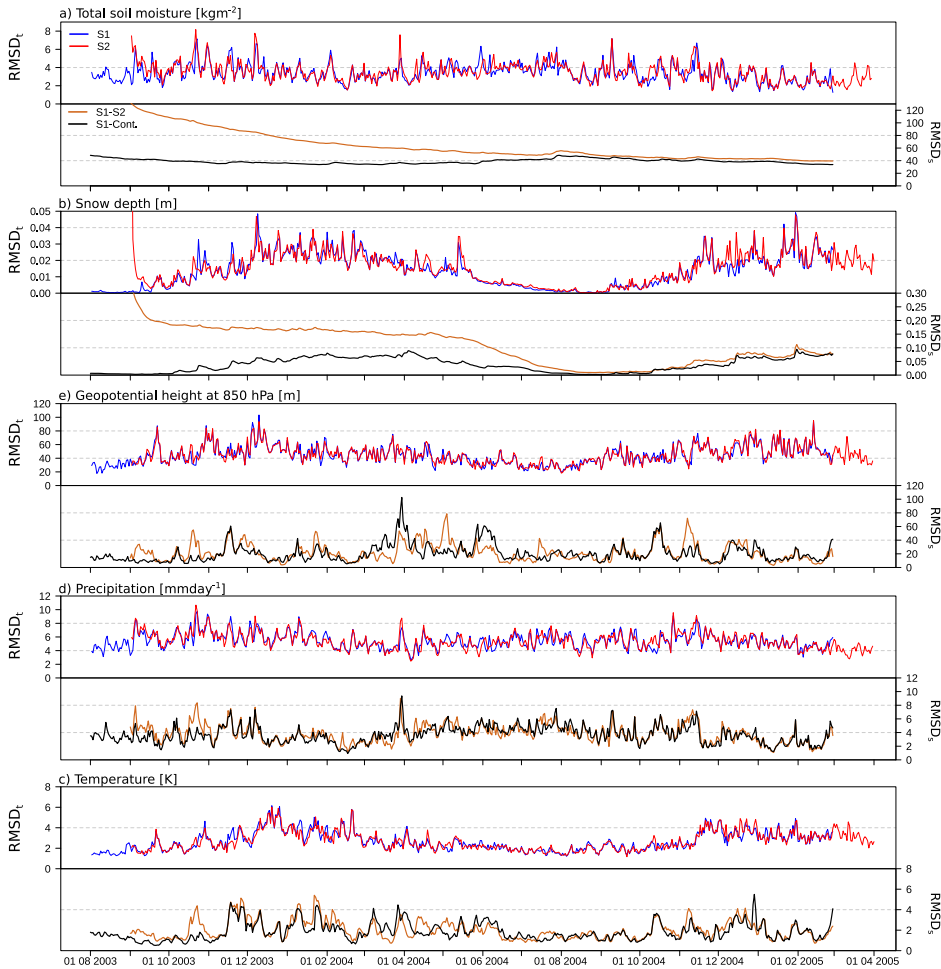


Figure 4.4: RMSD for (a) total soil moisture, in kg/m^2 , (b) snow depth, in m , (c) near-surface temperature, in K , (d) daily accumulated precipitation, in mm , and (e) geopotential height at 500 hPa, in m , for EUR-15 S1, S2 and continuous simulations; see Figure 4.1. For each variable, intra-slice daily tendencies ($RMSD_t X$) for each simulation (top panel) and inter-slice differences ($RMSD_s X$) between S1 and S2, and between S1 and continuous (bottom panel).

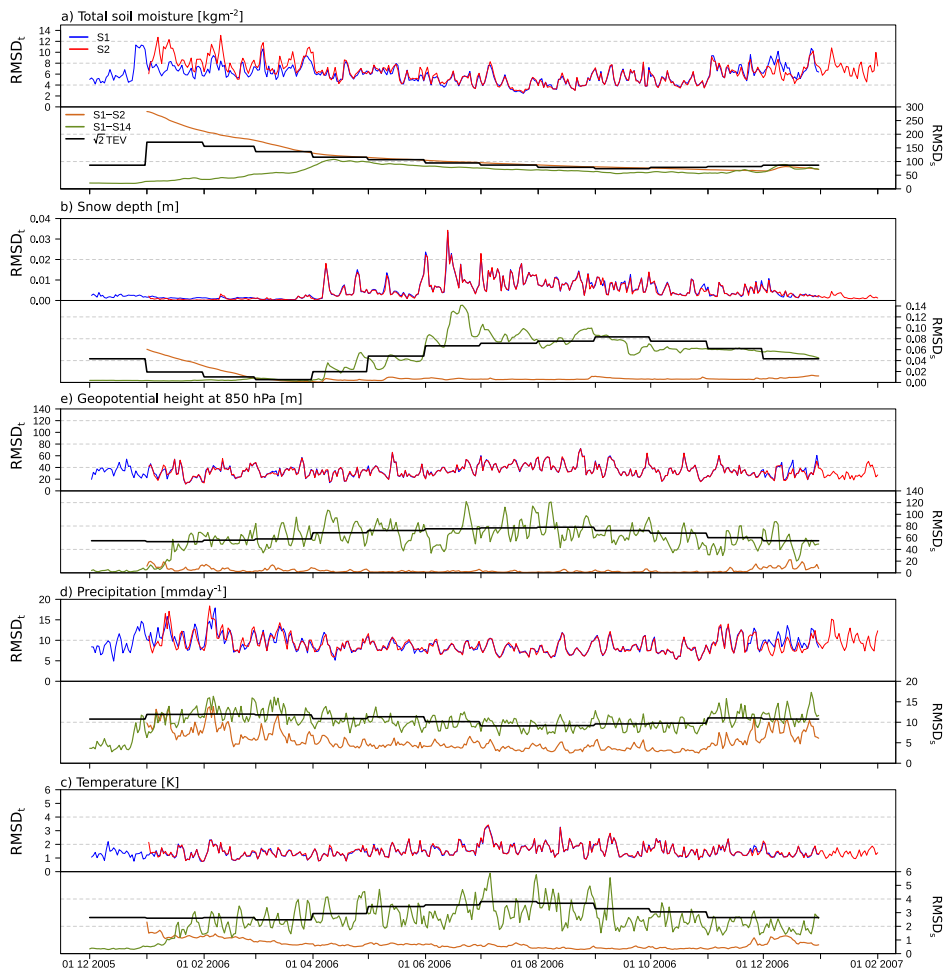


Figure 4.5: As Figure 4.4, but for the SAM-44 domain, and overlapping time slices S1 and S2.

sufficient spin-up. For this purpose, we compute the inter-slice difference between S1 (initialized 5 years before the overlapping period shown) and the continuous simulation (black line in Figure 4.4a). These differences are controlled by internal variability and set a lower limit for inter-slice differences. The results indicate that the overlap period chosen (at least 1 year) was long enough to spin up the slow-varying soil moisture and to get close to the internal variability limit.

It is worth noting the different scale of inter- and intra-slice differences for soil moisture, which is about one order of magnitude. This difference accounts for the $RMSD_t$ peaks in split simulations (soil moisture inhomogeneities) shown in the previous section. In particular, the first peak in Figure 4.3a has a contribution from both $RMSD_t(S2)$ and $RMSD_s(S1 - S2)$ lines (Figure 4.4a) at the end of the overlapping period, when slice S1 switches to S2 in the EUR-15 split simulation. In this sense, an earlier switch between S1 and S2 would have not lead to smaller inhomogeneities. For the rest of the variables (Figure 4.4b-e), $RMSD_s$ and $RMSD_t$ show the same order of magnitude.

Snow depth

Snow depth shows a different behavior than soil moisture in EUR-15 (Figure 4.4b, top panel). Initial $RMSD_t$ values in S2 are significantly higher than those in S1, but they balance in just a few days. In SAM-44 (Figure 4.5b, top panel), this initial difference is not evident as the snow depth is insignificant there during the austral summer, when the overlapped period starts. After balancing, $RMSD_t$ evolves coherently in time for both slices in both domains, with an evident seasonal cycle. The variability of day-to-day $RMSD_t$ is higher in winter and early spring, when snow depth changes due to snowfalls and snow melting, and lower values occur in summer when snow coverage is small and limited to areas with permanent snow.

Inter-slice differences ($RMSD_s$) are reduced fast, and a plateau is reached after a few days in EUR-15 (bottom panel in Figures 4.4b). The values drop to a minimum during summer, as the snow coverage is minimal. Afterwards, snow depth differences between the slices increase, following the seasonality of internal variability. However, the values of the previous winter plateau are not recovered. Therefore, the plateau in $RMSD_s$ is given as a result of an incomplete spin-up. For this simulation, an end-of-summer joint would minimize the snow depth inhomogeneity

while retaining a similar soil moisture inhomogeneity. Moreover, this is true for much shorter spin-up periods, with initializations in March (EUR-15 S3-S4) or even June (EUR-15 S2-S3), which can be seen in Figures A.2 and A.1 in the Supplementary Material, respectively. Minimal snow depth inhomogeneities across time slices are obtained by switching slices at the end of the summer (September) in all cases, although the initialization in June (just 3 months before) provides clearly insufficient spin-up for soil moisture. There is also a clear summer minimum arising in SAM-44 (Figure 4.5b) in which the joint would be more convenient. Although snow in SAM-44 is scarce, covering only some areas in the southern Andes, selecting austral summer to start the overlapping in SAM-44 is beneficial.

In EUR-44 (Figure A.3) there is a 2-year overlap that allows to better assess the annual cycles in the magnitude and variability of $RMSD_t$, in the slice switch differences $RMSD_s(S3-S2)$ and in the internal variability, as estimated by $RMSD_s(S2-continuous)$. This time slice overlap confirms all previous results for Europe, confirming late summer as a good season to switch slices regarding snow cover. It also reveals more clearly the seasonal cycle in soil moisture internal variability, peaking also in late summer. However, for this particular year, soil moisture seems not to be completely spun up. This highlights the need for an interannual assessment of soil moisture spin-up times.

Other variables

The other variables (Figures 4.4c-e) show no hint of spin-up period, with a coherent evolution of day-to-day changes ($RMSD_t$) and differences across time slices ($RMSD_s$) consistent with internal variability. The order of magnitude of both RMSD is the same, leading to no noticeable inhomogeneities.

Geopotential height exhibits typical high mid-latitude winter variability (Caya and Biner, 2004) in $RMSD_t$ in Europe (Figure 4.4c). There is a seasonal cycle with winter exhibiting larger day-to-day changes than summer. This seasonality is not evident in SAM-44 (Figure 4.5c), which covers large tropical areas. Nevertheless, the larger summer internal variability is apparent in the $RMSD_s$. Internal variability, as represented by the $RMSD_s$ between the continuous and S1 simulations in EUR-15, explains most of the differences between time slices. Similar results are obtained in near-surface temperature.

For precipitation, intra-slice daily tendencies evolve more coherently in

SAM-44, especially in the austral winter. In both domains, discrepancies between the two slices extend along all the overlapped period, regardless of the season. In turn, a seasonal cycle emerges in inter-slice differences, with higher (lower) differences between the slices in the austral summer (winter), following that observed in the geopotential height at 850 hPa. This seasonal behaviour is less apparent in EUR-15.

Horizontal resolution

Horizontal resolution does not seem to play any major role in the model spin-up and inhomogeneities of split simulations. We bilinearly remapped all EUR-15 variables to the ALP-3 domain (not shown). Apart from a slightly higher initial state of the soil moisture in ALP-3, all $RMSD_t$ and $RMSD_s$ time series for the overlap periods are virtually identical in the remapped EUR-15 and ALP-3 resolutions. Another example was shown in Figures 4.2 and 4.3, with very similar $RMSD_t$ evolution for both EUR-44 and EUR-15, regardless of the time slice considered and despite the different model version and configuration.

Another view on spin-up time

The SAM-44 simulation setup does not allow to estimate the internal variability limit, since the only year with two long-term overlapping simulations (S14 and S1) is 2006. In this year, the GCM boundary conditions driving S14 and S1 bifurcate into two different global climate realizations forced by the RCP 4.5 (S14) and 8.5 (S1 and S2) concentration scenarios. As a result, differences between S14 and S1 in 2006 do not represent RCM internal variability, but different global driving fields. In particular, the changes in the forcing between the RCP 4.5 and 8.5 scenarios is so small in 2006 that the two global climate realizations can be considered as resulting from the GCM internal variability. At least, regarding the atmospheric fields fed to the RCM. In a few weeks, the slight forcing differences make the GCM circulation diverge and the synoptic situation of corresponding days in the two global model realizations will be as different as two random days in the corresponding season. Note that no inhomogeneity occurs, since both GCM realizations are started from the same final state of the historical run at the end of 2005. Synoptic conditions depart smoothly as slight changes in the forcing introduce small perturbations which are amplified by the model dynamics to become finite perturbations.

From the point of view of the RCM, soil variables will evolve smoothly, with the land surface model responding in a physically consistent manner to the new atmospheric conditions. Snow cover should also adjust smoothly to the new synoptic conditions fed through the boundaries. This adjustment process is similar to the spin-up, since the RCM internal fields need to adjust to the new driving fields. Unlike the spin-up process, model states are physically consistent during the whole process; no tendencies develop in the model to account for the mismatch between the initial conditions and a balanced model state. The expected $RMSD_s(S1 - S14)$ value after the adjustment is not the RCM internal variability limit in this case (since the driving fields differ), but the GCM internal variability. This can be estimated from the transient eddy variability (TEV, Equation 4.11). In particular, for uncorrelated fields from two GCM realizations, $RMSD_s$ should reach $\sqrt{2}$ TEV (Caya and Biner, 2004).

This decorrelation time to reach the GCM internal variability level sets a minimum response time for the spin-up time. The RCM starts the adjustment process from an internally consistent state, unlike in the spin-up process, which needs to bring the initial state into line with the RCM dynamics. Therefore, spin-up times should be longer than the smooth adjustment time to decorrelated synoptic situations. This is illustrated in Figure 4.5, where the monthly $\sqrt{2}$ TEV lines have been included as reference. As expected, surface and upper air variables adjust in a few weeks. In fact, geopotential height will adjust almost immediately, since the 2-week delay shown in Figure 4.5e is likely the time taken by the GCM circulation to decorrelate. Soil moisture takes about 3 months to reach decorrelation ($\sqrt{2}$ TEV line in Figure 4.5a). Note that the Figure includes Dec-2005, which still represents RCM internal variability levels.

Snow depth takes longer to decorrelate, since the adjustment starts in austral summer, with no snow, and $RMSD_s$ keeps low until April (mid-autumn). Then, decorrelates relatively fast, growing along with the TEV line. This is different from the spin-up process, which efficiently uses the summer months to reset the snow cover fields.

Interestingly, for soil moisture, inter-slice differences between S2 and S1 stabilize at the $\sqrt{2}$ TEV level. This means that soil moisture differences between time slices subject to the same boundary conditions are as different as those in two random days in this month (note that TEV was computed considering interannual variability). This may indicate a generally low departure from average conditions in this variable. It could also be result of insufficient spin-up. The low internal variability level

($RMSD_s(S1 - S14)$) on Dec-2005 suggests that the soil moisture spin-up for $RMSD_s(S1 - S2)$ may have not finished in Dec-2006, despite the apparent stabilization.

Precipitation also gets close to the decorrelation limit during the austral summer months. In this case, summer convective precipitation is weakly forced by the boundaries and precipitation centers are likely mislocated between slices, even if forced by the same boundary conditions.

4.3.3 Meteorological inhomogeneities: spatial distribution

In the previous sections, we summarized day-to-day changes and changes across time slices by means of spatial root mean squared differences, hiding the spatial distribution of the inhomogeneities. In this section, we look into the spatial distribution of the inhomogeneities in split simulations. For this purpose, we show as an example (Figure 4.6) the differences that make up the $RMSD_t$ peak shown in Figure 4.3a on March 1st, 2005. The results for other joints are qualitatively similar. The first column shows the observed change at the time slice joint ($D_{st}X$) for the different variables. The changes shown will stand out as a noticeable inhomogeneity (peaking in Figures 4.2 or 4.3) if (and where) D_sX (second column) is larger than D_tX (third column). The fourth column shows the change in standard deviation units ($d_{st}X$) to have a relative measure to compare different variables.

For soil moisture content (Figure 4.6, first row), as already inferred from the $RMSD_t$ time series, the change between consecutive days (D_tX) is negligible as compared to change of time slice (D_sX). The differences are located at widely distributed spots across the domain. However, only two areas concentrate the most noticeable differences, above three standard deviations. On one hand, in north-eastern Europe, discrepancies are only explained by the joint from one slice to another one, as soil moisture has a very slow response time so that their changes between consecutive days are negligible. It is not clear that these inhomogeneities are a consequence of the internal variability since the joint takes place in a transitional time where the soil moisture reaches the full equilibrium and internal variability starts to dominate (Figure 4.4). On the other hand, a remarkable and extensive region with large differences emerges in northern Africa. These high values are a result of our standardization. Over areas where the variability is very small, such as very dry regions, very small absolute changes lead to huge relative changes in standard deviation units.

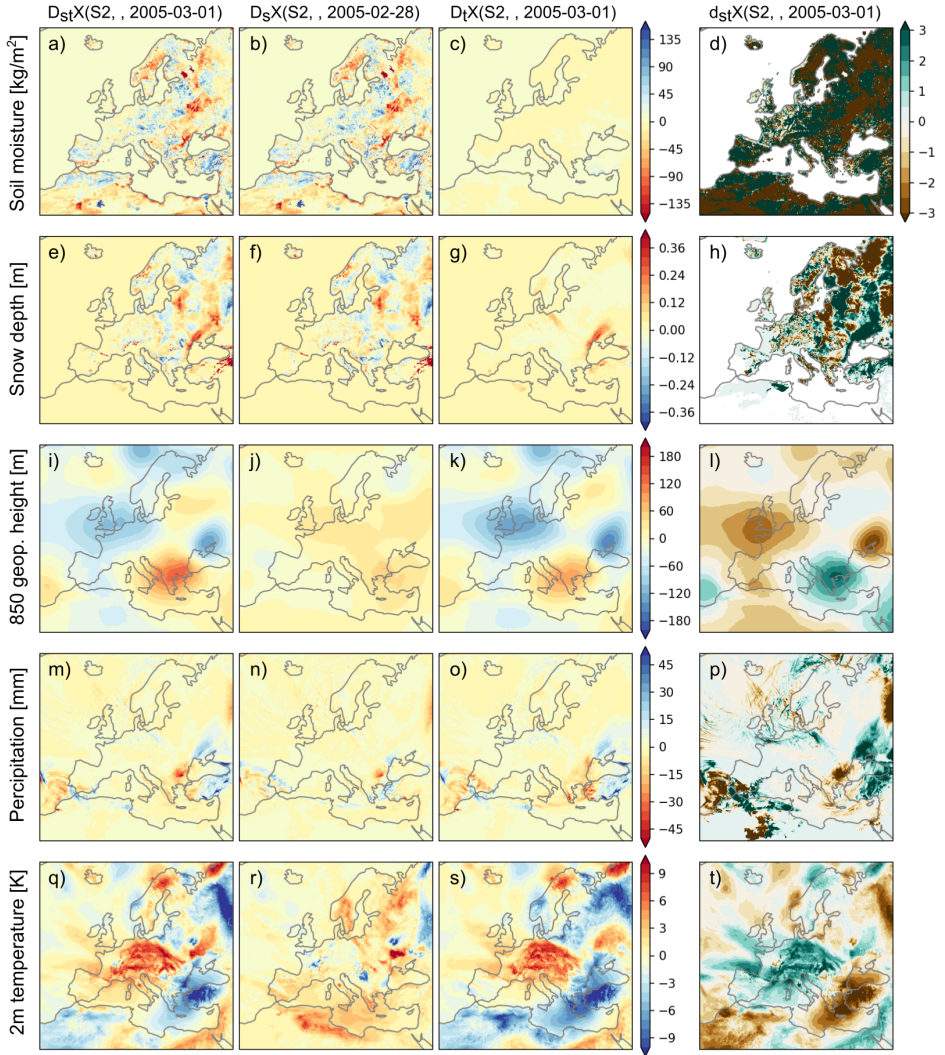


Figure 4.6: Spatial distribution of differences (Equations 4.1-4.3 and 4.5) for EUR-15 at the joint from 28th February ($t - 1$) to 1st March, 2005 (t) between slices S2 (s) and S1 ($s - 1$). From left to right: $D_{st}X(s, n, t)$, $D_sX(s, n, t - 1)$, $D_tX(s, n, t)$, and $d_{st}X(s, n, t)$. Note that the latter is non-dimensional and the same colorbar is used for all variables (from top to bottom): total soil moisture (kg/m^2), snow depth (m), geopotential height at 850 hPa (m), daily accumulated precipitation (mm) and near-surface temperature (K).

The results for snow depth are qualitatively similar. Due to its slow response time, most of the differences occur between the slices, except for an elongated area north of the Black Sea. Since the spin-up was sufficient (Figure 4.4b), we may attribute the discrepancies between both slices to the internal variability. These snow accumulation differences between slices (Figure 4.6f) have typical depths from individual misplaced snow-fall events, such as the one north of the Black Sea, occurring on this day (Figure 4.6g). As such, unlike soil moisture, which is relatively stable, the specific spatial pattern can fully differ from one joint to another for snow depth, even considering the same season. As an example, on March 1st, 2008 (Figure A.5), the synoptic conditions over Europe barely provided any snow and, as a result, inhomogeneities in snow depth are very small. This emphasizes the role of inter-annual variability at the joint, which in turn may increase or reduce the inhomogeneities.

Four areas with differences up to two standard deviations stand out in the 850 hPa geopotential height (Figure 4.6i,l). Unlike the previous slow-varying variables, they are almost exclusively due to changing synoptic conditions between consecutive days (Figure 4.6k). Along the day, two lows develop north of France and Scandinavia, and a third low moves and deepens from the west to the north of the Black Sea. Only west of the Black Sea the inhomogeneities have a slightly larger contribution because of the joint between the two slices (Figure 4.6j), which weakens and slightly shifts north the low there. The season is again an important factor. In winter (Figures 4.6 and A.5), when boundary forcing at mid latitudes is dominant, the differences are mainly attributed to the day-to-day natural variability of the atmosphere (e.g. low pressure systems entering or moving across the domain). However, by the end of the spring, the strength of the boundary forcing decreases and internal variability increases, allowing for larger discrepancies between time slices. Thus, at the joint on June 1st, 2006 (Figure A.4), the discrepancies between the two slices are larger, as it can be observed over northern Europe.

Even though differences found in the geopotential height are small, they may affect the results in other variables, especially those that are dependent on the synoptic circulation, such as precipitation. Discrepancies between both slices in the low pressure area west of the Black Sea (Figure 4.6f) drive precipitation changes there, giving rise to inhomogeneities up to 50 mm in northern Bulgaria. These are due to a northward shift in precipitation which accompanies the corresponding shift in the low pressure system. This is observed in the other domains, as well. For example,

in SAM-44 (not shown), the joint on January 1st, 2015 exhibits extended precipitation inhomogeneities east of Brazil, driven by time slice differences in simulating a low pressure system over the Atlantic.

There is no evident effect of joining the two slices for near-surface temperature, except for some discrepancies in Ukraine that, however, are within one standard deviation. Most of the inhomogeneities are explained by the day-to-day natural change of the variable.

4.3.4 Simulated climate

In previous sections, we have shown that discontinuities in split simulations can be relatively large, especially for slow-varying variables. These discontinuities occur on individual time steps and, therefore, they should not affect the simulated climate, especially when they have been shown to be within the model internal variability. In this section, we verify the split simulation climate against that of a continuous simulation. For this purpose, we used the EUR-44 split and continuous simulations, which share the longest period (20 years) among all of our simulations (see Figure 4.1).

Figure 4.7 shows the winter (DJF) and summer (JJA) differences in the seasonal climatology for the full overlapping period 1991-2010 (first and fourth columns). All variables considered are shown in different rows and differences use a common non-dimensional scale of seasonal standard deviation units. In winter, soil moisture and snow depth show significant differences, while upper air and surface variables show much lower, non-significant differences. Differences are spatially smooth for all variables except snow depth, which shows patchy differences over snow-dominated areas in the domain. In summer (Figure 4.7, fourth column), snow depth differences vanish due to lack of snow, and somewhat larger differences arise in upper air and surface variables. Patchy Mediterranean precipitation differences are significant and consistent with a weak summer mid-latitude lateral boundary forcing and the mainly convective origin of precipitation in the area. A relative low geopotential height develops in the split simulation over northern Africa/central Mediterranean Sea, which is consistent with the relatively cold region over northern Africa.

In order to check whether these differences are consistent with low frequency internal variability or a side effect of the splitting, we computed the seasonal climatology differences for two different 10-year periods. First, the years 1991-1995 and 2001-2005 (columns 2 and 5 in Figure 4.7) are considered as years which could potentially be affected by a long term spin-

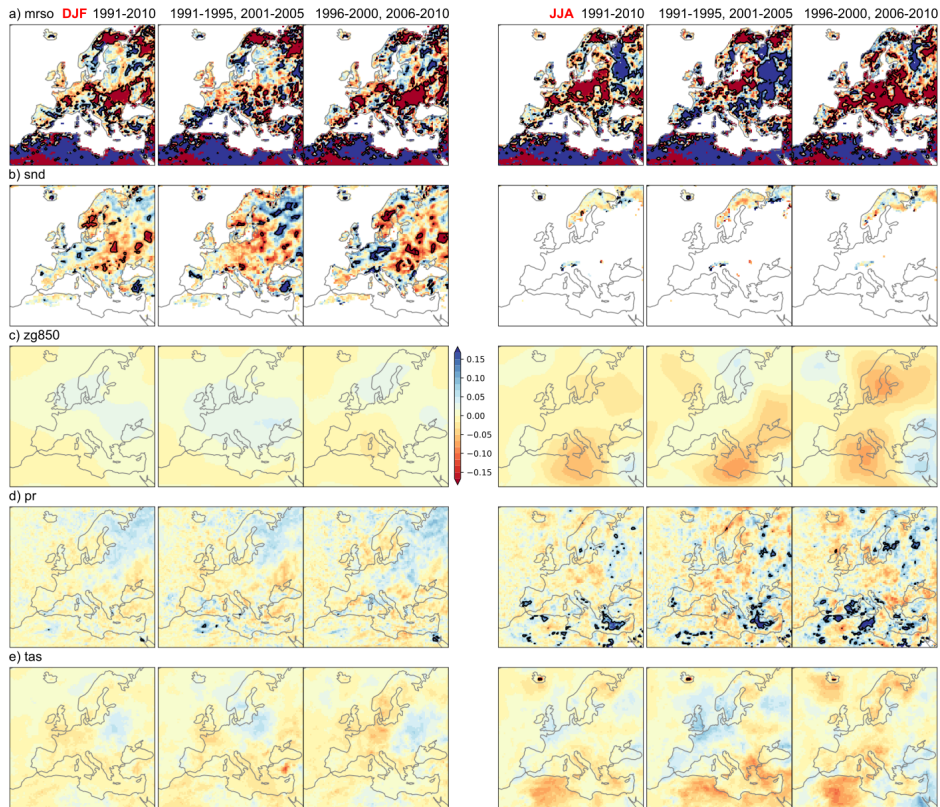


Figure 4.7: Seasonal climatology differences for different periods (in columns) and variables (in rows) between EUR-44 split and EUR-44 continuous. Differences are in non-dimensional standard deviation units. Black contours show statistically significant differences according to a two-sample t-test with 95% confidence. Snow depth (snd) differences are masked out where the variability is below 0.001 m.

up transient, since they were initialized less than 6 years before (see Figure 4.1). Second, we consider the years 1996-2000 and 2006-2010 (columns 3 and 6 in Figure 4.7) as dominated by the model internal variability, since the RCM initialization occurred at least 6 years before any of these years. Note that the 20-year seasonal climatology differences (columns 1 and 4 in Figure 4.7) are the average of these two 10-year climatology differences. In this way, differences in the long-term climatology can be ascribed to periods dominated either by potential spin-up or internal variability.

In general, no significant difference can be ascribed particularly to the period with a potential spin-up transient regime. Seasonal differences in the two 10-year periods show similar magnitudes for all variables. Moreover, some features in the 20-year climatology differences, such as summer differences in geopotential height or temperature, correspond to stronger differences during the internal variability dominated 10-year period. More or less co-located differences during the first 10-year period lead to significant differences during the full 20-year period. Patchy summer precipitation differences in the 20-year period also correspond to constructive averages with even patchier differences in the 10-year periods. The same is true for winter snow depth. This points to no spin-up transient effect in the first 10-year period, and to differences compatible with internal variability, even if statistically significant.

No systematic effect is apparent in both periods, except for the soil moisture differences over northern Africa, which are quite robust in all periods and seasons and reach several standard deviations. This is likely related to the extremely dry soils and low variability there, which would need further research. Unfortunately, for this simulations soil moisture at different depths is not available to investigate properly the source of this difference between the continuous and split runs. Differences in soil moisture over continental Europe are also fairly large (they reach about half the standard deviation). However, they are compatible with internal variability since there is no systematic location of differences across the 10-year periods. The differences found in the full 20-year period are the result of partly overlapping positive and negative differences in the other two time periods.

4.4 Conclusions

We presented a *post hoc* analysis of several regional climate simulation experiments carried out with the WRF RCM as a set of overlapping time slices. The simulations span different domains, boundary conditions, horizontal grid spacing and overlapping periods. Overlapping time slices were joined to build split simulations. Continuous simulations are available as reference to evaluate split simulations for some of these experiments. We evaluated the discontinuities in time and space introduced by this procedure at the joints of the time slices, devising a methodology to discern between insufficient spin-up and RCM internal variability effects. Finally, the effect of overlapping time slices on the regional climate was assessed.

The analysis was carried out on variables with different response times and, at the same time, variables typically saved in coordinated dynamical downscaling initiatives, such as CORDEX. For this purpose, we also focused on daily model output, commonly available in public repositories. An analysis at higher temporal frequencies would likely ease the location of meteorological discontinuities in the variables with the shortest response times (geopotential height, temperature, precipitation), which went unnoticed in our study. However, the output frequency does not affect spin-up times or seasonal climatology analyses.

We avoided spatial averaging and used root mean squared differences to highlight any mismatch between time slice simulations. The relative size of time slice switch differences with respect to daily variable tendencies only led to noticeable inhomogeneities in soil moisture. Locally, snow depth can also be used to reveal slice joints. Surface and upper air variables show larger day-to-day variations than across time slices.

Jerez *et al* (2020) showed that the optimal spin-up period is not always the longest, recommending an initialization in the warm season. We found that this depends on the region, though. As an example, unlike in Europe, the warm season in South America is also the wet season, due to deep convective events which lead to greater precipitation internal variability and, thus, more uncertain initial soil moisture conditions. The optimal starting point should therefore be found for each region to minimize the contents of slow-varying reservoirs (e.g. snow and soil water), thus avoiding gross errors in their initial levels. We also found that mismatches at the slice joints are also minimized during the warm/dry season. Therefore, a minimal overlapping time slice setup could be a 1-year spin-up period initialized at the end of the warm/dry season and entering the

split simulation one year later.

The largest and more spatially extended differences were found in total soil moisture, both regarding meteorological inhomogeneities and long term climatologies. This agrees with previous studies warning on the very long spin-up required by soil variables, and especially soil moisture (Christensen, 1999; Cosgrove et al, 2003; Yang et al, 2011; Jerez et al, 2020). We found that significant differences in the climatology over continental Europe might be ascribed to internal model variability. However, differences over low-precipitation, non-vegetated areas (northern Africa) present systematic differences which persist along the simulated period. This is likely due to initial soil moisture inconsistencies between the forcing reanalysis and the RCM equilibrium soil state over these areas. The land surface model takes a very long time to restore the equilibrium, especially from extremely dry initial conditions (Cosgrove et al, 2003). The situation is likely exacerbated due to the lack of precipitation and deep roots. A dedicated study with long-term, continuous simulations would be necessary to properly disentangle the internal variability and spin-up of soil variables in coupled simulations. Most studies on soil spin-up rely on off-line land surface model simulations (Cosgrove et al, 2003; Yang et al, 2011), where there is a target equilibrium soil moisture consistent with the prescribed atmospheric forcing. Coupled simulations, with an active soil-atmosphere feedback, are likely to develop greater internal variability with persistent anomalies in the slowest components.

For other variables, the discrepancies between the climatology in split simulations and continuous simulations can be ascribed to internal variability, even if statistically significant (e.g. for snow depth). No special effect on the climatology was found for periods closer to the initialization with respect to those farther away.

Our results are robust to interannual variability regarding the detection of meteorological inhomogeneities. Spin-up times for slow-varying variables can depend on the specific conditions of the initialization year. We showed examples with a long plateau in snow depth differences across time slices in EUR-15 in 2003 (Figure 4.4), which did not occur in other overlapping years (Figures A.1 or A.2). Also, the soil moisture spin-up time, as represented by the time to reach the internal variability limit, differs from year to year. While one year is usually enough, there are instances (e.g. 1999 in EUR-44, Figure A.3) when over two years seem necessary to reach equilibrium.

All in all, this work shows that the use of overlapping time slices to

accomplish long term regional climate simulations is a valid approach. This procedure can largely improve the efficiency of regional climate simulations, both for computationally heavy simulation (e.g. kilometer-scale simulation) or for a faster accomplishment of lower resolution runs, which do not scale efficiently to a large number of processors. Modelling workflow managers, such as WRF4G (Fernández-Quiruelas et al, 2015) —used in our simulations—, can help in the extra design, job submission and monitoring burden of this approach. In order to be on the safe side of soil spin-up, longer slices and spin-up times could be considered. For example, scenario simulations could be safely split into 30-year slices (near-, mid-, and far-future) with a 5-year spin-up each, especially if soil variables are initialized from an RCM soil climatology (Cosgrove et al, 2003; Rodell et al, 2005; Jerez et al, 2020).

Chapter 5

Synoptic forcing associated with extreme precipitation events over Southeastern South America as depicted by a CORDEX FPS set of convection-permitting RCMs

5.1 Introduction

During the austral spring and summer months, southeastern South America (SESA, Figure 5.1) is one of the regions of the world where deep moist convection presents the most extreme features (Zipser et al, 2006). In SESA, deep convection is associated with mesoscale convective systems (MCSs), which are the largest convective storms. They develop from individual convective cells which merge and organize into larger systems up to a scale of hundreds of kilometers. Extreme MCSs in SESA, with associated precipitation above the 30 mm/day (Solman and Blázquez, 2019), can account for up to $\sim 95\%$ of the summer precipitation and $\sim 70\%$ of the spring precipitation (Rasmussen et al, 2015), making these systems to be

often associated with severe weather events and, therefore, with property damage and agricultural impacts on the region.

Numerous works have studied the synoptic and mesoscale forcings that trigger deep moist convection associated with MCSs over SESA. Generally, isolated convective cells are triggered in the afternoon hours on the east side of the Andes mountain range, growing into mesoscale systems as they move eastward. They release intense showers between night hours and early morning up to finally decay in broad stratiform precipitation far east of the Andes (Rasmussen and Houze, 2011; Matsudo and Salio, 2011; Romatschke and Houze, 2013; Rasmussen et al, 2015). Salio et al (2007) showed that a higher frequency of subtropical MCSs are generated in the presence of the South American Low-Level Jet (SALLJ). This low-level flow advects warm moist air from the Amazon forest into subtropical latitudes (Figure 5.1) favouring organized deep moist convection in the region. The Andes mountain range plays a significant role in triggering deep moist convection. Insel et al (2010) concluded that high elevations of the Andes, exceeding 4 km over a large portion of the mountain range, not only guide the SALLJ into higher latitudes but also determine its intensity. Furthermore, the SALLJ penetration into higher latitudes is enhanced by mid-to-upper-level subsidence in the lee side of the Andes, that caps the low-level flow inhibiting convection up to Sierras de Cordoba (see Figure 5.1). In turn, low- to mid-level flow converges producing an optimal region for deep moist convection (Rasmussen and Houze, 2016; Salio et al, 2007). Another important feature of convection initiation is the cyclone formation on the lee side of the Andes mountain range. Rasmussen and Houze (2016) show that low-level westerly flow moving through southern Andes develops first into a trough and later into a lee cyclone that enhances northerly flow. This deepens warm moist inflow by increasing the intensity of the SALLJ and, finally, favors a strong convergence that fuels long-lived MSCs over SESA.

Given the relevance of MCSs in determining the climatic features of the SESA region and in triggering high-impact weather, it is worth exploring how these systems may respond in a warmer climate. However, modelling these extreme precipitation systems using either global or regional climate models may be challenging. The relatively small spatial and time scales of MCSs are often underrepresented in global climate models (GCMs, with grid spacing of ~ 100 km). Regional climate models (RCMs, grid spacing of ~ 10 -50 km) have been widely used to acquire more insight on the regional details that coarser GCMs cannot provide. Nevertheless, several

authors have demonstrated the difficulties that RCM simulations have in representing extreme precipitation, mainly due to the convective parameterization (Jankov et al, 2005; Prein et al, 2015, and references therein). Furthermore, RCMs available for South America systematically underestimate extreme precipitation intensity, especially in the SESA region (Solman et al, 2013; Solman, 2016; Solman and Blázquez, 2019). Computational advances made possible the implementation of high resolution convection-permitting (CP) RCMs, where deep convection is not parameterized but explicitly resolved. CP-RCMs, with spatial resolutions higher than 4 km (Weisman et al, 1997), have proved to better represent the diurnal cycle of convective summer precipitation, the intensity of extreme precipitation events and orography-triggered convection in both short-range and climate simulations (Weisman et al, 2008; Matsudo et al, 2015; Grell et al, 2000; Prein et al, 2013; Mahoney et al, 2012; Kendon et al, 2012). A recent study from Vergara-Temprado et al (2020) showed that even at coarser resolutions (up to 25 km), convection explicitly resolved is able to perform similarly or better than simulations parameterizing convection for some model skills.

Moreover, the increased spatial and temporal resolution of CP-RCMs facilitate the understanding of the behavior of the climate system at scales most relevant to policy makers. Due to the high computational costs, few groups have started implementing CP-RCMs under climate change scenarios (Kendon et al, 2014, 2016; Mahoney et al, 2012, 2013; Ban et al, 2015; Fosser et al, 2016; Coppola et al, 2020). Single-model CP-RCM simulations showed intensification and higher frequencies of subdaily heavy precipitation events that were not simulated by their driving RCM over the UK (Kendon et al, 2014). Mahoney et al (2013) showed that local maxima of extreme precipitation events over the Colorado Mountain Range could increase in a future climate. For an extensive review on climate CP-RCM simulations, see Prein et al (2015).

Despite the auspicious latest results of RCMs at convection permitting resolutions, there are still many processes that need to be parameterized. This makes CP-RCM results highly model-dependent. Therefore, a coordinated ensemble-model approach is recommended in order to assess the uncertainties and reliability of CP-RCM climate simulations. In this sense, the World Climate Research Program's (WCRP) Coordinated Regional climate Downscaling Experiment (CORDEX) Flagship Pilot Studies (FPS) program (Gutowski et al, 2016) aims, among several other targeted topics, for subcontinental coordinated CP simulations in or-

der to develop high resolution climate change information. This study is framed under the CORDEX-endorsed FPS “Extreme precipitation events in Southeastern South America: a proposal for a better understanding and modelling” which allowed building a consortium of several modelling groups for producing an ensemble of CP-RCMs with the aim of better reproducing extreme precipitation events associated with organized convective systems (Bettolli et al, 2021).

The synoptic-scale forcing exerts a dominant control in the development of organized convection and extreme rainfall over SESA. Therefore, the main objective of this study is to assess the quality of the simulated synoptic triggering mechanisms associated with extreme precipitation events over SESA in CP vs parameterized convection (non-CP) simulations. Two major questions motivate this main objective: To what extent simulating extreme precipitation events is limited by the cumulus parameterization?; Does high resolution have any impact on the local circulation leading to deep convection? In order to tackle these problems, three extreme precipitation events occurring during an anomalous spring/summer period were selected and a 3-member multi-model ensemble was produced in two modes: Weather Like (WL) and Climate Mode (CM), following Coppola et al (2020). WL consisted of short simulations of each extreme event while CM is a 6-month simulation of the extended summer season that includes the three extreme precipitation events selected. With these two sets of simulations, a secondary objective is to assess the capability of CP simulations of a set of individual events in WL simulations vs. climate simulations at CM. A more general overview of the capability of these CP simulations together with a set of statistical downscaling approaches in simulating individual extreme rainfall events can be found in Bettolli et al (2021).

5.2 Data & methods

The selection of the three extreme precipitation events is based on the analysis of the observational record from station data available over the SESA region for the period 1979-2015. Days with daily rainfall above the 95th percentile were first identified, considering rainy days only (days with precipitation above 1 mm per day). Then, the number of events were analysed for each extended warm season and the season with the largest number of events was selected. The particular events were chosen from

this subset of extreme events. Details of the spatial coverage of the observational data sets used can be found in [Bettolli et al \(2021\)](#). The events selected occurred in the extended summer of 2009-2010, an anomalous period regarding frequency and intensity of extreme precipitation events. Namely, the events took place in February 2010 (Case 1), January 2010 (Case 2) and November 2009 (Case 3). All three cases reached daily precipitation above 150 mm/day. Their precipitation intensity and spatial distribution are described with further detail in Section 5.3.

5.2.1 Observational data sets

Given the gaps of gauge measurements in the region, we used three different precipitation data sets to account for the observational uncertainty in our model evaluation. Since we are interested in peak convective rainfall and its spatial extent, we considered only data sets providing gridded sub-daily precipitation. Precipitation estimates are taken from the NOAA Climate Prediction Center (CPC) morphing method (CMORPH), which uses infrared sensor information from geostationary satellites to propagate the shape and intensity of precipitation estimates obtained from passive microwave (PMW) sensors onboard low Earth orbiting satellites. Essentially, the same satellite observations are considered by the PERSIANN (Precipitation Estimation from Remotely Sensed Information using Artificial Neural Networks) data set but, in this case, using an artificial neural network to fill the gaps in the PMW estimates. We also considered the Multi-Source Weighted-Ensemble Precipitation (MSWEP) data set, which combines information from several rain gauge-based data products, satellite products (CMORPH, among others) and reanalysis data (ERA-Interim). Several authors have assessed the uncertainty of the observational data sets based on satellite measurements in the SESA region (e.g. [Palharini et al, 2020](#); [Salio et al, 2014](#), among others). Moreover, when considering estimates of extreme precipitation from satellite data, the uncertainty in both the maximum intensity and the spatial coverage of the events can be quite large in the region ([Palharini et al, 2020](#)).

We evaluated not only precipitation, but also the key synoptic forcings associated with deep moist convection over SESA. Reference circulation and moisture fields were obtained from the European Center for Medium Range Weather Forecasts (ECMWF) ERA-Interim reanalysis. The uncertainty in the reanalysis is taken into account by considering also the National Centers for Environmental Prediction reanalysis (Reanalysis-1)

Dataset	Horizontal res.	Time res.	Time period	Reference
CMORPH	0.25°	3h	2003-present	Joyce et al (2004)
PERSIANN	0.25°	3h	2000-present	Nguyen et al (2019)
MSWEP	0.25°	3h	1979-2015	Beck et al (2018)
ERA-Interim	0.75°	6h	1979-2019	Dee et al (2011)
JRA55	0.56°	6h	1958-present	Kobayashi et al (2015)
Reanalysis-1	1.875°	6h	1948-present	Kalnay et al (1996)

Table 5.1: Datasets used in this study.

and the Japanese 55-year (JRA55) reanalysis (See Figures A.10-A.12 in Appendix A). The temporal and spatial resolution, time period covered and a reference for each of the data sets are summarized in Table 5.1.

5.2.2 Regional climate models

We used a 3-member ensemble composed of the Regional Climate Model version 4 (RegCM4; Giorgi et al, 2011) and two different versions (3.8.1 and 3.9.1) of the Weather Research and Forecasting (WRF) model (Skamarock et al, 2008), configured also with different physical parameterizations. WRF v3.8.1 was run by Universidad de Cantabria, matching exactly the setup (UCAN-WRF381BI) used in the EURO-CORDEX FPS on Convective phenomena at high resolution over Europe and the Mediterranean (FPS-CONV; Coppola et al, 2020). An alternative WRF setup (using version 3.9.1) was run by Centro de Investigaciones del Mar y la Atmósfera (CIMA-WRF391) and differs essentially in the parameterization of deep convection, surface layer and planetary boundary layer processes (Table 5.2). RegCM was used by Universidade de Sao Paulo (USP-RegCM4) and configured using the same physical options as RegCM4-ICTP in Coppola et al (2020). Note that, despite using two WRF configurations, the experimental set up for this model does not focus on the uncertainty associated with a given parameterization choice, as in Coppola et al (2020). The choice of physical schemes in the two WRF simulations is based on different criteria: CIMA-WRF391 uses the in-house model configuration for the area, while the UCAN-WRF381BI configuration has been transferred as-is (Takle et al, 2007) directly from the FPS-CONV in Europe.

All models run in a nested domain configuration using Mercator projection. A high-resolution (4 km) convection-permitting domain centered over La Plata basin (SESA) was nested into a coarser resolution (20 km) domain over central South America (CSAM). These domains cover the re-

Param. scheme	CIMA-WRF390	UCAN-WRF381BI	USP-RegCM4
Radiation	RRTMG	RRTMG	CCM3
Microphysics	WDM6	WDM6	SUBEX (CSAM), WSM5 (SESA)
Cumulus conv.	Kain-Fritsch	Grell-Freitas	Tiedke (land), Kain-Fritsch (sea)
Shallow conv.	-	GRIMS	-
Land Surface	NOAH	NOAH-MP	CLM4.5
PBL	MYJ	MYNN2	Holtslag
Surface-layer	ETA-Sim	MYNN	M-O

Table 5.2: Physical parameterizations used by each ensemble member. Note that the cumulus parameterizations shown were only active in the outer (CSAM) domain. See [Skamarock et al \(2008\)](#) and [Giorgi et al \(2011\)](#) for further details and references for each scheme.

spective common analysis domains (Figure 5.1) after removing the boundary relaxation zone. The deep convection parameterization was switched off in the SESA domain. Initial and boundary conditions for the coarser-resolution domain were taken from ECMWF 6-hourly ERA-Interim Reanalysis ([Dee et al, 2011](#)) fields at 0.75° horizontal resolution.

The experimental setup considered short-term (weather-like, WL) and long-term (climate mode, CM) simulations spanning the three selected heavy precipitation events. On the one hand, WL simulations were initialized around 24 hours before the occurrence of each event, which aimed at reproducing the events as close to reality as possible. The proximity in time of the initial condition constrains the simulation, acting as a source of predictability. On the other hand, CM was a 6-month simulation starting on October 1st 2009 and covering the complete wet season in SESA, including the three events. Unlike WL, initial conditions in CM are no longer a source of predictability for any of the events, as the simulation is not mainly driven by the initial conditions but by the information entering through the boundaries, in line with the regional climate modelling approach. It should be noted that, due to computational constraints, the multi-model ensemble in CM is composed of only 2 members (USP-RegCM and UCAN-WRF) which, however, is the minimum to cover multi-model uncertainty. Note that the number of modelling groups currently in FPS-SESA and their computational resources are much less than in other FPS, especially FPS-CONV in Europe, where 27 modelling groups and 6 different modelling systems are involved ([Coppola et al, 2020](#)). This will have an impact in the robustness of our results.

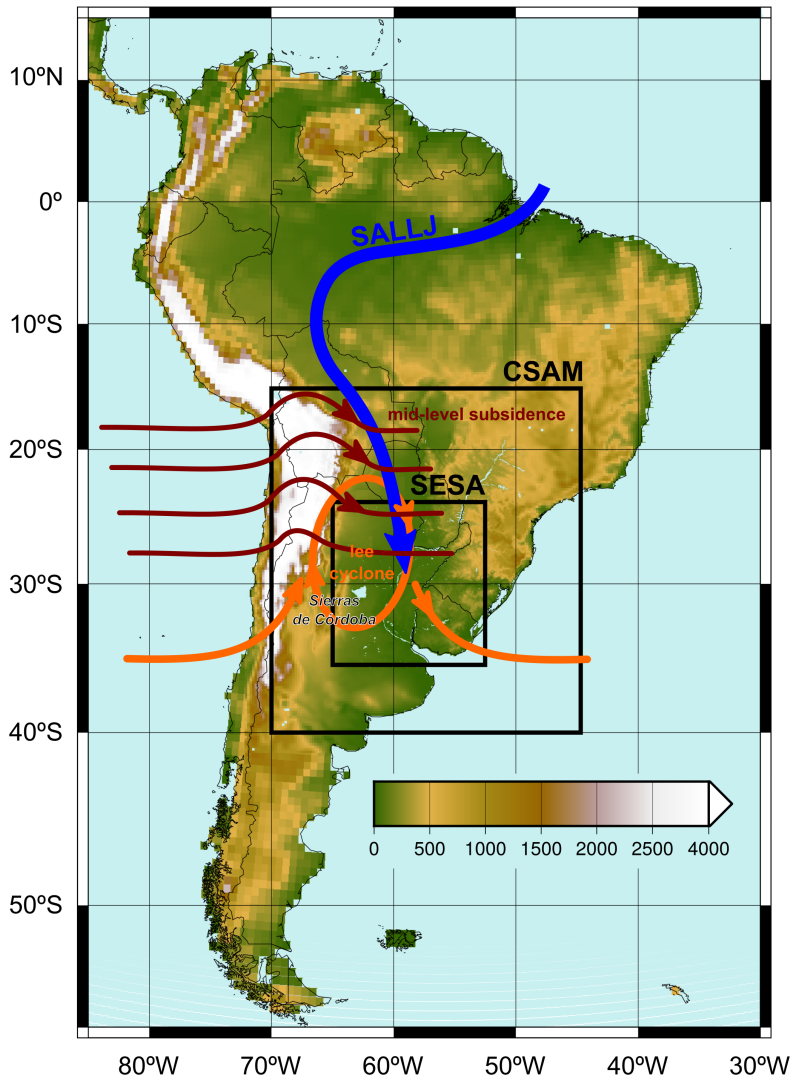


Figure 5.1: Analysis domains over central South America (CSAM) and Southeastern South America (SESA). A schematic depiction of the drivers of MCSs over SESA is also shown (adapted from [Rasmussen and Houze, 2016](#)). Blue arrow represents the low-level jet, red arrows refer to mid-to-upper level flow and orange arrows represent the low-level flow associated with the lee cyclone over Sierras de Córdoba.

5.2.3 Evaluation metrics

In this work, we characterized the low-level circulation by means of the meridional wind field and geopotential height at 850 hPa. These fields are associated with the intensity and occurrence of the SALLJ together with the low-level circulation, favouring the development of the cyclone leeward of the Andes. Additionally, the Vertically Integrated Moisture Flux Convergence (VIMFC) at low-levels, which contributes to organize convective precipitation, was computed from ERA-Interim using the meridional wind and moisture fields at 925, 850 and 700 hPa pressure levels. It is important to bear in mind that mid- and high-level circulation patterns are also relevant for the initiation and further development of organized convection leading to extreme precipitation events over SESA (Salio et al, 2007; Rasmussen and Houze, 2011, 2016). However, since the differences between CP and non-CP simulations are expected to be mainly at the lower levels of the atmosphere, our evaluation and analyses are focused on near surface variables.

The performance of the simulations in capturing extreme precipitation events was evaluated using the maximum 6-hourly accumulated precipitation during the whole event. Thus, the location, distribution and intensity of the simulated precipitation field were compared against each of the observational data sets. This was done both qualitatively, comparing maps of the spatial distribution of the precipitation maxima, and quantitatively, by computing spatially-averaged measures of precipitation flux and intensity. Intensity was quantified by averaging only those grid cells where precipitation occurred.

All data sets and simulations were interpolated to a regular latitude-longitude grid of $0.2^\circ \times 0.2^\circ$ spatial resolution covering a common spatial domain over central South America (CSAM in Figure 5.1). We used a bilinear interpolation scheme for all fields. This interpolation implies an upscaling of the CP 4-km spatial resolution simulations and, therefore, an apparent loss in high resolution information. However, it is still expected that high resolution information is transferred into the upscaled lower resolution domain (Torma et al, 2015; Fantini et al, 2018). There are also works showing that the improvement from upscaled high resolution information could also be potentially achieved by means of bias adjustment methods (Casanueva et al, 2016).

5.3 Results & discussion

5.3.1 Case studies: peak precipitation

The three selected cases are characterized by very high rates of convective precipitation. The discharge of the peak of precipitation is usually during the night or before sunrise, when synoptic conditions favour moist deep convection over La Plata basin. Although they share the same synoptic origin, each event has distinctive features which are discussed next.

Case 1 occurred between February 19th to 21st, 2010, and extended across the border between Argentina and Uruguay. The observations registered the 6-hourly maximum peak of precipitation on February 20th between 06 and 12 UTC (Figure 5.2). Observational data sets agree on the location of the event, but discrepancies are remarkable regarding precipitation intensity and spatial extent (Figure 5.2, top row). Spatially-averaged precipitation over the SESA region ranges from 5.4 (MSWEP) to 12.5 mm (PERSIANN). Precipitation intensity, as measured by the average precipitation rate over wet ($P > 0.1$ mm) grid cells, exceeds 26 mm in CMORPH and PERSIANN, while it remains slightly over 9 mm in MSWEP. Peak rainfall ranges from 45 mm exhibited by MSWEP to above 90 mm by PERSIANN. The resulting precipitation field is very similar, with PERSIANN showing spatially smoother precipitation extending over slightly larger areas. MSWEP, based on a weighted average of different precipitation sources (satellite, gauge and reanalyses) shows significantly less precipitation. This diverse behaviour of the observational databases is observed to some extent in the three cases analyzed, which indicates that observational uncertainty is not negligible. Inspection of the low-level circulation features along the lifecycle of this system (not shown) suggests the presence of a cold front progressing from the southwest inducing forced uplift that, together with the northerly low-level wind advecting wet and warm air into the SESA region, triggers the convection. Precipitation observations (Figure 5.2, top row) show this frontal rainfall band extending over the ocean. This feature was reproduced in all simulations. Indeed, both CP (4 km) and non-CP (20 km) simulations in WL tend to generate precipitation with frontal features, developing a northwest-to-southeast long band extended from the La Plata estuary and southern Uruguay to the Atlantic Ocean. In general, CP simulations showed higher rainfall intensities, closer to those observed. The coarser non-CP simulations showed lower intensities, especially in WRF members, since the precipita-

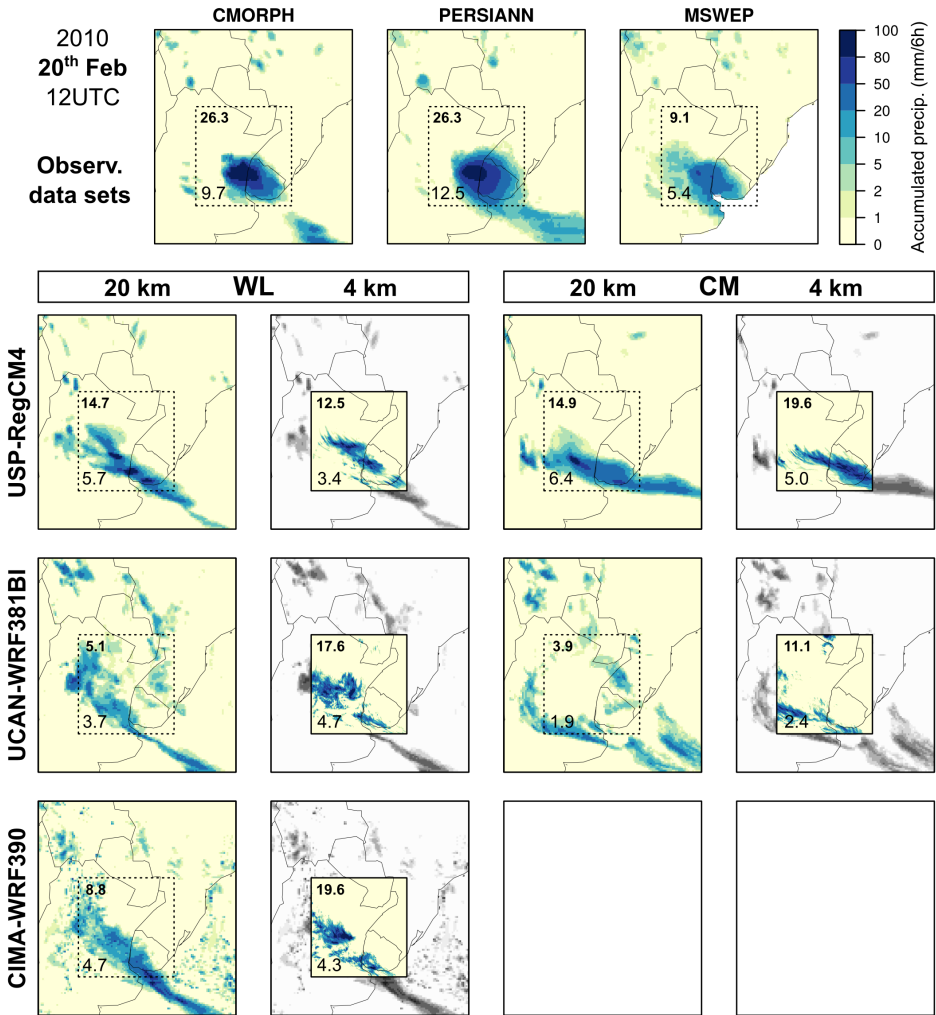


Figure 5.2: Accumulated 6-hourly precipitation (mm) on February 20th, 2010 between 06 to 12 UTC. Results for both CSAM (20km) and SESA (4km) domains are plotted for each ensemble member. These are displayed in weather-like (first and second columns) and climate mode (third and fourth columns). As reference, CSAM results are replicated (desaturated) around those of the SESA domain. Observational datasets (top) are shown only in the CSAM domain. Numbers in SESA denote the spatially-averaged precipitation rate (below) and the spatially-averaged precipitation rate over wet ($P > 0.1$ mm) grid cells (above) in this area.

tion spreads over larger areas. Total rainfall amounts over the SESA region were similar in CP and non-CP simulations, but the former concentrated higher peaks of precipitation in smaller areas. This is a characteristic feature of CP simulations that was previously noted by [Prein et al \(2015\)](#) and it is observed in all the three cases. Similar conclusions are derived from CM, as frontal features are clear in both sets of simulations. Peaks of maximum precipitation were also enhanced and centered over smaller areas at CP resolutions. When compared to observations, CP simulations in WL mode placed better the maximum, next to the border between Argentina and Uruguay. However, the maximum of these simulations in CM were located south of Uruguay.

Case 2 extended over a large area from the border between Argentina and Paraguay to the border between Brazil and Argentina. It occurred in the period from January 18th to 19th, 2010. The event developed the maximum 6-hourly precipitation rate on January 19th between 00 and 06 UTC. Again, there is a strong observational uncertainty, with 6-hourly intensities reaching up to 100 mm in PERSIANN and less than 50 mm in MSWEP (Figure 5.3). All models in WL showed two maxima in non-CP simulations, at a similar location (west of SESA) in both WRF members but southeasterly shifted in USP-RegCM, with a maximum over eastern Uruguay. This spatial pattern differs from observations. Strong discrepancies between the models were also found in CP simulations. Regarding CM, the 6-hourly accumulated precipitation patterns presented a maximum over La Plata basin, reaching up to 100 mm in CP simulations, with the location of maximum precipitation slightly shifted as compared with observations.

The event referred to as Case 3 was observed from November 21th to 22th, 2009. It consisted of a deep convective system affecting southern Brazil. The 6-hourly maximum precipitation occurred on November 22th between 06 and 12 UTC and extended mainly over southern Brazil. It is worth noting from Figure 5.4 that the observational uncertainty regarding the maximum intensity is smaller compared to the other cases, ranging from 50 to 80 mm. Simulations in WL mode reproduced most precipitation in southern Brazil but with some differences by placing the maximum, shifted out of the SESA domain in USP-RegCM. Unlike Case 2, models at CP resolution simulated a similar location of the maximum. Except for UCAN-WRF generating a secondary maximum over Uruguay, they placed most precipitation in southern Paraguay and northeastern Argentina. With the exception of UCAN-WRF, which reached higher in-

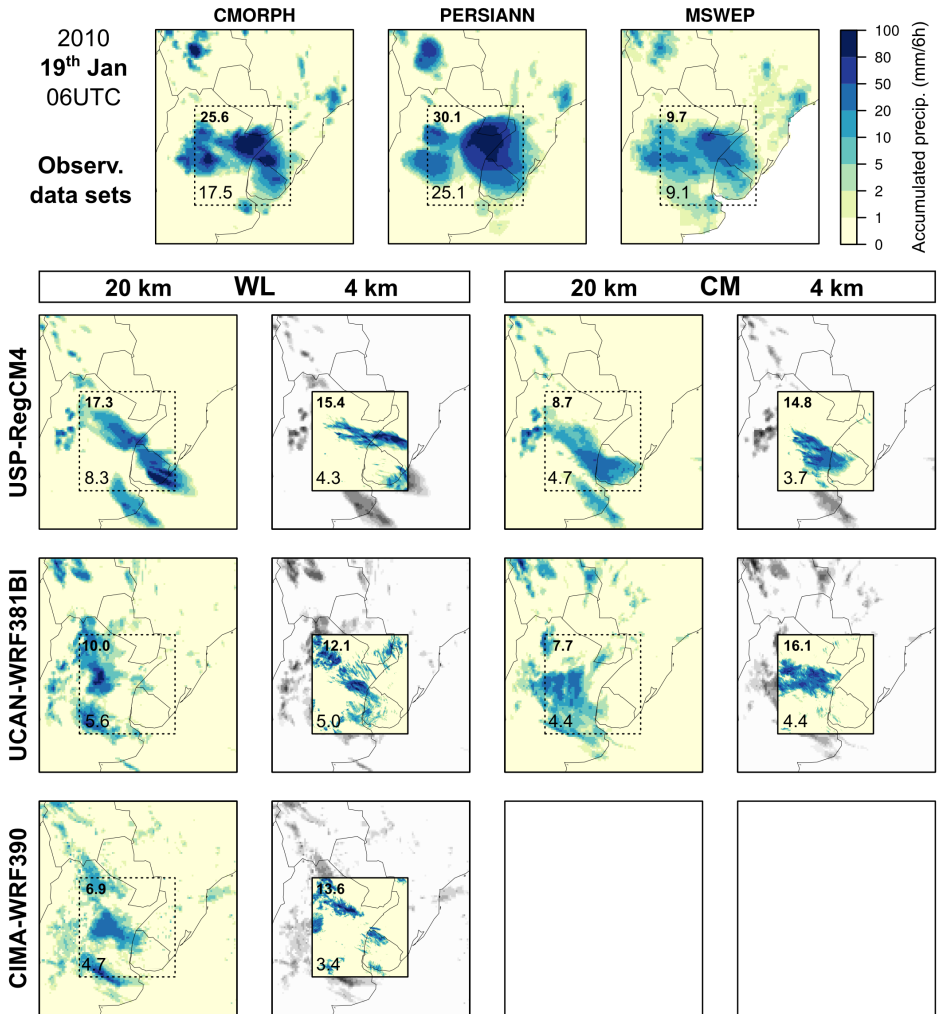


Figure 5.3: As Figure 5.2, but for Case 2.

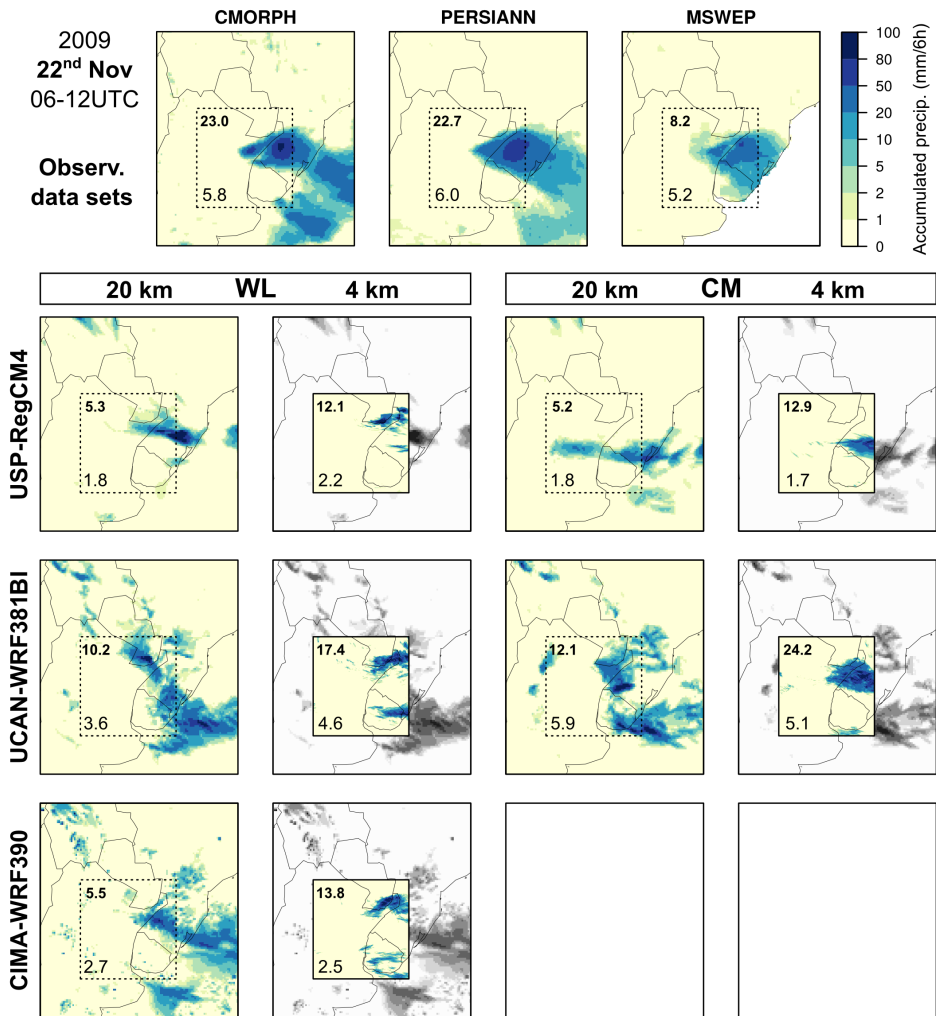


Figure 5.4: As Figure 5.2, but for Case 3.

tensities compared to the other models, mean precipitation over the SESA area and intensities of rainy pixels barely differed among the models. On the other hand, the results from CM show that CP simulations placed the maximum over southern Brazil, whereas they disagree regarding non-CP simulations. Interestingly, the former simulations captured the location of the maximum even better than in WL mode. Nevertheless, the most striking result emerging in both Case 2 and Case 3, is that the largest discrepancies were found between CP and non-CP simulations. Indeed, the former not only enhanced the intensity of the maximum, but also strongly modified its location. To a greater or lesser extent, this is also observed in CM.

It is worth noting that given the discrepancies among observational datasets in terms of the spatial extension and the intensity of the events, it is quite difficult to quantitatively assess model performance, since the skill of the models will strongly depend on which dataset is considered as the reference. Hence, the observational uncertainty poses an additional limitation towards assessing the capability of the models in reproducing the main features of extreme rainfall events in the region.

5.3.2 Synoptic forcing mechanisms

In order to understand the physical mechanisms explaining why the models are able (or not) to reproduce the main features of the selected extreme precipitation events, the synoptic forcing mechanisms associated with the development of deep convection over SESA were explored. The evaluation gave rise to very similar results in the three case studies, so here we only consider Case 3 (Figure 5.4). Observational uncertainty in this event is smaller than in the others, so the analysis is also more reliable. Corresponding analyses for Cases 1 and 2 are found in Appendix A (Figures A.6-A.9). The study focuses on the synoptic situation occurring 6 hours before the maximum of the event shown in Figure 5.4.

Figures 5.5 and 5.6 summarize the low-level circulation and low-level moisture flux convergence 6 hours before peak precipitation. After analysing the spatial distribution of the VIMFC for each of the individual case studies, it was found that the largest values were collocated with the maxima precipitation occurring 6 hours later. Accordingly, in order to identify a threshold for VIMFC associated with the occurrence of the precipitation peak, a test on different spatial percentiles of the VIMFC (not shown) was performed in order to match the pattern of maximum

accumulated precipitation 6 hours later. Results showed that the isoline for percentile 98 presents the best correspondence. Thus, in this study we consider this percentile (VIMFC98) to focus on VIMFC values leading to extreme precipitation.

Weather-like experiment

ERA-Interim Reanalysis (Figure 5.5, top row) places the mechanisms that favour deep convection over La Plata basin: a low pressure area favoured by a trough located in southern Bolivia and contributing to the extension of the SALLJ southward. Indeed, maximum meridional wind at 850 hPa, the northerly wind associated to the SALLJ coming from Amazonia, reaches high intensity (above 20 m/s) over Bolivia and Paraguay. Further south, the geopotential height at 850 hPa exhibits a deep low pressure system over Uruguay. Given these synoptic components, ERA-Interim exhibits large areas of VIMFC98 extending across northern Uruguay and Argentina. The same synoptic mechanisms are observed in JRA55 and NCEP Reanalysis 1 (See Figures A.10-A.12 in Appendix A). Nevertheless, relative differences are found in NCEP in terms of the magnitude of the geopotential height and the location of maximum meridional wind at 850 hPa, which extends further south than that in the other reanalysis. Similarly, NCEP exhibits a notably different pattern of VIMFC98. Similar discrepancies are found, to a greater or lesser extent, in Case 1 and Case 2.

All non-CP simulations captured a low pressure area leeward the Andes exhibiting similar magnitude as ERA-Interim, although slightly deeper in UCAN-WRF and CIMA-WRF. The wet and warm flow coming from Amazonia with maximum meridional wind at 850 hPa over Bolivia and Paraguay, referred to as SALLJ, was apparent in all simulations, though there was a notable extension of the northerly wind towards southern Brazil in WRF models. The non-CP simulations also agree on reproducing a deep low over Uruguay but with some differences in terms of its intensity. UCAN-WRF exhibited a deep low pressure system 50 m more intense than that in the reanalysis, whereas USP-RegCM depicted similar magnitude but showing an east-west stretched pattern. These differences in the low pressure system modulated the distribution of the low-level wind and, hence, had an impact on the moisture flux convergence. Note that all non-CP simulations located the maximum VIMFC over southern Brazil, where they placed the precipitation peak 6 hours later. It can be clearly

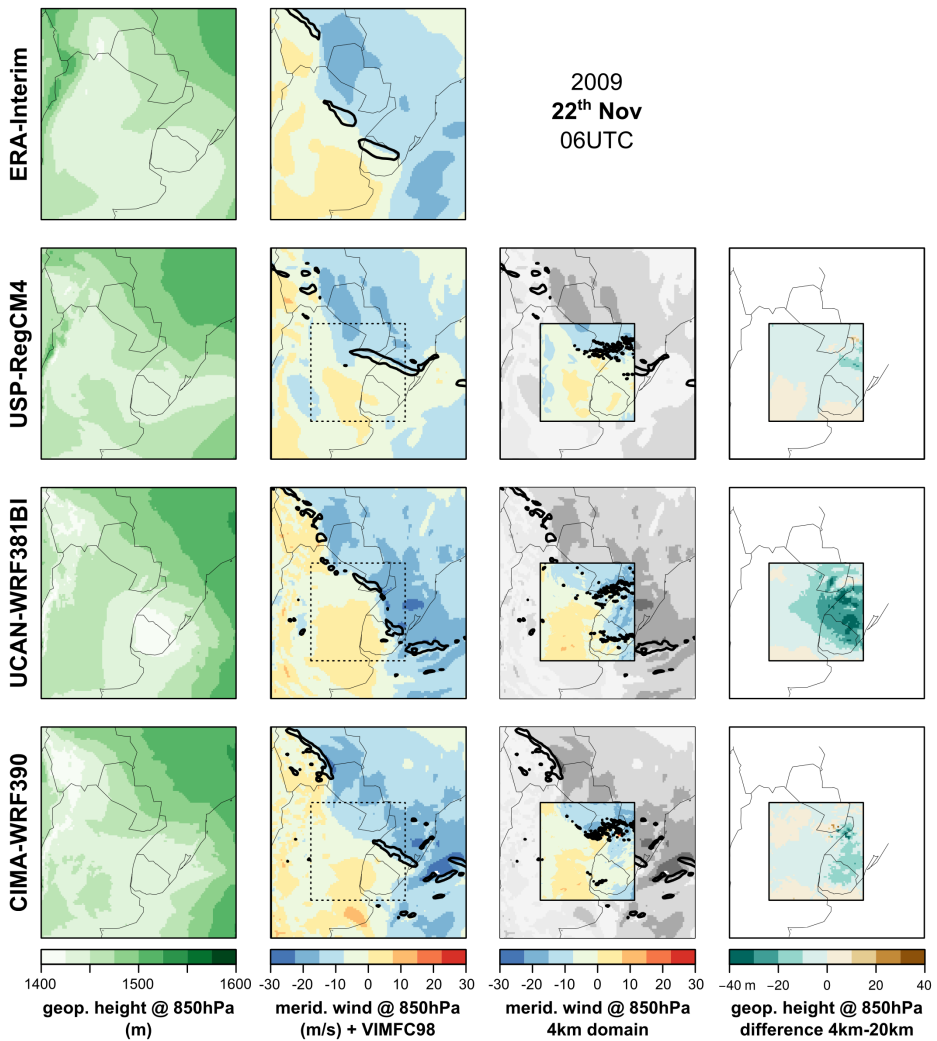


Figure 5.5: Synoptic drivers for WL simulations on 2009 November 22th at 06 UTC (Case 3). For each ensemble member, from left to right: Geopotential height at 850 hPa (m) in the CSAM domain, meridional wind at 850 hPa (m/s) for both CSAM and SESA domains and difference in geopotential height at 850 hPa (m) between CP and non-CP simulations. Black isolines on top of meridional wind panels show the 98th percentile of the vertically integrated moisture flux convergence (VIMFC98).

noted that the extent of the pattern of VIMFC98 is co-located with the distribution of precipitation maxima (displayed in Figure 5.4) occurring 6 hours later. This clear correspondence between the two fields is observed in all the members, in both CP and non-CP simulations. Therefore, VIMFC emerges as one important footprint of deep moist convection development in the models, independently whether convection was parameterized or not. Overall, all non-CP simulated a similar pattern of VIMFC, which is consistent with their capability of capturing adequately the observed maximum rainfall.

At upper levels, the synoptic components required to produce deep convection were also captured in all the models. Thus, geopotential height at 500 hPa (not shown) exhibited a short-wave negative anomaly (trough) centered south of SESA, whereas the zonal wind at 200 hPa (not shown) extended from the east of the Andes to the exit of the SALLJ over Uruguay. It produced the required divergence at upper levels that triggers the deep convection in accordance with convergence at lower levels (Salio et al, 2007).

The most striking feature found in the CP simulations is that they differed from their lower resolution driving counterparts not only on the simulated precipitation but also on the low-level circulation. CP simulations seem to strongly modulate the atmospheric circulation going into the domain through the boundaries (Figure 5.5, last column), despite the relatively small domain size and the short-term simulation. At these resolutions, models tend to strengthen the deep low pressure system over Uruguay. This was especially noticeable in UCAN-WRF, where the low pressure system was up to 40 m deeper. This strengthening implied in turn differences in the associated meridional wind as compared to that in the non-CP. Accordingly, discrepancies arose in the pattern of VIMFC98 as well. However, all CP simulations agree on locating the maximum VIMFC over northeastern Argentina, where the models produced the precipitation peak 6 hour later (Figure 5.4). The differences of VIMFC98 between CP and non-CP simulations could only be explained by the model deepening of the low pressure system, since the flux of humidity coming from Amazonia was ensured by the boundary data forcing from the non-CP domain. Note again that the differences in the spatial distribution of the areas of maximum moisture flux convergence between the CP and non-CP simulations drove the differences in the simulated precipitation. Therefore, the low-level circulation arises as a key element to produce the corresponding convergence that is fundamental for triggering convection

and, consequently, extreme precipitation. The result agrees with previous studies that highlight the importance of the SALLJ and the low-level circulation to initiate and to develop deep convection in SESA (Cerón et al, 2020; Giles et al, 2020).

Climate mode

Similarly to WL, non-CP simulations in CM (Figure 5.6) captured the synoptic-scale features needed to trigger convection 6 hours later. All models reproduced the low pressure system leeward to the Andes, favouring the extension of the SALLJ southward. Thus, the core of the SALLJ was captured with a maximum (~ 30 m/s) between Bolivia and Paraguay. On the other hand, the interaction between upper level divergence and lower level convergence was also captured by reproducing the deep low over Uruguay. However, its magnitude was again model-dependent, with UCAN-WRF yielding the deepest one. As a consequence, northerly meridional wind is more intense and extends well southward. The synoptic configuration favoured VIMFC98 to extend over northern Uruguay towards Argentina. A secondary area of high values of VIMFC developed over southern Uruguay in UCAN-WRF, likely associated with a deeper low.

At CP resolutions, the differences in the spatial pattern of the 850 hPa geopotential height as compared with the non-CP were more evident than in WL. It is noticeable the deepening of the low in UCAN-WRF, above 40 m more intense than that in the non-CP simulation. Thereby, the meridional wind at 850 hPa is modified so that the largest VIMFC values are shifted to southern Brazil, where the model placed the precipitation peak 6 hours later. The role of the CP modifying the large-scale features was also observed in USP-RegCM. Nevertheless, unlike UCAN-WRF, the CP displayed a weakened low over Uruguay and the northerly wind was enhanced southward, placing the maximum VIMFC over southern Brazil. Clearly, we can extract from this analysis that the two CP simulations agree on extending the VIMFC98 area over southern Brazil, where precipitation peak was observed. The mechanisms for which the low pressure system is strongly modified in the CP simulations are not clear. However, unlike the WL, these differences in the CM resulted in the improvement of the simulated extreme precipitation.

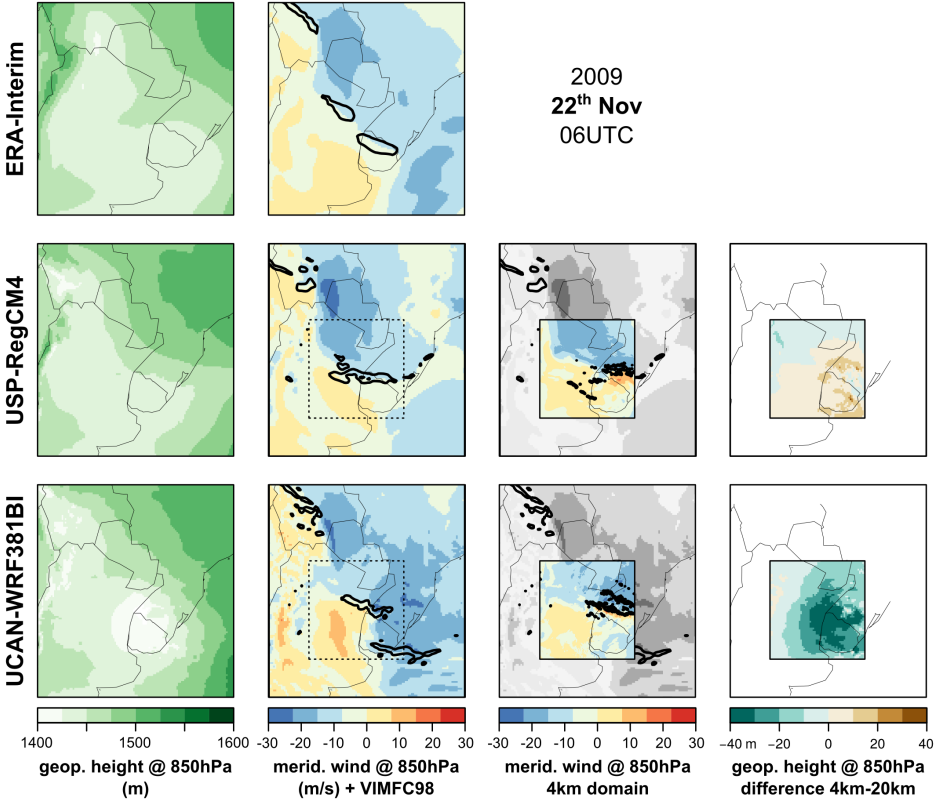


Figure 5.6: As Figure 5.5, but for CM simulations.

Weather-like vs. Climate mode

VIMFC is driven by low-level circulation features together with the moisture distribution, whose magnitudes are strongly affected by the intensity of the low pressure system generated over La Plata basin. There is an agreement among the ensemble members to place the low-level pressure system properly in both WL and CM simulations, but with different magnitudes. Depending on the model, CP simulations modulated this pressure system by weakening or deepening it. Despite the different physical configurations and models, members in each mode tend to depict a preferential region of VIMFC98. Indeed, major discrepancies were mainly found when comparing both modes. It could be explained by the fact that this mechanism is strongly determined by the synoptic pattern, which in turn depends on the lead time of the simulation.

As seen previously, CM simulations of Case 3 were able to reproduce extreme precipitation in terms of magnitude and location in both models. In spite of the longer lead time, these simulations properly captured the synoptic triggering mechanisms that force deep convection. In [Coppola et al \(2020\)](#) the comparison between WL and CM was carried out in order to use the former as a reference. However, in our study, WL presented more difficulty with capturing synoptic forcings as the peak of the event was eventually misplaced. This is observed across the different models and physical configurations. We speculate that the complex orography of the Andes and surrounding areas is not sufficiently well represented by the coarse resolution of the reanalysis (~ 75 km). Therefore, the low-level flow used as initial conditions in WL simulations could be more unrealistic than the flow developed by the CM simulations. Despite CM simulations are also forced by the reanalysis, they are long enough to develop a better interaction with the orography.

Similar conclusions can be inferred from the other cases (see Online Resource 2 in [Lavin-Gullon et al, 2021a](#)). The CP simulations strongly modify the circulation in both Case 1 and Case 2, more remarkable in Case 2. This is clearly observed in WL mode. As an example, non-CP simulation from USP-RegCM generated a non-observed low pressure system over Uruguay that was even strengthened in the CP simulation. In turn, the modification of these large-scale features lead to differences of VIMFC between CP and non-CP simulations. As observed in Case 3, the VIMFC emerges as an important imprint of deep convection development.

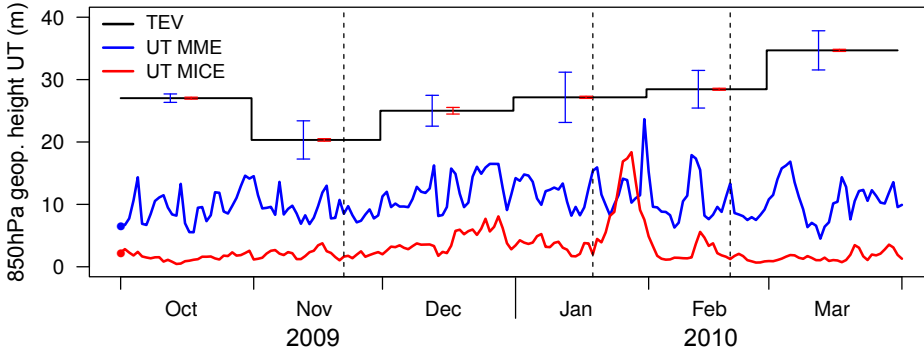


Figure 5.7: Inter-member variance in time (UT) for 850hPa geopotential height (m) in CSAM-20 of experiment CM (from 1st October, 2009). The uncertainty is computed separately for MME (blue) and MICE (red). Transient-eddy variability (TEV, black line) was computed from the UCAN configuration and error bars show its standard deviation for MME and MICE. Dashed lines indicate the three selected cases.

Multi-model uncertainty vs. Internal variability

The analysis in CM must be put in perspective to discern how internal variability is affecting the results. TEV presents higher values in the austral winter, so that boundary forcing is higher in this season. However, a comparison between the multi-model ensemble and an additional MICE (Figure 5.7) shows that multi-model uncertainty exceeds internal variability for the whole year, with a remarkable exception arising at the end of January 2010. Here, internal variability clearly exceeds the multi-model uncertainty. The 850 hPa geopotential height fields exhibit strong discrepancies between the MICE members by simulating a low-pressure system East of Uruguay (not shown). Similarly to the observed in EUR-15 (see Section 3.3.1), MICE exhibits mixed results, with two members differing in the magnitude and location of the event and another member missing it. The spatial distribution of the inter-member variance for the peak in 28th January, 2010 (Figure 5.8) reflects these discrepancies with high internal variability over Uruguay and East of Uruguay. Nevertheless, it is important to note that internal variability is lower than multi-model uncertainty in the three cases, so that we cannot attribute the differences described in Sections 5.3.1 and 5.3.2 to the internal variability. On the other hand, the behaviour of the internal variability is transmitted from

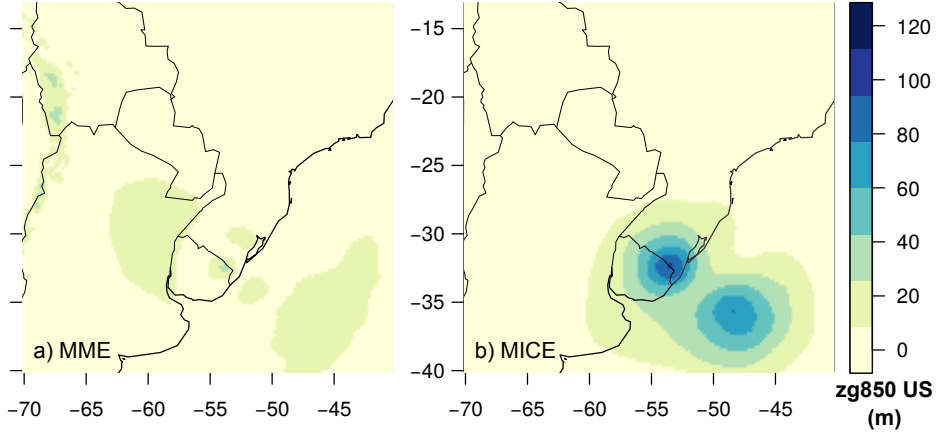


Figure 5.8: Spatial distribution of the inter-member variance (US) for the 850 hPa geopotential height (m) in CSAM-20 of experiment CM. The results are shown for 28th January, 2010 in a) multi-model ensemble. b) multi-initial-conditions ensemble.

CSAM-20 to the CP domain (SESA-4) and as a consequence, the results in both domains are qualitatively similar (not shown).

5.4 Conclusions

We analysed RCM ability in reproducing the mechanisms behind extreme precipitation over the SESA region. The simulations consisted of two different RCMs run in two modes (WL and CM) and in two nested domains at 20 km and 4 km spatial resolutions. The latter is a so-called convection-permitting resolution and, therefore, the deep convection parameterization was deactivated. We focused mainly on three extreme precipitation events and considered three observational data sets to account for observational uncertainty. We paid particular attention to peak 6-hourly rainfall during each event. Forcing mechanisms, identified in previous studies, were characterized by means of the low-level circulation and moisture transport from reanalysis and compared to model results.

The main conclusions derived from these analyses can be summarized as follows:

- All simulations captured the mechanisms favoring deep convection

over La Plata basin. This was observed in both resolutions, CP and non-CP, and modes, WL and CM.

- As compared to parameterized-convection simulations, convection-permitting simulations reproduce higher precipitation intensities but centered over smaller areas, in agreement with other studies (Prein et al, 2015; Kendon et al, 2012, among others).
- A strong correspondence between the vertically integrated moisture flux convergence and the generation of extreme precipitation 6 hours later was identified in each simulation, independently on whether convection was explicitly resolved or not. As a result, we could consider VIMFC as one important footprint of deep convection.
- Discrepancies among members are found in the location of the synoptic patterns, which leads to discrepancies in the moisture flux convergence and, hence, in the simulated precipitation pattern.
- Convection-permitting simulations strongly modulated the flow of forcing data coming from the parameterized simulation. Surprisingly, this was observed in both modes in spite of the small size of the domain.
- Based on the case study approach, it is apparent that the evaluation of simulated extreme precipitation events in the region is challenging due to the large uncertainty in observational datasets available, most of them based on satellite products, given the scarcity of in situ observations.
- There is a clear added value in CP simulations in terms of the capability of capturing the spatial distribution of extreme precipitation in SESA and the corresponding triggering mechanisms.
- Internal variability seems not to play any important role in the results of the selected extreme precipitation events. However, some peak of increased internal variability was found and therefore, the analysis for other periods must be taken with caution.

Besides these relevant results, several questions arose from the analysis. One of these questions is related to understanding the causes behind the poor performance of WL simulations. Another important issue, not

evaluated here, is related to the timing of the peak precipitation in CP versus non-CP. There are several examples of CP simulations in the literature that highlight a major improvement in the representation of the diurnal cycle of precipitation (e.g. [Kendon et al, 2012](#), and references therein). These issues will be tackled in a separate study. SESA region is a unique natural laboratory for developing high impact weather systems leading to extreme precipitation accounting for the interaction of dynamical forcings with the complex Andes orography, the Sierras de Córdoba topographic features, the SALLJ and the large-scale baroclinic systems affecting the area. Further studies are needed to better understand the added value of CP in reproducing these triggering mechanisms that may help to improve the simulation of deep moist convection and, hence, extreme precipitation events. These convection mechanisms are one of the main differences with respect to the study by [Coppola et al \(2020\)](#). In SESA, the role of the Andes orography in placing the synoptic components that favour deep convection is more decisive than in the Alps. Also, our target region is not centered on the mountain range (unlike the Alps in [Coppola et al \(2020\)](#)), but to the lee, well beyond the Andes.

Finally, it should be noted that this study is based on a limited number of coordinated CP simulations which may limit the robustness of the results. Moreover, the analysis is based on a few individual cases which may also impact on the conclusions. However, even based on a limited number of events and models, a clear message arises from the case study approach that helps identify why CP and non-CP simulations differ. In order to draw more robust conclusions, future work should focus on increasing the number of models and the length of CP-simulations (to include at least interannual variability) in the area. An improved ensemble design (e.g. including a sensitivity study on the effect of relevant model components, such as shallow convection) would help in better understanding model-to-model differences. Another venue for enlarging the ensemble of convection-permitting simulations with a moderate computational cost is the use of a coarser resolution, since recent results ([Vergara-Temprado et al, 2020](#)) show that RCMs might explicitly develop realistic convective processes at much coarser resolutions than those typically considered.

Chapter 6

General Conclusions

This thesis deepens on quantifying different sources of uncertainty that arise in regional climate modeling. The investigation is carried out by means of multi-physics and multi-model ensembles generated under two CORDEX FPS. We quantify against the noise of internal variability the uncertainty from multi-physics and multi-model ensembles at different timescales. For slow-varying variables, an adequate timescale is key to consider the required spin-up time. In this sense, we analyze the internal variability in split simulations, where this uncertainty is distinguished from the effect of spin-up time. In turn, the impact of splitting simulations on the simulated climate is analyzed. The study is extended to also cover domain and horizontal resolution uncertainties. Simulations from both CORDEX FPS initiatives are focused on convective heavy precipitation events, and therefore, we explore the synoptic mechanisms that lead to extreme precipitation, paying especial attention to the results at convection-permitting resolution. In particular, we search for footprints which determine the onset of deep convection.

Detailed conclusions of these assessments are found in each Chapter. Here, we provide a general overview of the main conclusions for each of the objectives presented in Section 1.6.

- *Simulate the regional climate of heavy precipitation areas at very high, convection-permitting resolution using a state-of-the-art RCM.*

The CORDEX FPS-Convection and FPS-SESA initiatives offered an opportunity to coordinate very high, convection-permitting multi-model ensembles. In this thesis, we have contributed to all the evaluation simulations in both initiatives. Large multi-physics and

multi-model ensembles have been used to simulate the climate of areas of occurrence of heavy precipitation events.

Synoptic mechanisms that favour deep convection were captured in all the standard resolution, parameterized convection domains. However, discrepancies were found regarding the location of the synoptic patterns. This is key, since the different results generated by the ensemble members led to discrepancies reproducing the events at convection-permitting resolution. Interestingly, it was observed that convection-permitting resolution may modulate the low-level atmospheric circulation from the parameterized convection domain and as a result, to modify the location of maximum precipitation.

- *Quantify the role of different uncertainty sources. Namely, horizontal resolution, domain uncertainty, internal variability, multi-physics and multi-model uncertainties.*

In this thesis, we quantify different sources of uncertainty, with an especial emphasis on the internal variability, as a hint of the relative size of the other uncertainties. Internal variability has been demonstrated to be decisive to explain the variability of atmospheric variables, where multi-physics uncertainty may be of comparable magnitude to internal variability. Here, uncertainty arising from perturbations of the model physics are seen from the circulation point of view as perturbations of initial conditions. However, for surface variables, the effect from internal variability is less relevant and it is more feasible to discern the multi-physics uncertainty from internal variability. In agreement with previous RCM internal variability studies, an increased (decreased) uncertainty emerged in summer (winter) together with a spatial pattern of enhanced uncertainty towards the outflow boundaries of the domain.

The quantification of multi-model uncertainty showed that its magnitude exceeds internal variability. This was observed for atmospheric variables in the standard CORDEX South America domain. Nevertheless, short periods of enhanced internal variability emerged, with internal variability exhibiting similar magnitude than that of multi-model uncertainty.

For simulations that are divided into time slices, the magnitude of the meteorological inhomogeneities at the joints depends on the domain. In this sense, domain uncertainty should be considered as at-

mospheric conditions over a particular region may lead to dry or wet conditions and in turn, to reduce or increase the inhomogeneities.

On the other hand, results showed that internal variability is not sensitive to the horizontal resolution and in turn, horizontal resolution does not seem to play any major role in the model spin-up and inhomogeneities of split simulations.

- *Explore the uncertainty associated to the initialization of variables with long response time, and their impact on the time slicing of costly RCM simulations.*

Our work confirms that splitting simulations into time slices is valid to improve the efficiency of costly RCM simulations or to speed up lower resolution simulations which do not scale to a large number of processors. In the simulated regional climatologies we mainly found a potential impact of splitting simulations in soil moisture, albeit attributed to internal variability.

The analysis showed that long-response time variables, such as soil moisture or snow depth, present the largest meteorological discontinuities at the joints of split simulations. In addition, these variables exhibited the largest and more spatially extended meteorological inhomogeneities. Unlike surface and upper air variables, where discontinuities went unnoticed, long-response time variables can be used to reveal slice joints.

The optimal time to switch between time slices strongly depends on the season. In order to optimize the spin-up period, the starting point should be selected so that the content of slow-varying reservoirs (e.g. soil water) is minimized. Besides, our results showed that interannual variability is an important factor, as spin-up times of slow-varying variables may depend on the specific conditions at the initialization year.

- *Improve the understanding of the mechanisms leading to heavy precipitation events.*

Both FPS-Convection and FPS-SESA provide two target regions with different synoptic features giving rise to extreme precipitation, although they have in common the important role of orography. In particular the Andes, which determines the strength of the South American Low Level Jet and in turn, the occurrence of extreme

events in southeastern South America. In this region, we found that the largest values of vertically integrated moisture flux convergence were collocated with precipitation maxima occurring 6 h later, that is, a strong correspondence between the vertically integrated moisture flux convergence and the later generation of extreme precipitation was identified. This was observed regardless of whether convection was explicitly resolved or not. As a result, vertically integrated moisture flux convergence arose as an important footprint of deep convection. Nevertheless, the climate conditions in the target domains determine the forcing mechanisms leading to heavy precipitation events, so that the generalization of the results to other domains should be taken with caution.

Appendix A

Supplementary figures

A set of figures with supplementary information for different chapters is provided in this appendix. They are as other figures in the body of the thesis, but for different dates, seasons, etc. They are all referenced when appropriate in the main text.

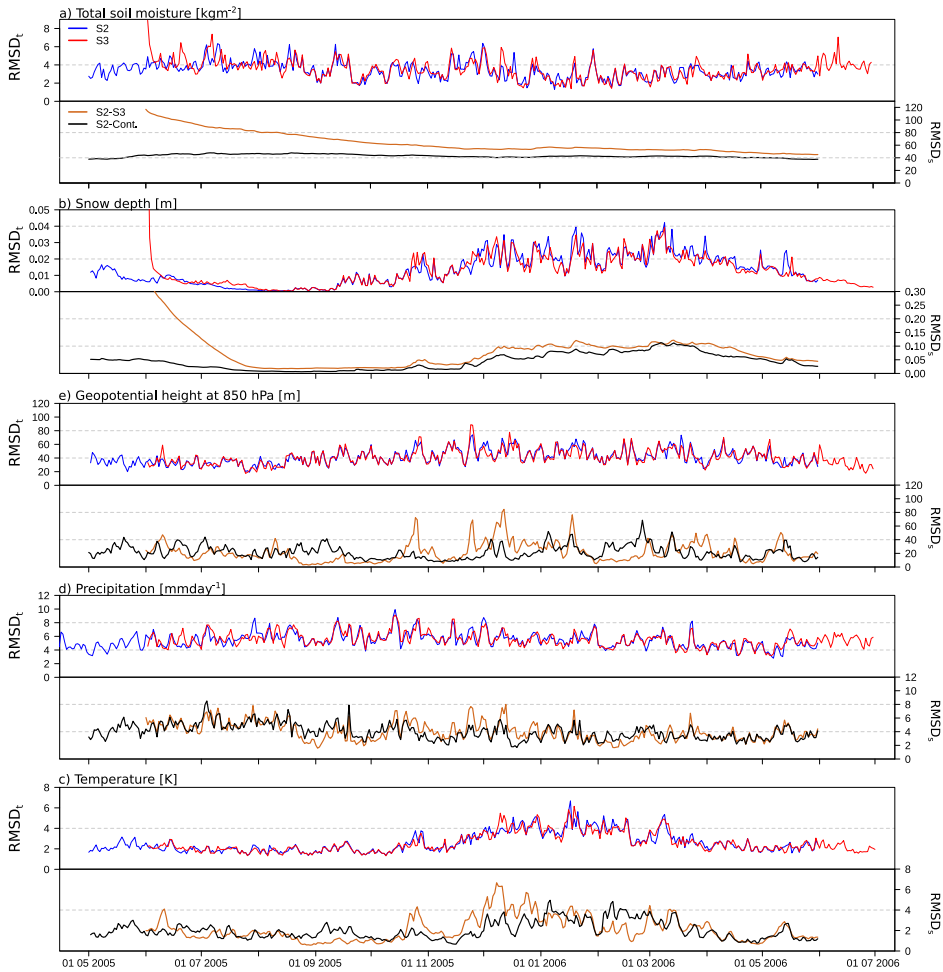


Figure A.1: As Figure 4.4, but for overlapping time slice simulations S2 and S3.

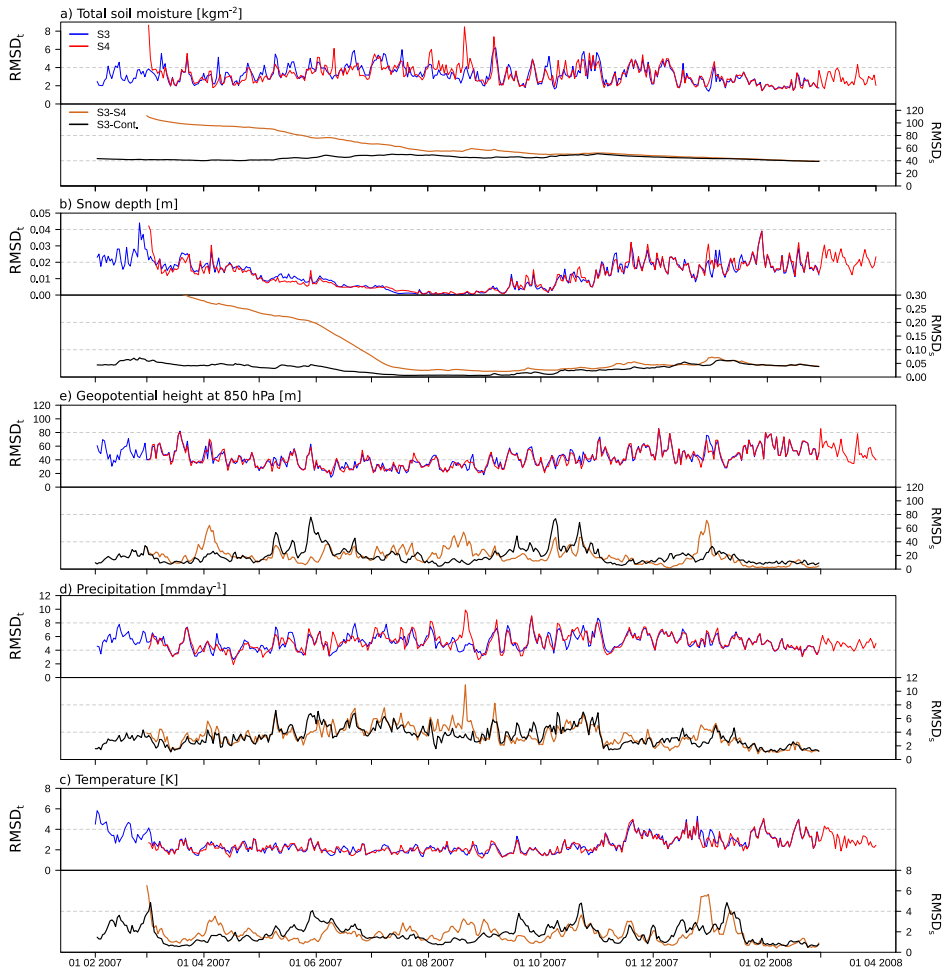


Figure A.2: As Figure 4.4, but for overlapping time slice simulations S3 and S4.

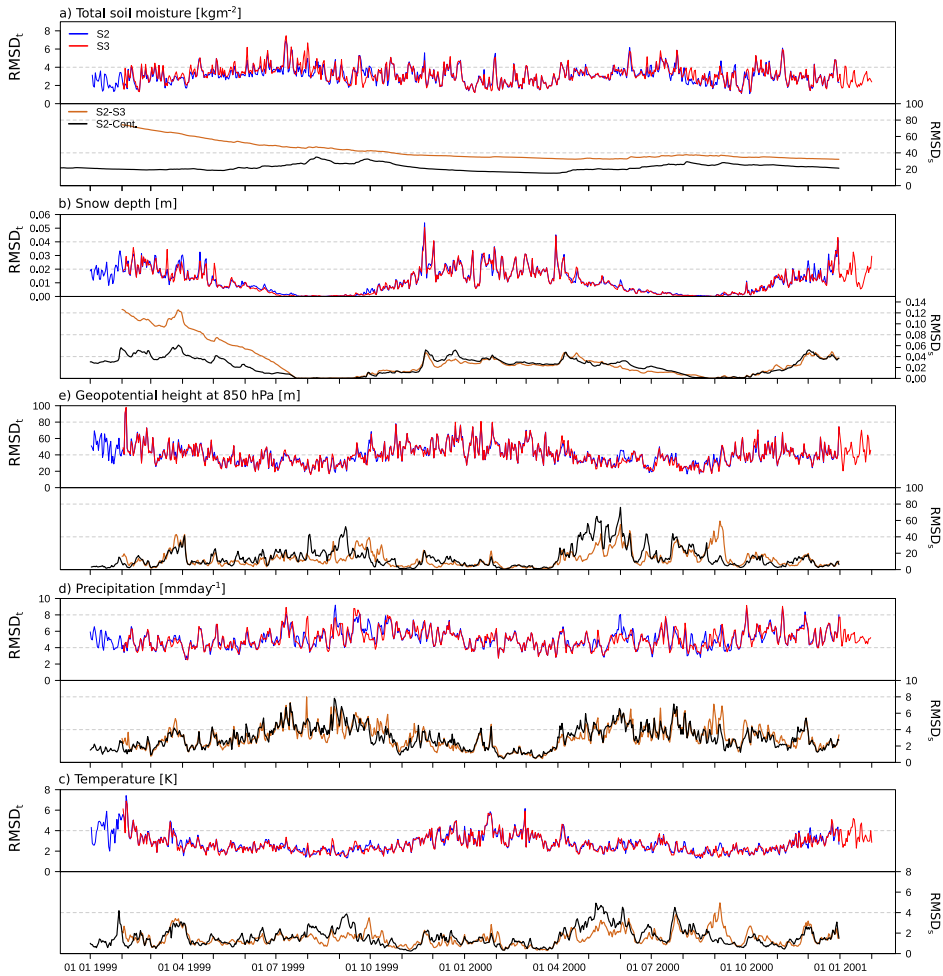


Figure A.3: The same as Figure 4.4 but for the EUR-44 domain, and slices S2 and S3.

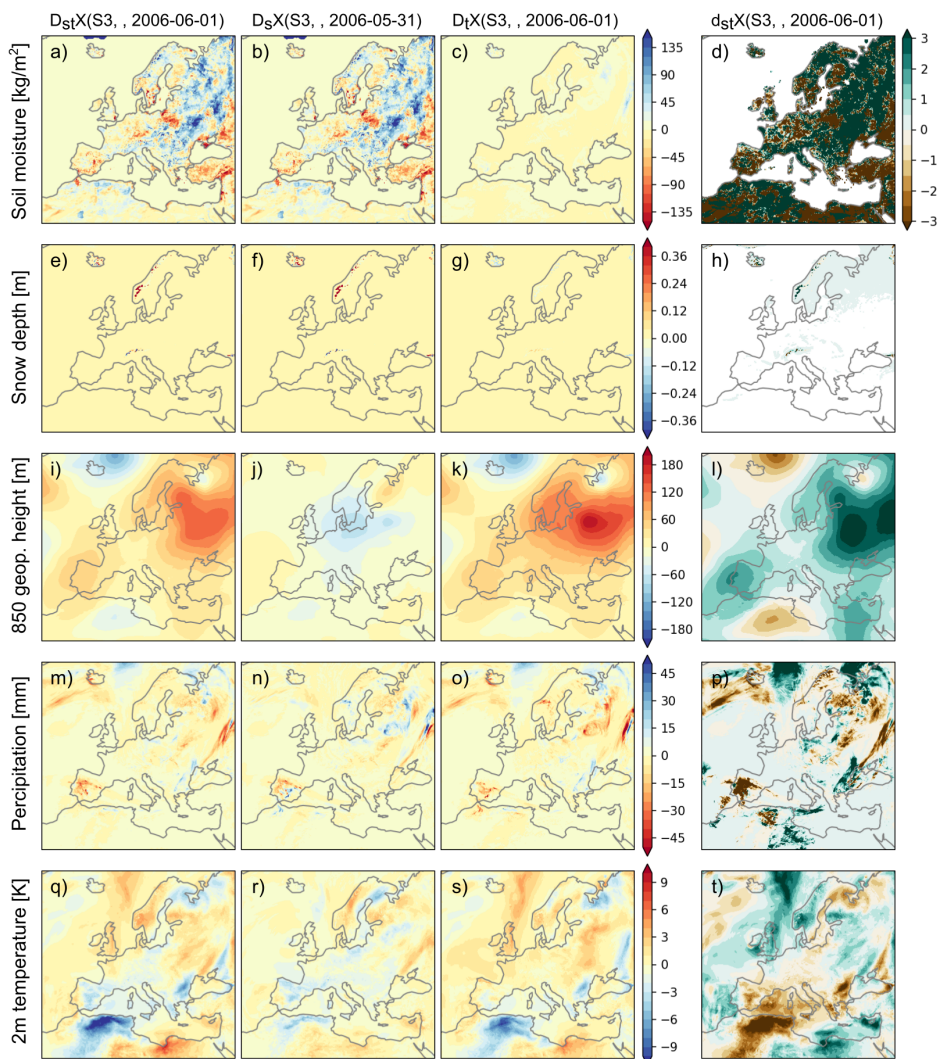


Figure A.4: As Figure 4.6 but for the joint between S2 and S3 (1st June, 2006).

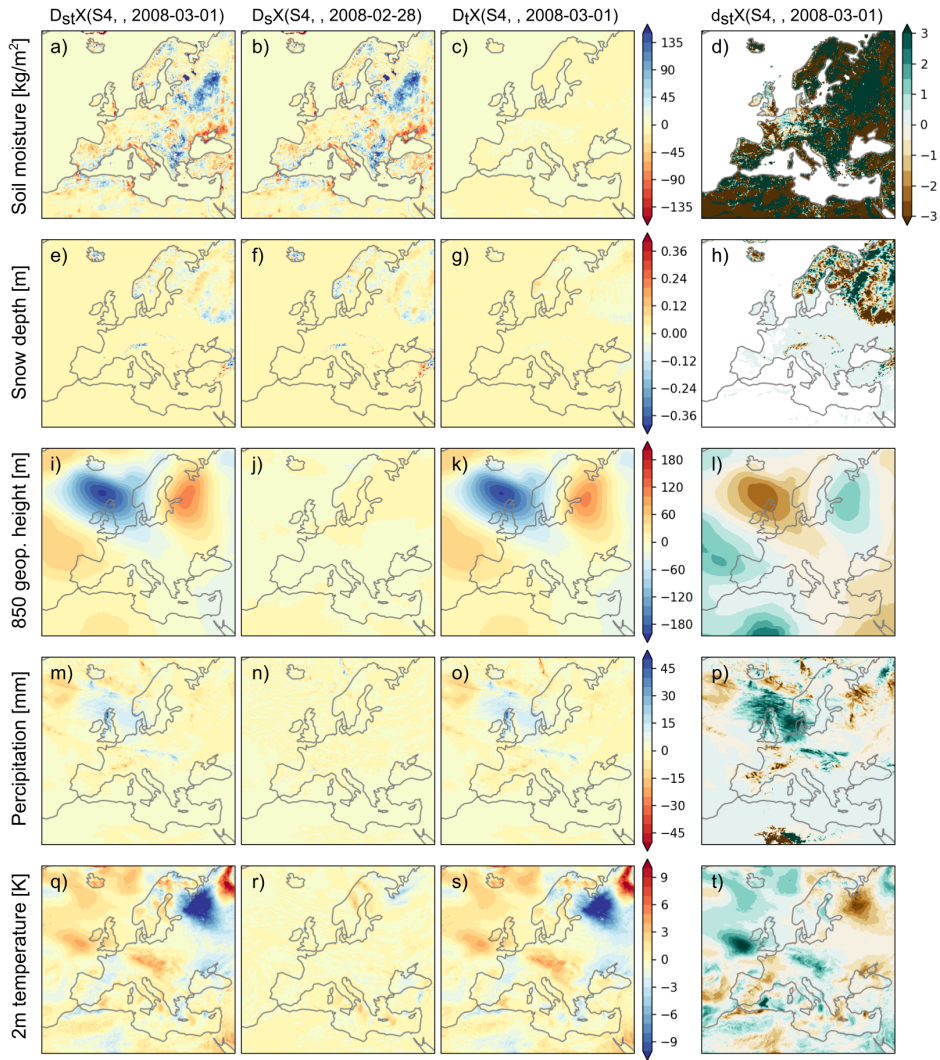


Figure A.5: As Figure 4.6 but for the joint between S3 and S4 (1st March, 2008).

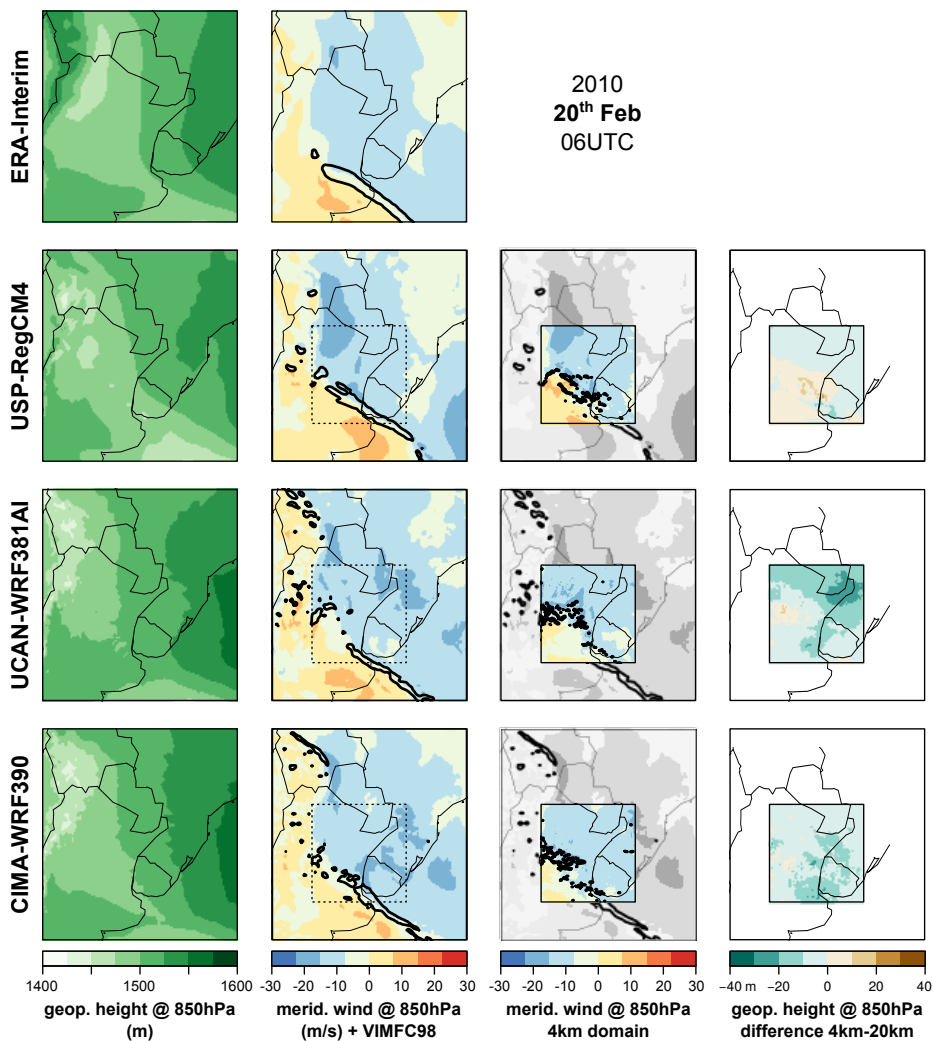


Figure A.6: Synoptic drivers for weather-like simulations on 2010 February 20th at 06 UTC (Case 1). For each ensemble member, from left to right: Geopotential height at 850 hPa (m) in the CSAM domain, meridional wind at 850 hPa (m/s) for both CSAM and SESA domains and difference in geopotential height at 850 hPa (m) between CP and non-CP simulations. Black isolines on top of meridional wind panels show the 98th percentile of the vertically integrated moisture flux convergence (VIMFC98).

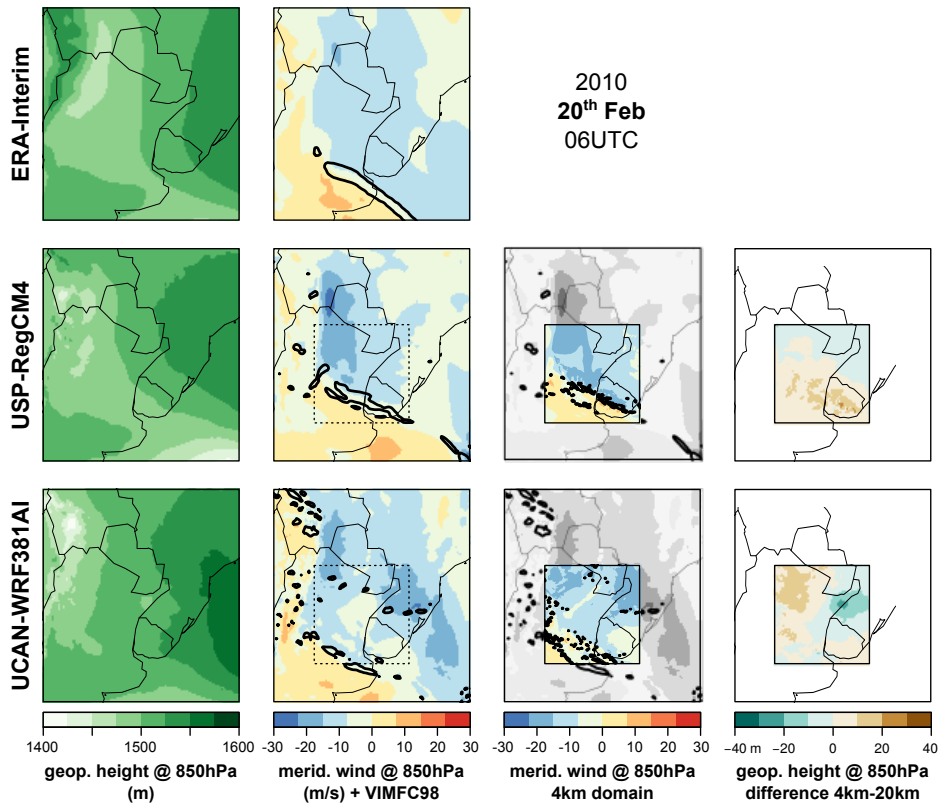


Figure A.7: As Figure A.6, but for CM.

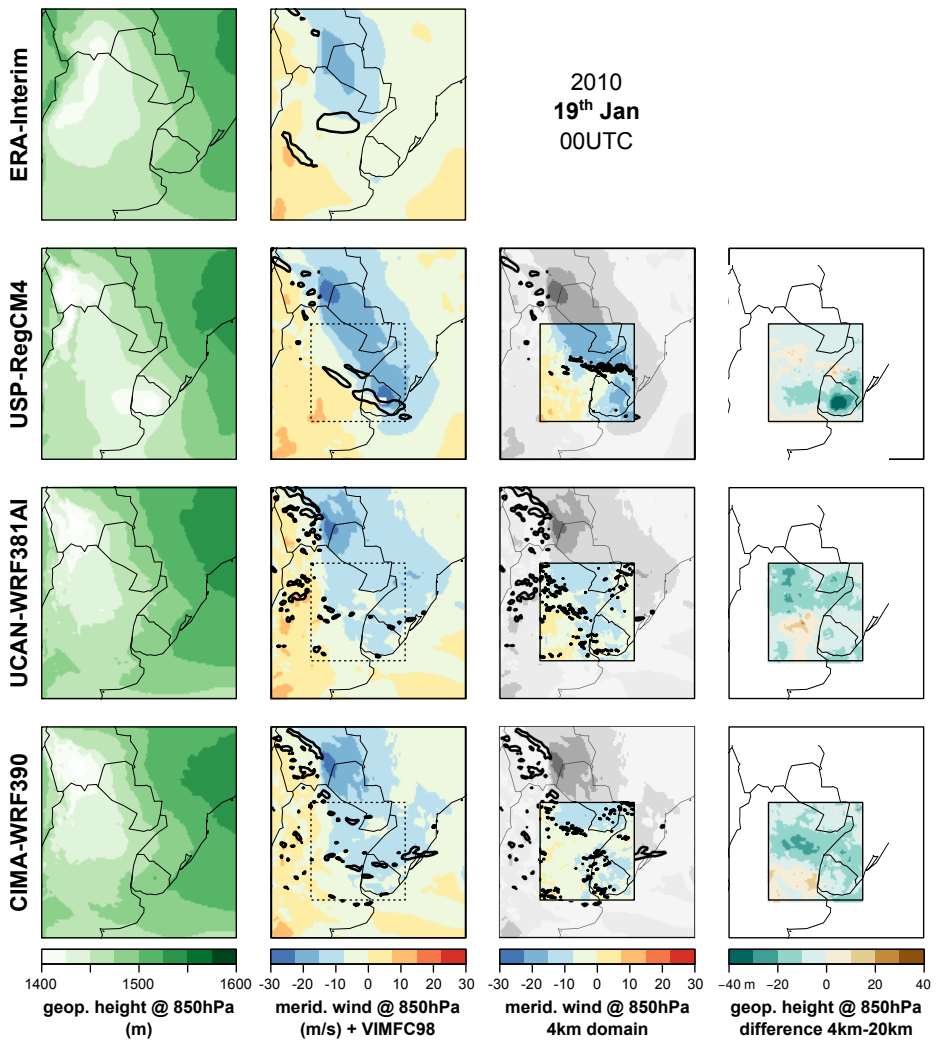


Figure A.8: Synoptic drivers for weather-like simulations on 2010 January 19th at 00 UTC (Case 2). For each ensemble member, from left to right: Geopotential height at 850 hPa (m) in the CSAM domain, meridional wind at 850 hPa (m/s) for both CSAM and SESA domains and difference in geopotential height at 850 hPa (m) between CP and non-CP simulations. Black isolines on top of meridional wind panels show the 98th percentile of the vertically integrated moisture flux convergence (VIMFC98).

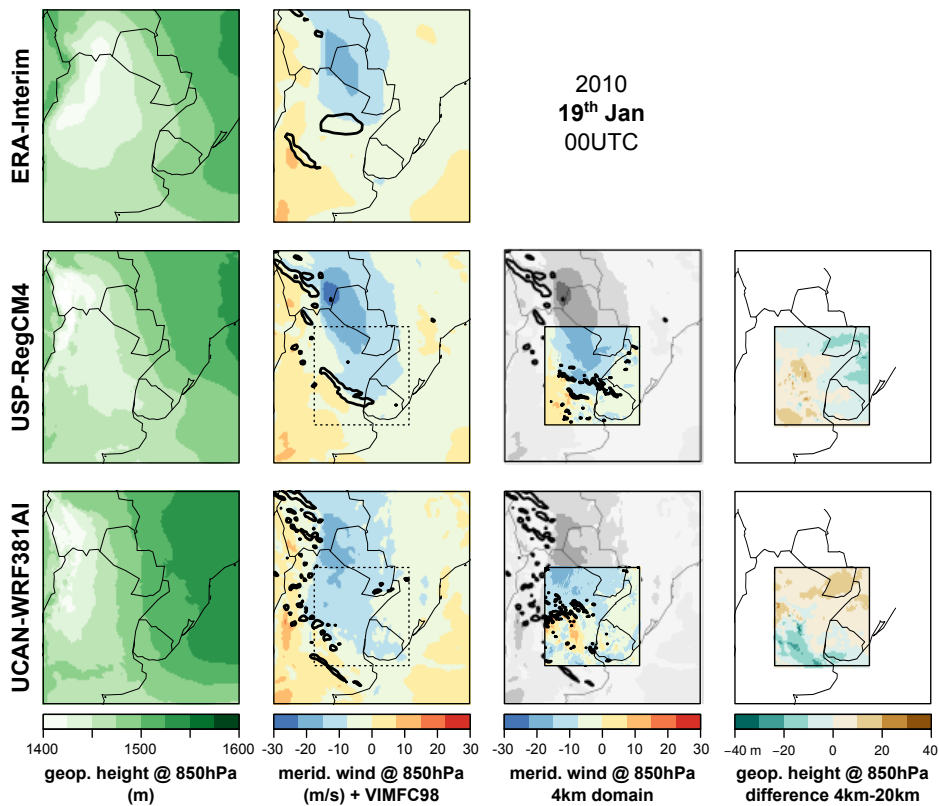


Figure A.9: As Figure A.8, but for CM.

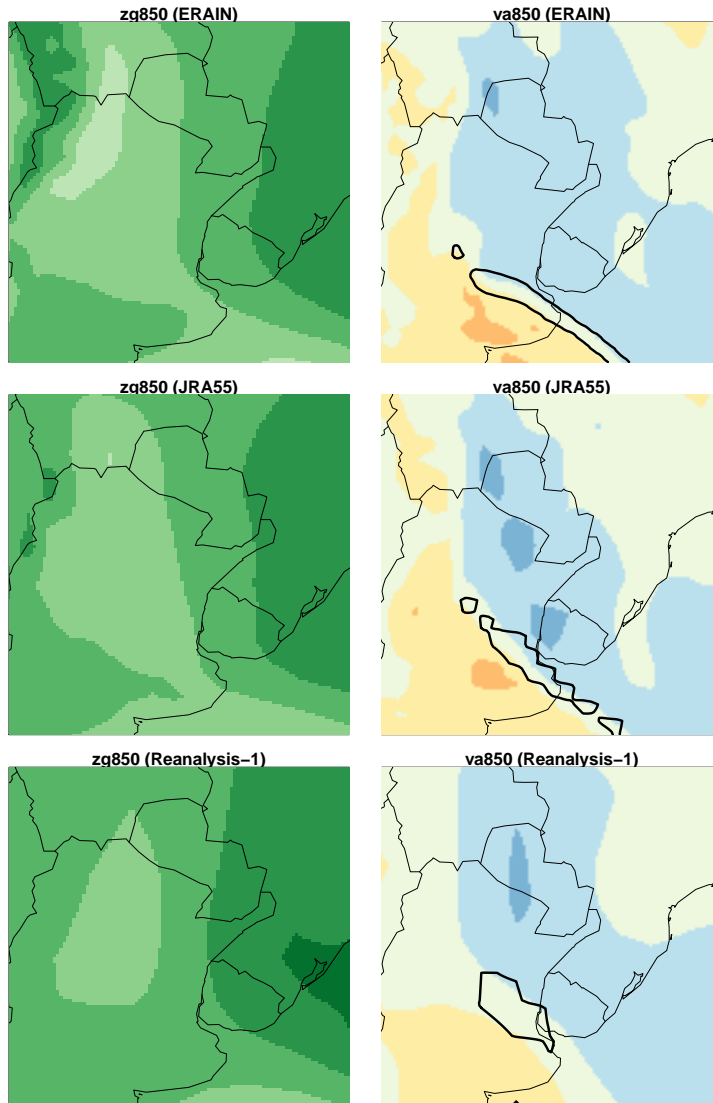


Figure A.10: Synoptic drivers on 2010 February 20th at 06 UTC (Case 1) for ERA-Interim, JRA-55 and Reanalysis-1 in the CSAM domain. Results are shown for geopotential height at 850 hPa (m) in the first column and meridional wind at 850 hPa (m/s) in the second column. Black isolines on top of meridional wind panels show the 98th percentile of the vertically integrated moisture flux convergence (VIMFC98).

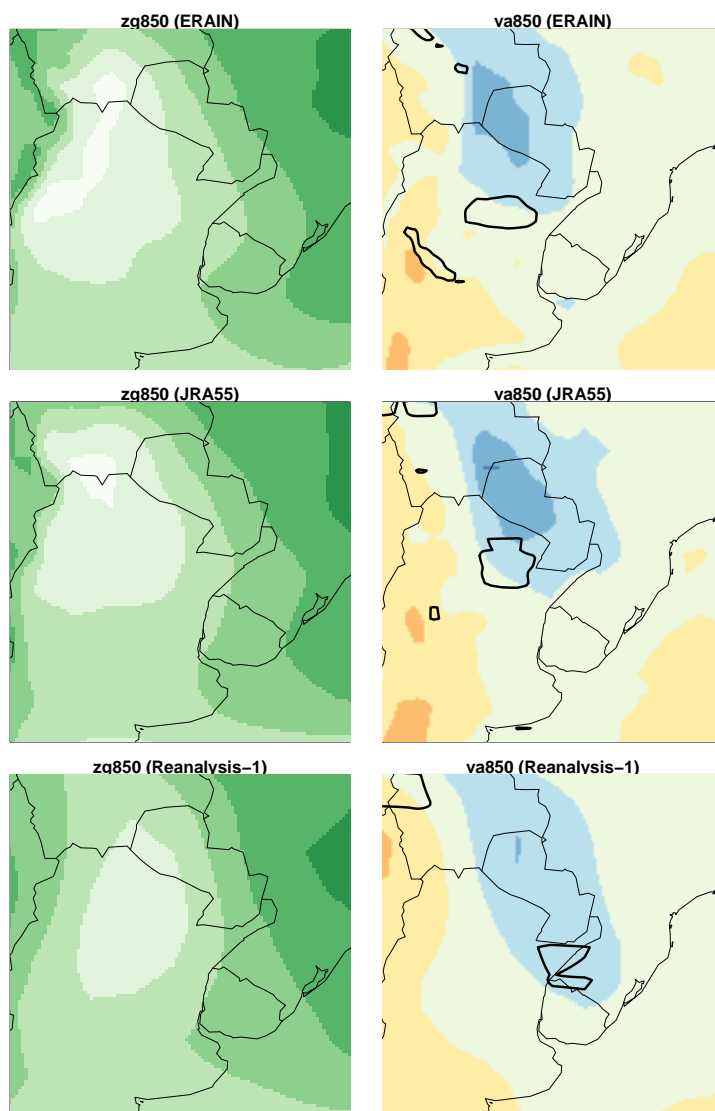


Figure A.11: As Figure A.10, but for Case 2 (2010 January 19th at 00 UTC).

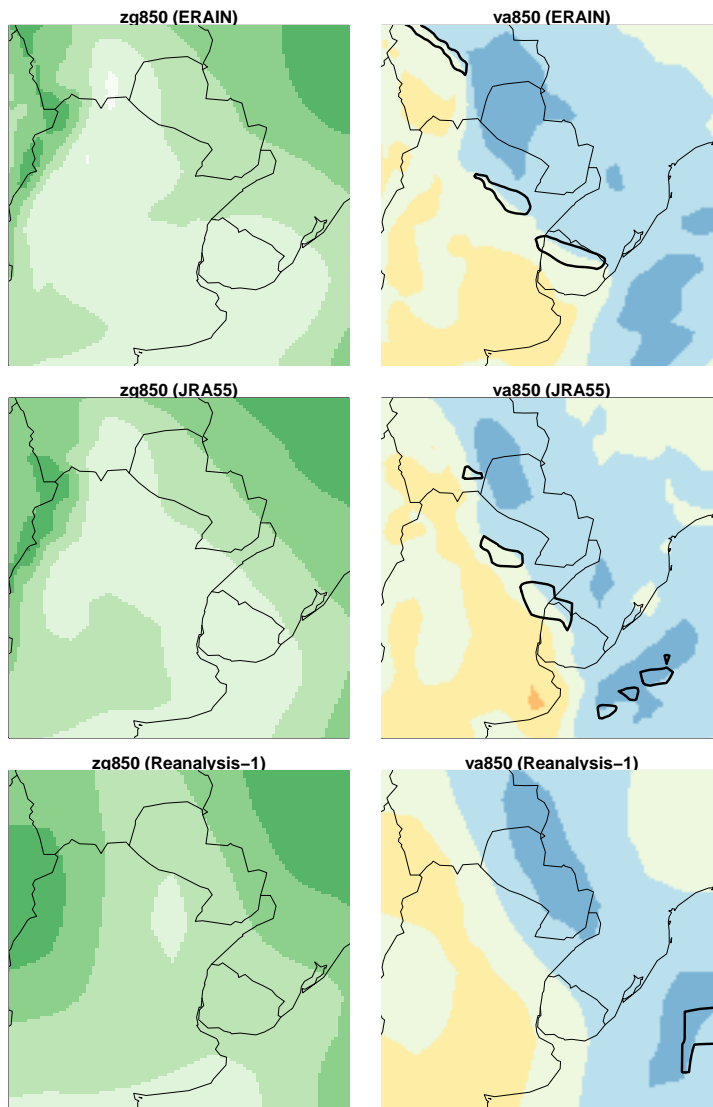


Figure A.12: As Figure A.10, but for Case 3 (2009 November 22nd at 06 UTC).

Bibliography

- Ahrens C (2009) *Meteorology Today: An Introduction to Weather, Climate, and the Environment*. International student edition, Brooks/Cole, CengageLearning
- Alexandru A, de Elia R, Laprise R, Separovic L, Biner S (2009) Sensitivity study of regional climate model simulations to large-scale nudging parameters. *Monthly Weather Review* 137(5):1666–1686, [DOI: [10.1175/2008MWR2620.1](https://doi.org/10.1175/2008MWR2620.1)]
- Alexandru A, de Elia R, Laprise R (2007) Internal variability in regional climate downscaling at the seasonal scale. *Monthly Weather Review* 135(9):3221–3238, [DOI: [10.1175/MWR3456.1](https://doi.org/10.1175/MWR3456.1)]
- Arakawa A (2004) The cumulus parameterization problem: Past, present, and future. *Journal of Climate* 17(13):2493–2525, [DOI: [10.1175/1520-0442\(2004\)017;2493:RATCPP;2.0.CO;2](https://doi.org/10.1175/1520-0442(2004)017;2493:RATCPP;2.0.CO;2)]
- Arora VK, Scinocca JF, Boer GJ, Christian JR, Denman KL, Flato GM, Kharin VV, Lee WG, Merryfield WJ (2011) Carbon emission limits required to satisfy future representative concentration pathways of greenhouse gases. *Geophysical Research Letters* 38(5), [DOI: [10.1029/2010GL046270](https://doi.org/10.1029/2010GL046270)]
- Ban N, Schmidli J, Schär C (2015) Heavy precipitation in a changing climate: Does short-term summer precipitation increase faster? *Geophysical Research Letters* 42, [DOI: [10.1002/2014GL062588](https://doi.org/10.1002/2014GL062588)]
- Ban N, Caillaud C, Coppola E, Pichelli E, Sobolowski S, Adinolfi M, Ahrens B, Alias A, Anders I, Bastin S, Belusic D, Berthou S, Brisson E, Cardoso RM, Chan S, Christensen OB, Fernandez J, Fita L, Frisius T, Gašparac G, Giorgi F, Goergen K, Haugen JE, Hodnebrog O, Kartsios

- S, Katragkou E, Kendon EJ, Keuler K, Lavin-Gullon A, Lenderink G, Leutwyler D, Lorenz T, Maraun D, Mercogliano P, Milovac J, Panitz HJ, Raffa M, Remedio AR, Schär C, Soares PM, Srnec L, Steensen BM, Stocchi P, Tölle MH, Truhetz H, Vergara-Temprado J, de Vries H, Warrach-Sagi K, Wulfmeyer V, Zander M (2021) The first multi-model ensemble of regional climate simulations at kilometer-scale resolution, Part I: Evaluation of precipitation. *Climate Dynamics* En prensa, [DOI: [10.1007/s00382-021-05708-w](https://doi.org/10.1007/s00382-021-05708-w)]
- Ban N, Schmidli J, Schaer C (2014) Evaluation of the convection-resolving regional climate modeling approach in decade-long simulations. *Journal of Geophysical Research - Atmospheres* 119(13), [DOI: [10.1002/2014JD021478](https://doi.org/10.1002/2014JD021478)]
- Barry R, Chorley R (2003) *Atmosphere, Weather and Climate*. Taylor & Francis Group
- Bassett R, Young P, Blair G, Samreen F, Simm W (2020) A Large Ensemble Approach to Quantifying Internal Model Variability Within the WRF Numerical Model. *Journal of Geophysical Research: Atmospheres* 125(7):e2019JD031,286, [DOI: [10.1029/2019JD031286](https://doi.org/10.1029/2019JD031286)]
- Beck H, Wood E, Pan M, Fisher C, Miralles D, van Dijk A, McVicar T, Adler R (2018) MSWEP v2 global 3-hourly 0.1° precipitation: Methodology and quantitative assessment. *Bulletin of the American Meteorological Society* 100, [DOI: [10.1175/BAMS-D-17-0138.1](https://doi.org/10.1175/BAMS-D-17-0138.1)]
- Bellprat O, Kotlarski S, Lüthi D, Schär C (2012) Exploring perturbed physics ensembles in a regional climate model. *Journal of Climate* 25(13):4582–4599, [DOI: [10.1175/JCLI-D-11-00275.1](https://doi.org/10.1175/JCLI-D-11-00275.1)]
- Berg P, Christensen J (2008) Poor man's re-analysis over Europe. Tech. rep., WATCH Technical 5 Report No. 2
- Berg P, Wagner S, Kunstmann H, Schaedler G (2013) High resolution Regional Climate Model simulations for Germany: Part I-Validation. *Climate Dynamics* 40(1-2):401–414, [DOI: [10.1007/s00382-012-1508-8](https://doi.org/10.1007/s00382-012-1508-8)]
- Bettolli M, Solman S, da Rocha R, Llopart M, Gutierrez J, Fernandez J, Olmo M, Lavin-Gullon A, Chou S, Carneiro-Rodrigues D, Coppola E, Balmaceda-Huarte R, Barreiro M, Blazquez J, Doyle M, Feijoo M,

- Huth R, Machado L, Vianna-Cuadra S (2021) The CORDEX Flagship Pilot Study in Southeastern South America: A comparative study of statistical and dynamical downscaling models in simulating daily extreme precipitation events. *Climate Dynamics* 56:1589–1608, [DOI: [10.1007/s00382-020-05549-z](https://doi.org/10.1007/s00382-020-05549-z)]
- Brockhaus P, Luethi D, Schaer C (2008) Aspects of the diurnal cycle in a regional climate model. *Meteorologische Zeitschrift* 17(4, SI):433–443, [DOI: [10.1127/0941-2948/2008/0316](https://doi.org/10.1127/0941-2948/2008/0316)]
- Busalacchi AJ, Asrar GR (2009) World Climate Research Programme: achievements, activities and challenges. *WMO Bulletin* 58 (3):151–161
- Casanueva A, Kotlarski S, Herrera García S, Fernández J, Gutiérrez J, Boberg F, Colette A, Christensen O, Goergen K, Jacob D, Keuler K, Nikulin G, Teichmann C, Vautard R (2016) Daily precipitation statistics in a EURO-CORDEX RCM ensemble: Added value of raw and bias-corrected high-resolution simulations. *Climate Dynamics* 47, [DOI: [10.1007/s00382-015-2865-x](https://doi.org/10.1007/s00382-015-2865-x)]
- Caya D, Biner S (2004) Internal variability of RCM simulations over an annual cycle. *Climate Dynamics* 22(1):33–46, [DOI: [10.1007/s00382-003-0360-2](https://doi.org/10.1007/s00382-003-0360-2)]
- Cerón W, Kayano M, Andreoli R, Avila-Diaz A, Ayes I, Freitas E, Martins J, Souza R (2020) Recent intensification of extreme precipitation events in the La Plata basin in Southern South America (1981–2018). *Atmospheric Research* [DOI: [10.1016/j.atmosres.2020.105299](https://doi.org/10.1016/j.atmosres.2020.105299)]
- Charney J, Fjortoft R, von Neuman J (1950) Numerical integration of the barotropic vorticity equation. *Tellus*
- Chen F, Dudhia J (2001) Coupling an advanced land surface–hydrology model with the penn state–NCAR MM5 modeling system. part i: Model implementation and sensitivity. *Monthly Weather Review* 129(4):569–585, [DOI: [10.1175/1520-0493\(2001\)129<0569:caalsh>2.0.co;2](https://doi.org/10.1175/1520-0493(2001)129<0569:caalsh>2.0.co;2)]
- Christensen JH, Christensen OB (2007) A summary of the PRUDENCE model projections of changes in European climate by the end of this century. *Climatic change* 81(1):7–30

- Christensen JH, Carter TR, Rummukainen M, Amanatidis G (2007) Evaluating the performance and utility of regional climate models: the PRUDENCE project. *Climate Change* 81(1):1–6, [DOI: [10.1007/s10584-006-9211-6](https://doi.org/10.1007/s10584-006-9211-6)]
- Christensen OB (1999) Relaxation of soil variables in a regional climate model. *Tellus A* 51:674–685, [DOI: [10.1034/j.1600-0870.1999.00010.x](https://doi.org/10.1034/j.1600-0870.1999.00010.x)]
- Coppola E, Sobolowski S, Pichelli E, Raffaele F, Ahrens B, Anders I, Ban N, Bastin S, Belda M, Belusic D, Caldas-Alvarez A, Cardoso RM, Davolio S, Dobler A, Fernandez J, Fita L, Fumiere Q, Giorgi F, Gørgen K, Güttler I, Halenka T, Heinzeller D, Hodnebrog Ø, Jacob D, Kartsios S, Katragkou E, Kendon E, Khodayar S, Kunstmann H, Knist S, Lavín-Gullón A, Lind P, Lorenz T, Maraun D, Marelle L, van Meijgaard E, Milovac J, Myhre G, Panitz HJ, Piazza M, Raffa M, Raub T, Rockel B, Schär C, Sieck K, Soares PMM, Somot S, Srnec L, Stocchi P, Tölle MH, Truhetz H, Vautard R, de Vries H, Warrach-Sagi K (2020) A first-of-its-kind multi-model convection permitting ensemble for investigating convective phenomena over Europe and the Mediterranean. *Climate Dynamics* 55:3–34, [DOI: [10.1007/s00382-018-4521-8](https://doi.org/10.1007/s00382-018-4521-8)]
- Cosgrove BA, Lohmann D, Mitchell KE, Houser PR, Wood EF, Schaake JC, Robock A, Sheffield J, Duan Q, Luo L, Higgins RW, Pinker RT, Tarpley JD (2003) Land surface model spin-up behavior in the North American Land Data Assimilation System (NL-DAS). *Journal of Geophysical Research: Atmospheres* 108(D22), [DOI: [10.1029/2002JD003316](https://doi.org/10.1029/2002JD003316)]
- Crétat J, Pohl B (2012) How physical parameterizations can modulate internal variability in a Regional Climate Model. *Journal of the Atmospheric Sciences* 69(2):714–724, [DOI: [10.1175/JAS-D-11-0109.1](https://doi.org/10.1175/JAS-D-11-0109.1)]
- Davin EL, Rechid D, Breil M, Cardoso RM, Coppola E, Hoffmann P, Jach LL, Katragkou E, de Noblet-Ducoudré N, Radtke K, Raffa M, Soares PM, Sofiadis G, Strada S, Strandberg G, Tölle MH, Warrach-Sagi K, Wulfmeyer V (2020) Biogeophysical impacts of forestation in Europe: first results from the LUCAS (Land Use and Climate Across Scales) regional climate model intercomparison. *International Journal of Climatology* 11:183–200, [DOI: [10.5194/esd-11-183-2020](https://doi.org/10.5194/esd-11-183-2020)]
- Dee DP, Uppala SM, Simmons AJ, Berrisford P, Poli P, Kobayashi S, Andrae U, Balmaseda MA, Balsamo G, Bauer P, Bechtold P, Beljaars

- ACM, van de Berg L, Bidlot J, Bormann N, Delsol C, Dragani R, Fuentes M, Geer AJ, Haimberger L, Healy SB, Hersbach H, Hólm EV, Isaksen L, Kållberg P, Köhler M, Matricardi M, McNally AP, Monge-Sanz BM, Morcrette JJ, Park BK, Peubey C, de Rosnay P, Tavolato C, Thépaut JN, Vitart F (2011) The ERA-Interim reanalysis: configuration and performance of the data assimilation system. *Quarterly Journal of the Royal Meteorological Society* 137(656):553–597, [DOI: [10.1002/qj.828](https://doi.org/10.1002/qj.828)]
- Dee DP, Balsameda M, Balsamo G, Engelen R, Simmons AJ, Thépaut JN (2014) Toward a consistent reanalysis of the climate system. *Bulletin of the American Meteorological Society* 95(8):1235–1248, [DOI: [10.1175/BAMS-D-13-00043.1](https://doi.org/10.1175/BAMS-D-13-00043.1)]
- Deser C, Phillips A, Bourdette V, Teng H (2012) Uncertainty in climate change projections: the role of internal variability. *Climate Dynamics* 38(3):527–546, [DOI: [10.1007/s00382-010-0977-x](https://doi.org/10.1007/s00382-010-0977-x)]
- Devanand A, Ghosh S, Paul S, Karmakar S, Niyogi D (2018) Multi-ensemble regional simulation of Indian monsoon during contrasting rainfall years: role of convective schemes and nested domain. *Climate Dynamics* 50(11):4127–4147, [DOI: [10.1007/s00382-017-3864-x](https://doi.org/10.1007/s00382-017-3864-x)]
- Dickinson R (1986) The climate system and modeling of climate. *The Greenhouse Effect, Climatic Change, and Ecosystems* pp 207–270
- Dickinson RE, Giorgi F, Bates G (1989) A regional climate model for the western United States. *Climatic Change* 15:1573–1480, [DOI: [10.1007/BF00240465](https://doi.org/10.1007/BF00240465)]
- Doblas-Reyes FJ, Weisheimer A, Déqué M, Keenlyside N, McVean M, Murphy JM, Rogel P, Smith D, Palmer TN (2009) Addressing model uncertainty in seasonal and annual dynamical ensemble forecasts. *Quarterly Journal of the Royal Meteorological Society* 135(643):1538–1559, [DOI: <https://doi.org/10.1002/qj.464>]
- Donner LJ, Wyman BL, Hemler RS, Horowitz LW, Ming Y, Zhao M, Golaz JC, Ginoux P, Lin SJ, Schwarzkopf MD, Austin J, Alaka G, Cooke WF, Delworth TL, Freidenreich SM, Gordon CT, Griffies SM, Held IM, Hurlin WJ, Klein SA, Knutson TR, Langenhorst AR, Lee HC, Lin Y, Magi BI, Malyshev SL, Milly PCD, Naik V, Nath MJ, Pincus

- R, Ploshay JJ, Ramaswamy V, Seman CJ, Shevliakova E, Sirutis JJ, Stern WF, Stouffer RJ, Wilson RJ, Winton M, Wittenberg AT, Zeng F (2011) The Dynamical Core, Physical Parameterizations, and Basic Simulation Characteristics of the Atmospheric Component AM3 of the GFDL Global Coupled Model CM3. *Journal of Climate* 24(13):3484–3519, [DOI: [10.1175/2011JCLI3955.1](https://doi.org/10.1175/2011JCLI3955.1)]
- Durrán D (1999) *Numerical Methods for Wave Equations in Geophysical Fluid Dynamics*. Springer-Verlag
- Evans JP, Ekström M, Ji F (2012) Evaluating the performance of a WRF physics ensemble over South-East Australia. *Climate Dynamics* 39(6):1241–1258, [DOI: [10.1007/s00382-011-1244-5](https://doi.org/10.1007/s00382-011-1244-5)]
- Falco M, Carril AF, Menéndez CG, Zaninelli PG, Li LZ (2019) Assessment of CORDEX simulations over South America: added value on seasonal climatology and resolution considerations. *Climate Dynamics* 52:4771–4786, [DOI: [10.1007/s00382-018-4412-z](https://doi.org/10.1007/s00382-018-4412-z)]
- Fantini A, Raffaele F, Torma C, Bacer S, Coppola E, Giorgi F, Ahrens B, Dubois C, Sanchez E, Verdecchia M (2018) Assessment of multiple daily precipitation statistics in ERA-Interim driven Med-CORDEX and EURO-CORDEX experiments against high resolution observations. *Climate Dynamics* 51, [DOI: [10.1007/s00382-016-3453-4](https://doi.org/10.1007/s00382-016-3453-4)]
- Fathalli B, Pohl B, Castel T, Safi MJ (2019) Errors and uncertainties in regional climate simulations of rainfall variability over Tunisia: a multi-model and multi-member approach. *Climate Dynamics* 52(1):335–361, [DOI: [10.1007/s00382-018-4150-2](https://doi.org/10.1007/s00382-018-4150-2)]
- Fernández J, Primo C, Cofiño AS, Gutiérrez JM, Rodríguez MA (2009) MVL spatiotemporal analysis for model intercomparison in EPS: application to the DEMETER multi-model ensemble. *Climate Dynamics* 33(2):233–243, [DOI: [10.1007/s00382-008-0456-9](https://doi.org/10.1007/s00382-008-0456-9)]
- Fernández J, Montavez JP, Saenz J, Gonzalez-Rouco JF, Zorita E (2007) Sensitivity of the MM5 mesoscale model to physical parameterizations for regional climate studies: Annual cycle. *Journal of Geophysical Research - Atmospheres* 112:D04,101, [DOI: [10.1029/2005JD006649](https://doi.org/10.1029/2005JD006649)]
- Fernández-Quiruelas V, Blanco C, Cofiño A, Fernández J (2015) Large-scale climate simulations harnessing clusters, grid and cloud in-

- frastructures. *Future Generation Computer Systems* 51:36–44, [DOI: 10.1016/j.future.2015.04.009]
- Fosser G, Khodayar S, Berg P (2016) Climate change in the next 30 years: What can a convection-permitting model tell us that we did not already know? *Climate Dynamics* [DOI: 10.1007/s00382-016-3186-4]
- Fosser G, Khodayar S, Berg P (2015) Benefit of convection permitting climate model simulations in the representation of convective precipitation. *Climate Dynamics* 44(1-2):45–60, [DOI: 10.1007/s00382-014-2242-1]
- García-Díez M, Fernández J, Vautard R (2015) An RCM multi-physics ensemble over Europe: multi-variable evaluation to avoid error compensation. *Climate Dynamics* 45(11):3141–3156, [DOI: 10.1007/s00382-015-2529-x]
- García-Díez M, Fernández J, Fita L, Yagüe C (2013) Seasonal dependence of WRF model biases and sensitivity to PBL schemes over Europe. *Quarterly Journal of the Royal Meteorological Society* 139(671):501–514, [DOI: <https://doi.org/10.1002/qj.1976>]
- van Geel B, Raspopov O, Renssen H, van der Plicht J, Dergachev V, Meijer H (1999) The role of solar forcing upon climate change. *Quaternary Science Reviews* 18(3):331–338, [DOI: 10.1016/S0277-3791(98)00088-2]
- Geyer B, Ludwig T, von Storch H (2021) Limits of reproducibility and hydrodynamic noise in atmospheric regional modelling. *Commun Earth Environ* 2, [DOI: 10.1038/s43247-020-00085-4.]
- Giles J, Ruscica RC, Menéndez C (2020) Warm-season precipitation drivers in northeastern Argentina: Diurnal cycle of the atmospheric moisture balance and land–atmosphere coupling. *International Journal of Climatology* [DOI: 10.1002/joc.6724]
- Giorgi F (1990a) Sensitivity of wintertime precipitation and soil hydrology simulation over the western United-States to lower boundary specifications. *Atmosphere-Ocean* 28(1):1–23, [DOI: 10.1080/07055900.1990.9649365]
- Giorgi F (1990b) Simulation of Regional Climate using a limited are model nested in a general-circulation model. *Journal of Climate* 3(9):941–963, [DOI: 10.1175/1520-0442(1990)003;0941:SORCUA;2.0.CO;2]

- Giorgi F (2005) Climate Change Prediction. *Climatic Change* 73:239–265, [DOI: [10.1007/s10584-005-6857-4](https://doi.org/10.1007/s10584-005-6857-4)]
- Giorgi F (2006) Regional climate modeling: Status and perspectives. *Journal of Physique IV* 139:101–118, [DOI: [10.1051/jp4:2006139008](https://doi.org/10.1051/jp4:2006139008)]
- Giorgi F (2019) Thirty years of regional climate modeling: Where are we and where are we going next? *Journal of Geophysical Research: Atmospheres* [DOI: [10.1029/2018JD030094](https://doi.org/10.1029/2018JD030094)]
- Giorgi F, Bates G (1989) The Climatological Skill of a Regional Model over complex terrain. *Monthly Weather Review* 117(11):2325–2347, [DOI: [10.1175/1520-0493\(1989\)117<2325:TCSOARj2.0.CO;2](https://doi.org/10.1175/1520-0493(1989)117<2325:TCSOARj2.0.CO;2)]
- Giorgi F, Bi X (2000) A study of internal variability of a regional climate model. *Journal of Geophysical Research: Atmospheres* 105(D24):29,503–29,521, [DOI: [10.1029/2000JD900269](https://doi.org/10.1029/2000JD900269)]
- Giorgi F, Gutowski WJ (2015) Regional Dynamical Downscaling and the CORDEX Initiative. *Annual Review of Environment and Resources* 40(1):467–490, [DOI: [10.1146/annurev-environ-102014-021217](https://doi.org/10.1146/annurev-environ-102014-021217)]
- Giorgi F, Mearns L (1999) Introduction to special section: Regional climate modeling revisited. *Journal of Geophysical Research - Atmospheres* 104(D6):6335–6352, [DOI: [10.1029/98JD02072](https://doi.org/10.1029/98JD02072)]
- Giorgi F, Bates GT, Nieman SJ (1993) The Multiyear Surface Climatology of a Regional Atmospheric Model over the Western United States. *Journal of Climate* 6(1):75–95, [DOI: [10.1175/1520-0442\(1993\)006<0075:TMSCOA;2.0.CO;2](https://doi.org/10.1175/1520-0442(1993)006<0075:TMSCOA;2.0.CO;2)]
- Giorgi F, Hewitson B, Christensen J, Hulme M, von Storch H, Whetton P, Jones R, Mearns L, Fu C (2001) Regional climate information – evaluation and projections, Chapter 10. In: Houghton J et al (eds) *Climate change 2001: the scientific basis. Contribution of working group I to the third assessment report of the intergovernmental panel on climate change*. Intergovernmental Panel on Climate Change p 583–638
- Giorgi F, Jones C, Asrar GR (2009) Addressing climate information needs at the regional level: the CORDEX framework. *WMO Bulletin* 58:175–183

- Giorgi F, Coppola E, Solmon F, Mariotti L, Sylla M, Bi X, Elguindi N, Diro G, Nair VS, Giuliani G, Turuncoglu U, Cozzini S, Güttler I, O'Brien T, Tawfik A, Shalaby A, Zakey S, Steiner A, Stordal F, Brankovic C (2011) RegCM4: Model description and preliminary tests over multiple CORDEX domains. *Climate research* 53:577X, [DOI: [10.3354/cr01018](https://doi.org/10.3354/cr01018)]
- Giorgi F, Bates G, Errico R, Dickinson R (1989) Modeling the climate of the western United-States with a limited area model coupled to a general-circulation model. In: *Sixth Conference on Applied Climatology*, American Meteorological Society, pp 201–208
- Giorgi F, Brodeur C, Bates G (1994) Regional Climate-Change scenarios over the United-States produced with a nested regional climate model. *Journal of Climate* 7(3):375–399, [DOI: [10.1175/1520-0442\(1994\)007<0375:RCCSOT>2.0.CO;2](https://doi.org/10.1175/1520-0442(1994)007<0375:RCCSOT>2.0.CO;2)]
- Girard E, Bekcic B (2005) Sensitivity of an Arctic regional climate model to the horizontal resolution during winter: Implications for aerosol simulation. *International Journal of Climatology* 25(11):1455–1471, [DOI: [10.1002/joc.1205](https://doi.org/10.1002/joc.1205)]
- Gómez-Navarro JJ, Montávez JP, Jerez S, Jiménez-Guerrero P, Lorente-Plazas R, González-Rouco JF, Zorita E (2011) A regional climate simulation over the iberian peninsula for the last millennium. *Climate of the Past* 7(2):451–472, [DOI: [10.5194/cp-7-451-2011](https://doi.org/10.5194/cp-7-451-2011)]
- Grell G, Schade L, Knoche R, Pfeiffer A, Egger J (2000) Nonhydrostatic climate simulations of precipitation over complex terrain. *Journal of Geophysical Research* 105:29,595–29,608, [DOI: [10.1029/2000JD900445](https://doi.org/10.1029/2000JD900445)]
- Gu H, Yu Z, Yang C, Ju Q, Yang T, Zhang D (2018) High-resolution ensemble projections and uncertainty assessment of regional climate change over China in CORDEX East Asia. *Hydrology and Earth System Sciences* 22(5):3087–3103, [DOI: [10.5194/hess-22-3087-2018](https://doi.org/10.5194/hess-22-3087-2018)]
- Gutowski WJ Jr, Giorgi F, Timbal B, Frigon A, Jacob D, Kang HS, Raghavan K, Lee B, Lennard C, Nikulin G, O'Rourke E, Rixen M, Solman S, Stephenson T, Tangang F (2016) WCRP COordinated Regional Downscaling EXperiment (CORDEX): a diagnostic MIP for CMIP6. *Geoscientific Model Development* 9(11):4087–4095, [DOI: [10.5194/gmd-9-4087-2016](https://doi.org/10.5194/gmd-9-4087-2016)]

- Güttler I, Stepanov I, Brankovic C, Nikulin G, Jones C (2015) Impact of Horizontal Resolution on Precipitation in Complex Orography Simulated by the Regional Climate Model RCA3. *Monthly Weather Review* 143(9):3610–3627, [DOI: [10.1175/MWR-D-14-00302.1](https://doi.org/10.1175/MWR-D-14-00302.1)]
- Hagedorn R, Doblas-Reyes FJ, Palmer TN (2005) The rationale behind the success of multi-model ensembles in seasonal forecasting — I. Basic concept. *Tellus A: Dynamic Meteorology and Oceanography* 57(3):219–233, [DOI: [10.3402/tellusa.v57i3.14657](https://doi.org/10.3402/tellusa.v57i3.14657)]
- Haltiner G, Williams R (1980) *Numerical Prediction and Dynamic Meteorology*. John Wiley and Sons
- Hartmann D (1994) *Global Physical Climatology*. Academic Press
- Haughton N, Abramowitz G, Pitman A, Phipps SJ (2014) On the generation of climate model ensembles. *Climate Dynamics* 43(7):2297–2308, [DOI: [10.1007/s00382-014-2054-3](https://doi.org/10.1007/s00382-014-2054-3)]
- Hawkins E, Sutton R (2009) The potential to narrow uncertainty in regional climate predictions. *Bulletin of the American Meteorological Society* 90(8):1095–1108, [DOI: [10.1175/2009BAMS2607.1](https://doi.org/10.1175/2009BAMS2607.1)]
- Haylock MR, Hofstra N, Klein Tank AMG, Klok EJ, Jones PD, New M (2008) A European daily high-resolution gridded data set of surface temperature and precipitation for 1950–2006. *Journal of Geophysical Research: Atmospheres* 113(D20), [DOI: [10.1029/2008JD010201](https://doi.org/10.1029/2008JD010201)]
- Hewitt CD, Lowe JA (2018) Toward a European Climate Prediction System. *Bulletin of the American Meteorological Society* 99(10):1997 – 2001, [DOI: [10.1175/BAMS-D-18-0022.1](https://doi.org/10.1175/BAMS-D-18-0022.1)]
- Houghton J, Ding Y, Griggs D, Noguer M, van der Linden P, Dai X, Maskell M, Johnson C (2001) *Climate Change 2001: The Scientific Basis*, vol 881., Cambridge University Press, p 881
- Insel N, Poulsen C, Ehlers T (2010) Influence of the Andes mountains on South American moisture transport, convection, and precipitation. *Climate Dynamics* 35:1477–1492, [DOI: [10.1007/s00382-009-0637-1](https://doi.org/10.1007/s00382-009-0637-1)]
- Jacob D, Teichmann C, Sobolowski S, Katragkou E, Anders I, Belda M, Benestad R, Boberg F, Buonomo E, Cardoso RM, Casanueva A, Christensen OB, Christensen JH, Coppola E, De Cruz L, Davin EL, Dobler

- A, Dominguez M, Fealy R, Fernandez J, Gaertner MA, Garcia-Diez M, Giorgi F, Gobiet A, Goergen K, Gomez-Navarro JJ, Aleman JJG, Gutierrez C, Gutierrez JM, Guettler I, Haensler A, Halenka T, Jerez S, Jimenez-Guerrero P, Jones RG, Keuler K, Kjellstrom E, Knist S, Kotlarski S, Maraun D, van Meijgaard E, Mercogliano P, Montavez JP, Navarra A, Nikulin G, de Noblet-Ducoudre N, Panitz HJ, Pfeifer S, Piazza M, Pichelli E, Pietikainen JP, Prein AF, Preuschmann S, Rechid D, Rockel B, Romera R, Sanchez E, Sieck K, Soares PMM, Somot S, Srnec L, Sorland SL, Termonia P, Truhetz H, Vautard R, Warrach-Sagi K, Wulfmeyer V (2020) Regional climate downscaling over Europe: perspectives from the EURO-CORDEX community. *Regional Environmental Change* 20:51, [DOI: [10.1007/s10113-020-01606-9](https://doi.org/10.1007/s10113-020-01606-9)]
- Jacob D, Petersen J, Eggert B, Alias A, Christensen OB, Bouwer LM, Braun A, Colette A, Deque M, Georgievski G, Georgopoulou E, Gobiet A, Menut L, Nikulin G, Haensler A, Hempelmann N, Jones C, K K, Kovats S, Kroener N, Kotlarski S, Kriegsmann A, Martin E, van Meijgaard E, Moseley C, Pfeifer S, Preuschmann S, Radermacher C, Radtke K, Rechid D, Rounsevell M, Samuelsson P, Somot S, Soussana JF, Teichmann C, Valentini R, Vautard R, Weber B, Yiou P (2014) EURO-CORDEX: new high-resolution climate change projections for European impact research. *Regional Environmental Change* 14(2, SI):563–578, [DOI: [10.1007/s10113-013-0499-2](https://doi.org/10.1007/s10113-013-0499-2)]
- Jankov I, Gallus W, Segal M, Koch S (2005) The impact of different WRF model physical parameterizations and their interactions on warm season MCS rainfall. *Weather and Forecasting* 20, [DOI: [10.1175/WAF888.1](https://doi.org/10.1175/WAF888.1)]
- Jerez S, Gimenez D, Montáñez JP (2009) Optimizing the execution of a parallel meteorology simulation code. IPDPS 2009 - Proceedings of the 2009 IEEE International Parallel and Distributed Processing Symposium [DOI: [10.1109/IPDPS.2009.5161154](https://doi.org/10.1109/IPDPS.2009.5161154)]
- Jerez S, López-Romero JM, Turco M, Lorente-Plazas R, Gómez-Navarro JJ, Jiménez-Guerrero P, Montáñez JP (2020) On the spin-up period in WRF simulations over europe: Trade-offs between length and seasonality. *Journal of Advances in Modeling Earth Systems* 12(4):e2019MS001,945, [DOI: [10.1029/2019ms001945](https://doi.org/10.1029/2019ms001945)]
- Jerez S, Pedro Montavez J, Jimenez-Guerrero P, Jose Gomez-Navarro J, Lorente-Plazas R, Zorita E (2013a) A multi-physics ensemble of present-

- day climate regional simulations over the Iberian Peninsula. *Climate Dynamics* 40(11-12):3023–3046, [DOI: [10.1007/s00382-012-1539-1](https://doi.org/10.1007/s00382-012-1539-1)]
- Jerez S, Pedro Montavez J, Jose Gomez-Navarro J, Lorente-Plazas R, Andres Garcia-Valero J, Jimenez-Guerrero P (2013b) A multi-physics ensemble of regional climate change projections over the Iberian Peninsula. *Climate Dynamics* 41(7-8):1749–1768, [DOI: [10.1007/s00382-012-1551-5](https://doi.org/10.1007/s00382-012-1551-5)]
- Jimenez PA, Gonzalez-Rouco JF, Garcia-Bustamante E, Navarro J, Montavez JP, de Arellano JVG, Dudhia J, Muñoz-Roldan A (2010) Surface Wind Regionalization over Complex Terrain: Evaluation and Analysis of a High-Resolution WRF Simulation. *Journal of Applied Meteorology and Climatology* 49:268–287, [DOI: [10.1175/2009JAMC2175.1](https://doi.org/10.1175/2009JAMC2175.1)]
- Joyce R, Janowiak J, Arkin P, Xie P (2004) CMORPH: A method that produces global precipitation estimates from passive microwave and infrared data at high spatial and temporal resolution. *Journal of Hydrometeorology* 5, [DOI: [10.1175/1525-7541\(2004\)005;0487:CAMTPG;2.0.CO;2](https://doi.org/10.1175/1525-7541(2004)005;0487:CAMTPG;2.0.CO;2)]
- Kalnay E (2002) *Atmospheric Modeling, Data Assimilation and Predictability*. Cambridge University Press, [DOI: [10.1017/CBO9780511802270](https://doi.org/10.1017/CBO9780511802270)]
- Kalnay E, Kanamitsu M, Kistler R, Collins W, Deaven D, Gandin L, Iredell M, Saha S, White G, Woollen J, Zhu Y, Chelliah M, Ebisuzaki W, Higgins W, Janowiak J, Mo K, Ropelewski C, Wang J, Leetmaa A, Reynolds R, Jenne R, Joseph D (1996) The NCEP/NCAR 40-year reanalysis project. *Bulletin of the American Meteorological Society* 77(3):437–471, [DOI: [10.1175/1520-0477\(1996\)077;0437:TNYRP;2.0.CO;2](https://doi.org/10.1175/1520-0477(1996)077;0437:TNYRP;2.0.CO;2)]
- Katragkou E, García-Díez M, Vautard R, Sobolowski S, Zanis P, Alexandri G, Cardoso RM, Colette A, Fernandez J, Gobiet A, Goergen K, Karacostas T, Knist S, Mayer S, Soares PMM, Pytharoulis I, Tegoulis I, Tsikerdekis A, Jacob D (2015) Regional climate hindcast simulations within EURO-CORDEX: evaluation of a WRF multi-physics ensemble. *Geoscientific Model Development* 8(3):603–618, [DOI: [10.5194/gmd-8-603-2015](https://doi.org/10.5194/gmd-8-603-2015)]

- Kendon E, Roberts N, Fowler H, Roberts M, Chan S, Senior C (2014) Heavier summer downpours with climate change revealed by weather forecast resolution model. *Nature Climate Change* 4:570–576, [DOI: [10.1038/nclimate2258](https://doi.org/10.1038/nclimate2258)]
- Kendon E, Ban N, Roberts N, Fowler H, Roberts M, Chan S, Evans J, Fosse G, Wilkinson J (2016) Do convection-permitting regional climate models improve projections of future precipitation change? *Bulletin of the American Meteorological Society* 98, [DOI: [10.1175/BAMS-D-15-0004.1](https://doi.org/10.1175/BAMS-D-15-0004.1)]
- Kendon EJ, Roberts NM, Senior CA, Roberts MJ (2012) Realism of rainfall in a very high-resolution regional climate model. *Journal of Climate* 25(17):5791–5806, [DOI: [10.1175/JCLI-D-11-00562.1](https://doi.org/10.1175/JCLI-D-11-00562.1)]
- Khodayar S, Sehlinger A, Feldmann H, Kottmeier C (2015) Sensitivity of soil moisture initialization for decadal predictions under different regional climatic conditions in Europe. *International Journal of Climatology* 35(8):1899–1915, [DOI: [10.1002/joc.4096](https://doi.org/10.1002/joc.4096)]
- Kiehl JT, Trenberth KE (1997) Earth's annual global mean energy budget. *Bulletin of the American Meteorological Society* 78(2):197 – 208, [DOI: [10.1175/1520-0477\(1997\)078<0197:EAGMEB>2.0.CO;2](https://doi.org/10.1175/1520-0477(1997)078<0197:EAGMEB>2.0.CO;2)]
- Kobayashi S, Ota Y, Harada Y, Ebata A, Moriya M, Onoda H, Onogi K, Kamahori H, Kobayashi C, Endo H, Miyaoka K, Takahashi K (2015) The JRA-55 Reanalysis: General specifications and basic characteristics. *Journal of the Meteorological Society of Japan Ser II* 93(1):5–48, [DOI: [10.2151/jmsj.2015-001](https://doi.org/10.2151/jmsj.2015-001)]
- Kumar D, Ganguly AR (2018) Intercomparison of model response and internal variability across climate model ensembles. *Climate Dynamics* 51(1):207–219, [DOI: [10.1007/s00382-017-3914-4](https://doi.org/10.1007/s00382-017-3914-4)]
- Laux P, Nguyen PNB, Cullmann J, Van TP, Kunstmann H (2017) How many RCM ensemble members provide confidence in the impact of land-use land cover change? *International Journal of Climatology* 37(4):2080–2100, [DOI: [10.1002/joc.4836](https://doi.org/10.1002/joc.4836)]
- Lavin-Gullon A, Fernández J, Cardoso R, Goergen K, Knist S, Lorenz T, Milovac J, Soares PM, Sobolowski S, Truhetz H, Warrach-Sagi K (2018) Convective processes in high resolution models: Impact of the lead time

- of the simulation. *Acta de las Jornadas Científicas de la Asociación Meteorológica Española* 35, [DOI: [10.30859/ameJrCn35p388](https://doi.org/10.30859/ameJrCn35p388)]
- Lavin-Gullon A, Fernandez J, Bastin S, Cardoso RM, Fita L, Giannaros TM, Goergen K, Gutierrez JM, Kartsios S, Katragkou E, Lorenz T, Milovac J, Soares PMM, Sobolowski S, Warrach-Sagi K (2020) Internal variability versus multi-physics uncertainty in a regional climate model. *International Journal of Climatology* 41, [DOI: [10.1002/joc.6717](https://doi.org/10.1002/joc.6717)]
- Lavin-Gullon A, Feijoo M, Solman S, Fernandez J, da Rocha P, Bettolli M (2021a) Synoptic forcing associated with extreme precipitation events over Southeastern South America as depicted by a CORDEX FPS set of convection-permitting RCMs. *Climate Dynamics* [DOI: [10.1007/s00382-021-05637-8](https://doi.org/10.1007/s00382-021-05637-8)]
- Lavin-Gullon A, Milovac J, Fernandez J (2021b) Spin-up time and internal variability analysis for overlapping time slices in a regional climate model. Submitted
- Leduc M, Laprise R (2009) Regional climate model sensitivity to domain size. *Climate Dynamics* 32(6):833–854, [DOI: [10.1007/s00382-008-0400-z](https://doi.org/10.1007/s00382-008-0400-z)]
- Leduc M, Laprise R, Moretti-Poisson M, Morin JP (2011) Sensitivity to domain size of mid-latitude summer simulations with a regional climate model. *Climate Dynamics* 37(1-2):343–356, [DOI: [10.1007/s00382-011-1008-2](https://doi.org/10.1007/s00382-011-1008-2)]
- Leutwyler D, Fuhrer O, Lapillonne X, Lüthi D, Schär C (2016) Towards European-scale convection-resolving climate simulations with GPUs: a study with COSMO 4.19. *Geoscientific Model Development* 9(9):3393–3412, [DOI: [10.5194/gmd-9-3393-2016](https://doi.org/10.5194/gmd-9-3393-2016)]
- Liebmann B, Mechoso CR (2011) *The South American Monsoon System*, 2nd edn, World Scientific Publishing Co Pte Ltd, pp 137–157
- Lo JCF, Yang ZL, Pielke Sr RA (2008) Assessment of three dynamical climate downscaling methods using the weather research and forecasting (WRF) model. *Journal of Geophysical Research: Atmospheres* 113(D9), [DOI: [10.1029/2007JD009216](https://doi.org/10.1029/2007JD009216)]

- Lucas-Picher P, Caya D, Biner S, Laprise R (2008a) Quantification of the lateral boundary forcing of a Regional Climate Model using an aging tracer. *Monthly Weather Review* 136(12):4980–4996, [DOI: [10.1175/2008MWR2448.1](https://doi.org/10.1175/2008MWR2448.1)]
- Lucas-Picher P, Caya D, de Elía R, Laprise R (2008b) Investigation of regional climate models' internal variability with a ten-member ensemble of 10-year simulations over a large domain. *Climate Dynamics* 31(7):927–940, [DOI: [10.1007/s00382-008-0384-8](https://doi.org/10.1007/s00382-008-0384-8)]
- Lucas-Picher P, Boberg F, Christensen JH, Berg P (2013) Dynamical downscaling with reinitializations: A method to generate finescale climate datasets suitable for impact studies. *Journal of Hydrometeorology* 14(4):1159–1174, [DOI: [10.1175/JHM-D-12-063.1](https://doi.org/10.1175/JHM-D-12-063.1)]
- Mahoney K, Thompson G, J Barsugli J, D Scott J, Alexander M (2012) Changes in hail and flood risk in high-resolution simulations over Colorado's mountains. *Nature Climate Change* 2, [DOI: [10.1038/nclimate1344](https://doi.org/10.1038/nclimate1344)]
- Mahoney K, Alexander M, D Scott J, Barsugli J (2013) High-resolution downscaled simulations of warm-season extreme precipitation events in the Colorado front range under past and future climates. *Journal of Climate* 26:8671–8689, [DOI: [10.1175/JCLI-D-12-00744.1](https://doi.org/10.1175/JCLI-D-12-00744.1)]
- Manzanas R, Gutiérrez J, Fernández J, van Meijgaard E, Calmanti S, Magariño M, Cofiño A, Herrera S (2018) Dynamical and statistical downscaling of seasonal temperature forecasts in europe: Added value for user applications. *Climate Services* 9:44–56, [DOI: <https://doi.org/10.1016/j.cliser.2017.06.004>]
- Mass CF, Ovens D, Westrick K, Colle BA (2002) Does increasing horizontal resolution produce more skillful forecasts?: The results of two years of real-time numerical weather prediction over the pacific northwest. *Bulletin of the American Meteorological Society* 83(3):407 – 430, [DOI: [10.1175/1520-0477\(2002\)083<0407:DIHRPM>2.3.CO;2](https://doi.org/10.1175/1520-0477(2002)083<0407:DIHRPM>2.3.CO;2)]
- Matsudo C, Salio P (2011) Severe weather reports and proximity to deep convection over Northern Argentina. *Atmospheric Research* 100:523–537, [DOI: [10.1016/j.atmosres.2010.11.004](https://doi.org/10.1016/j.atmosres.2010.11.004)]

- Matsudo C, García Skabar Y, Ruiz J, Vidal L, Salio P (2015) Verification of WRF-ARW convective-resolving forecasts over Southeastern South America. *Mausam* 66:445–456
- McAvaney B, Covey C, Joussaume S, Kattsov V, Kitoh A, Ogana W, Pitman A, Weaver A, Wood R, Zhao ZC (2001) "Model Evaluation. Chapter 8 of Intergovernmental Panel on Climate Change (IPCC), 2001: Climate Change 2001: The Scientific Basis. Contribution of Working Group I to the Third Assessment Report of the Intergovernmental Panel on Climate Change". Cambridge University Press
- McFarlane N (2011) Parameterizations: representing key processes in climate models without resolving them. *Wiley Interdisciplinary Reviews - Climate Change* 2(4):482–497, [DOI: [10.1002/wcc.122](https://doi.org/10.1002/wcc.122)]
- McGregor J, Katzfey J, Nguyen K (1999) Recent regional climate modelling experiments at CSIRO. *Research Activities in Atmospheric and Oceanic Modelling* H Ritchie(ed) (CAS/JSC Working Group on Numerical Experimentation Report; 28; WMO/TD – no 942) pp 7.37–7.38
- Menendez M, Garcia-Diez M, Fita L, Fernandez J, Mendez FJ, Gutierrez JM (2014) High-resolution sea wind hindcasts over the Mediterranean area. *Climate Dynamics* 42:1857–1872, [DOI: [10.1007/s00382-013-1912-8](https://doi.org/10.1007/s00382-013-1912-8)]
- Nguyen P, Shearer EJ, Tran H, Ombadi M, Hayatbini N, Palacios T, Huynh P, Braithwaite D, Updegraff G, Hsu K, Kuligowski B, Logan WS, Sorooshian S (2019) The CHRS data portal, an easily accessible public repository for PERSIANN global satellite precipitation data. *Scientific Data* 6(180296), [DOI: [10.1038/sdata.2018.296](https://doi.org/10.1038/sdata.2018.296)]
- Niu GY, Yang ZL, Mitchell KE, Chen F, Ek MB, Barlage M, Kumar A, Manning K, Niyogi D, Rosero E, et al (2011) The community Noah land surface model with multiparameterization options (Noah-MP): 1. model description and evaluation with local-scale measurements. *Journal of Geophysical Research: Atmospheres* 116(D12), [DOI: [10.1029/2010JD015139](https://doi.org/10.1029/2010JD015139)]
- Palharini R, Vila D, Rodrigues D, Pareja Quispe D, Palharini R, Siqueira R, Afonso J (2020) Assessment of the extreme precipitation by satellite estimates over South America. *Remote Sensing* 12:2085, [DOI: [10.3390/rs12132085](https://doi.org/10.3390/rs12132085)]

- Palmer T (2005) Global warming in a nonlinear climate. Can we be sure? *Europhysics news* 36(2):42–46
- Pan Z, Takle E, Gutowski W, Turner R (1999) Long Simulation of Regional Climate as a Sequence of Short Segments. *Monthly Weather Review* 127(3):308–321, [DOI: [10.1175/1520-0493\(1999\)127<0308:LSORCA;2.0.CO;2](https://doi.org/10.1175/1520-0493(1999)127<0308:LSORCA;2.0.CO;2)]
- Peixoto J, Oort AH (1992) *Physics of Climate*. American Institute of Physics
- van Pelt SC, Beersma JJ, Buishand TA, van den Hurk BJJM, Schellekens J (2015) Uncertainty in the future change of extreme precipitation over the Rhine basin: the role of internal climate variability. *Climate Dynamics* 44(7):1789–1800, [DOI: [10.1007/s00382-014-2312-4](https://doi.org/10.1007/s00382-014-2312-4)]
- Pielke R (2002) *Mesoscale Meteorological Modeling*. Academic Press
- Prein A, Gobiet A, Suklitsch M, Truhetz H, Awan N, Keuler K, Georgievski G (2013) Added value of convection permitting seasonal simulations. *Climate Dynamics* 41, [DOI: [10.1007/s00382-013-1744-6](https://doi.org/10.1007/s00382-013-1744-6)]
- Prein AF, Langhans W, Fosser G, Ferrone A, Ban N, Goergen K, Keller M, Toelle M, Gutjahr O, Feser F, Brisson E, Kollet S, Schmidli J, van Lipzig NPM, Leung R (2015) A review on regional convection-permitting climate modeling: Demonstrations, prospects, and challenges. *Reviews of Geophysics* 53(2):323–361, [DOI: [10.1002/2014RG000475](https://doi.org/10.1002/2014RG000475)]
- Qian JH, Seth A, Zebiak S (2003) Reinitialized versus Continuous Simulations for Regional Climate Downscaling. *Monthly Weather Review* 131(11):2857–2874, [DOI: [10.1175/1520-0493\(2003\)131<2857:RVCSFR;2.0.CO;2](https://doi.org/10.1175/1520-0493(2003)131<2857:RVCSFR;2.0.CO;2)]
- Rasmussen K, Houze R (2011) Orographic convection in subtropical South America as seen by the TRMM satellite. *Monthly Weather Review* 139:2399–2420, [DOI: [10.1175/MWR-D-10-05006.1](https://doi.org/10.1175/MWR-D-10-05006.1)]
- Rasmussen K, Houze R (2016) Convective initiation near the Andes in subtropical South America. *Monthly Weather Review* 144, [DOI: [10.1175/MWR-D-15-0058.1](https://doi.org/10.1175/MWR-D-15-0058.1)]

- Rasmussen K, Chaplin M, Zuluaga M, Houze R (2015) Contribution of extreme convective storms to rainfall in South America. *Journal of Hydrometeorology* 17, [DOI: [10.1175/JHM-D-15-0067.1](https://doi.org/10.1175/JHM-D-15-0067.1)]
- Rinke A, Dethloff K (2000) On the sensitivity of a regional Arctic climate model to initial and boundary conditions. *Climate Research* 14(2):101–113, [DOI: [10.3354/cr014101](https://doi.org/10.3354/cr014101)]
- Rodell M, Houser PR, Berg AA, Famiglietti JS (2005) Evaluation of 10 methods for initializing a land surface model. *Journal of Hydrometeorology* 6:146–155, [DOI: [10.1175/JHM414.1](https://doi.org/10.1175/JHM414.1)]
- Romatschke U, Houze R (2013) Characteristics of precipitating convective systems accounting for the summer rainfall of tropical and subtropical South America. *Journal of Hydrometeorology* 14:25–46, [DOI: [10.1175/JHM-D-12-060.1](https://doi.org/10.1175/JHM-D-12-060.1)]
- Salio P, Nicolini M, Zipser E (2007) Mesoscale convective systems over southeastern south america and their relationship with the South American Low-Level Jet. *Monthly Weather Review* 135, [DOI: [10.1175/MWR3305.1](https://doi.org/10.1175/MWR3305.1)]
- Salio P, Hobouchian M, García Skabar Y, Vila D (2014) Evaluation of high-resolution satellite precipitation estimates over southern South America using a dense rain gauge network. *Atmospheric Research* 163, [DOI: [10.1016/j.atmosres.2014.11.017](https://doi.org/10.1016/j.atmosres.2014.11.017)]
- Sanchez-Gomez E, Somot S, Déqué M (2009) Ability of an ensemble of regional climate models to reproduce weather regimes over Europe-Atlantic during the period 1961–2000. *Climate Dynamics* 33(5):723–736, [DOI: [10.1007/s00382-008-0502-7](https://doi.org/10.1007/s00382-008-0502-7)]
- Sela JG (1980) Spectral modeling at the National Meteorological Center. *Monthly Weather Review* 108(9):1279–1292, [DOI: [10.1175/1520-0493\(1980\)108;1279:smatnm;2.0.co;2](https://doi.org/10.1175/1520-0493(1980)108;1279:smatnm;2.0.co;2)]
- Seneviratne SI, Lüthi D, Litschi M, Schär C (2006) Land–atmosphere coupling and climate change in Europe. *Nature* 443(7108):205–209, [DOI: [10.1038/nature05095](https://doi.org/10.1038/nature05095)]
- Seth A, Giorgi F (1998) The effects of domain choice on summer precipitation simulation and sensitivity in a regional climate

- model. *Journal of Climate* 11(10):2698–2712, [DOI: 10.1175/1520-0442(1998)011<2698:TEODCO>2.0.CO;2]
- Shin HH, Hong SY (2011) Intercomparison of Planetary Boundary-Layer Parametrizations in the WRF Model for a Single Day from CASES-99. *Boundary-Layer Meteorology* 139(2):261–281, [DOI: 10.1007/s10546-010-9583-z]
- Shuman FG, Hovermale JB (1968) An operational six-layer Primitive Equation Model. *Journal of Applied Meteorology* 7(4):525–547, [DOI: 10.1175/1520-0450(1968)007<0525:aoslpe>2.0.co;2]
- Sieck K (2013) Internal variability in the Regional Climate Model REMO. PhD Thesis. PhD thesis, Universität Hamburg, Hamburg, URL <http://hdl.handle.net/11858/00-001M-0000-001A-2C89-B>
- Skamarock WC, Klemp JB, Dudhia J, Gill DO, Barker M, Duda KG, Y Huang X, Wang W, Powers JG (2008) A description of the Advanced Research WRF Version 3. NCAR Technical Note pp 1–113, [DOI: 10.5065/D68S4MVH]
- Solman S (2016) Systematic temperature and precipitation biases in the CLARIS-LPB ensemble simulations over South America and possible implications for climate change projections. *Climate Research* 68, [DOI: 10.3354/cr01362]
- Solman S, Blázquez J (2019) Multiscale precipitation variability over South America: Analysis of the added value of CORDEX RCM simulations. *Climate Dynamics* 53:1547–1565, [DOI: 10.1007/s00382-019-04689-1]
- Solman S, Sanchez E, Samuelsson P, P da Rocha R, Li L, Marengo J, Pessacg N, Remedio AR, Chou SC, Berbery H, Le Treut H, de Castro M, Jacob D (2013) Evaluation of an ensemble of regional climate model simulations over South America driven by the ERA-Interim reanalysis: Model performance and uncertainties. *Climate Dynamics* 41, [DOI: 10.1007/s00382-013-1667-2]
- Solman SA, Pessacg NL (2012) Regional climate simulations over South America: sensitivity to model physics and to the treatment of lateral boundary conditions using the MM5 model. *Climate Dynamics* 38(1):281–300, [DOI: 10.1007/s00382-011-1049-6]

- Stahl K, Tallaksen LM, Gudmundsson L, Christensen JH (2011) Streamflow Data from Small Basins: A Challenging Test to High-Resolution Regional Climate Modeling. *Journal of Hydrometeorology* 12(5):900–912, [DOI: [10.1175/2011JHM1356.1](https://doi.org/10.1175/2011JHM1356.1)]
- Stegehuis AI, Vautard R, Ciais P, Teuling AJ, Miralles DG, Wild M (2015) An observation-constrained multi-physics WRF ensemble for simulating european mega heat waves. *Geoscientific Model Development* 8(7):2285–2298, [DOI: [10.5194/gmd-8-2285-2015](https://doi.org/10.5194/gmd-8-2285-2015)]
- Stensrud D (2007) *Parameterization Schemes. Keys to Understanding Numerical Weather Prediction Models*. Cambridge University Press
- von Storch H (2006) *Models of Global and Regional Climate*, American Cancer Society, chap 32. [DOI: <https://doi.org/10.1002/0470848944.hsa035>]
- Takle ES, Roads J, Rockel B, Gutowski WJ, Arritt RW, Meinke I, Jones CG, Zadra A (2007) Transferability intercomparison: An opportunity for new insight on the global water cycle and energy budget. *Bulletin of the American Meteorological Society* 88(3):375–384, [DOI: [10.1175/BAMS-88-3-375](https://doi.org/10.1175/BAMS-88-3-375)]
- Tans P (2009) An Accounting of the Observed Increase in Oceanic and Atmospheric CO₂ and an Outlook for the Future. *Oceanography* 22(4, SI):26–35, [DOI: [10.5670/oceanog.2009.94](https://doi.org/10.5670/oceanog.2009.94)]
- Taylor KE, Stouffer RJ, Meehl GA (2012) An overview of CMIP5 and the experiment design. *Bulletin of the American Meteorological Society* 93(4):485–498, [DOI: [10.1175/BAMS-D-11-00094.1](https://doi.org/10.1175/BAMS-D-11-00094.1)]
- Thompson G, Field PR, Rasmussen RM, Hall WD (2008) Explicit forecasts of winter precipitation using an improved bulk microphysics scheme. Part II: Implementation of a new snow parameterization. *Monthly Weather Review* 136(12):5095–5115, [DOI: [10.1175/2008MWR2387.1](https://doi.org/10.1175/2008MWR2387.1)]
- Torma C, Giorgi F, Coppola E (2015) Added value of regional climate modeling over areas characterized by complex terrain—precipitation over the Alps. *Journal of Geophysical Research: Atmospheres* 120(9):3957–3972, [DOI: [10.1002/2014JD022781](https://doi.org/10.1002/2014JD022781)]

- Torseth K, Aas W, Breivik K, Fjaeraa AM, Fiebig M, Hjellbrekke AG, Myhre CL, Solberg S, Yttri KE (2012) Introduction to the European Monitoring and Evaluation Programme (EMEP) and observed atmospheric composition change during 1972-2009. *Atmospheric Chemistry and Physics* 12(12):5447–5481, [DOI: 10.5194/acp-12-5447-2012]
- Tourpali K, Zanis P (2013) Winter anticyclonic blocking effects over Europe during 1960-2000 from an ensemble of regional climate models. *Climate Research* 57:81–91, [DOI: 10.3354/cr01169]
- van Ulden A, van Oldenborgh G (2006) Large-scale atmospheric circulation biases and changes in global climate model simulations and their importance for climate change in Central Europe. *Atmospheric Chemistry and Physics* 6:863–881, [DOI: 10.5194/acp-6-863-2006]
- Vautard R, Gobiet A, Jacob D, Belda M, Colette A, Deque M, Fernandez J, Garcia-Diez M, Goergen K, Guettler I, Halenka T, Karacostas T, Katragkou E, Keuler K, Kotlarski S, Mayer S, van Meijgaard E, Nikulin G, Patarcic M, Scinocca J, Sobolowski S, Suklitsch M, Teichmann C, Warrach-Sagi K, Wulfmeyer V, Yiou P (2013) The simulation of European heat waves from an ensemble of regional climate models within the EURO-CORDEX project. *Climate Dynamics* 41(9-10):2555–2575, [DOI: 10.1007/s00382-013-1714-z]
- Vergara-Temprado J, Ban N, Panosetti D, Schlemmer L, Schär C (2020) Climate models permit convection at much coarser resolutions than previously considered. *Journal of Climate* 33(5):1915–1933, [DOI: 10.1175/JCLI-D-19-0286.1]
- Weisheimer A, Doblus-Reyes FJ, Palmer TN, Alessandri A, Arribas A, Déqué M, Keenlyside N, MacVean M, Navarra A, Rogel P (2009) ENSEMBLES: A new multi-model ensemble for seasonal-to-annual predictions—Skill and progress beyond DEMETER in forecasting tropical Pacific SSTs. *Geophysical Research Letters* 36(21), [DOI: <https://doi.org/10.1029/2009GL040896>]
- Weisman M, Davis C, Wang W, Manning K, Klemp J (2008) Experiences with 0–36-h explicit convective forecasts with the WRF-ARW model. *Weather and Forecasting* 23, [DOI: 10.1175/2007WAF2007005.1]
- Weisman M, Skamarock W, Klemp J (1997) The resolution dependence of explicitly modeled convective systems.

- Monthly Weather Review 125(4):527–548, [DOI: 10.1175/1520-0493(1997)125;0527:TRDOEM;2.0.CO;2]
- Wilks DS (2011) Statistical methods in the atmospheric sciences, vol 100. Academic press
- WMO (2017) WMO guidelines on the calculation of climate normals. Tech. Rep. WMO-No. 12031, World Meteorological Organization, URL https://library.wmo.int/doc_num.php?explnum_id=4166
- Yang Y, Uddstrom M, Duncan M (2011) Effects of short spin-up periods on soil moisture simulation and the causes over new zealand. Journal of Geophysical Research: Atmospheres 116(D24), [DOI: 10.1029/2011JD016121]
- Yang Z, Arritt RW (2002) Tests of a Perturbed Physics Ensemble Approach for Regional Climate Modeling. Journal of Climate 15(20):2881–2896, [DOI: 10.1175/1520-0442(2002)015;2881:TOAPPE;2.0.CO;2]
- Zappa G (2019) Regional climate impacts of future changes in the mid-latitude atmospheric circulation: a storyline view. Current Climate Change Reports 5(4):358–371, [DOI: 10.1007/s40641-019-00146-7]
- Zikova N, Holtanova E, Kalvova J (2013) Annual precipitation cycle in regional climate models: the influence of horizontal resolution. Theoretical and Applied Climatology 112(3-4):521–533, [DOI: 10.1007/s00704-012-0749-0]
- Zipser E, J Cecil D, Liu C, Nesbitt S, Yorty D (2006) Where are the most intense thunderstorms on Earth? Bulletin of the American Meteorological Society 87, [DOI: 10.1175/BAMS-87-8-1057]